DOKUZ EYLÜL UNIVERSITY
GRADUATE SCHOOL OF NATURAL AND APPLIED SCIENCES

PREPARATION, CHARACTERIZATION AND APPLICATIONS OF ZnO NANOPARTICLES

Tuğçe KARATAŞ

February, 2018
İZMİR

PREPARATION, CHARACTERIZATION AND APPLICATIONS OF ZnO NANOPARTICLES

A Thesis Submitted to the
Graduate School of Natural and Applied Sciences of Dokuz Eylül University
In Partial Fulfillment of the Requirements for the Degree of Master of Science in Department of Nanoscience and Nanoengineering

Tuğçe KARATAŞ

February, 2018
İZMİR

M.SC THESIS EXAMINATION RESULT FORM

We have read the thesis entitled **"PREPARATION, CHARACTERIZATION AND APPLICATIONS OF ZnO NANOPARTICLES"** completed by **TUĞÇE KARATAŞ** under supervision of **PROF. DR. MEHMET KADİR YURDAKOÇ** and we certify that in our opinion it is fully adequate, in scope and in quality, as a thesis for the degree of Master of Science.

Prof. Dr. Mehmet Kadir YURDAKOÇ

Supervisor

Prof. Dr. Levent Ballice

(Jury Member)

Prof. Dr. Yoldaş Seki

(Jury Member)

Prof. Dr. Kadriye ERTEKİN
Director
Graduate School of Natural and Applied Sciences

ACKNOWLEDGMENTS

First of all, I would like to thank my advisor Prof. Dr. Kadir Yurdakoç for his constructive ideas, help, constant support, guidance and contributions. I wish to extend my sincere thanks to Research Assistant Dr. Aylin Altınışık Tağaç and BSc İdil Özel for their collaboration in the laboratory studies and sharing her valuable experiences with me.

Due to fact that I would like to thank MOLUMER Construction Chemicals, the company I work, for its economical and infrastructural supports.

Finally, a special thank goes to my dear family for their concern, confidence and support.

Tuğçe KARATAŞ

PREPARATION, CHARACTERIZATION AND APPLICATIONS OF ZnO NANOPARTICLES

ABSTRACT

It has been well-known that Zinc Oxide is an inorganic material and has several applications in industry, such as photocatalysts, solar cells, light-emitting devices, gas sensors, biological probes and antibacterial agents, etc. In this study, Zinc Oxide nanoparticles were synthesized by using different methods and conditions. The synthesized samples were then characterized by Fourier transform infrared spectroscopy (FTIR), X-Ray Diffraction Analysis (XRD), Scanning Electron Microscopy (SEM) and Thermogravimetric analysis (TG/DTG).

We modified the surface of Zinc oxide with (3-Aminopropyl) triethoxysilane, Cetyl trimethyl ammonium bromide and Sodium dodecyl sulfate. The effects of surface modifications on the size, structure, morphology, and optical properties of Zinc Oxide nanoparticles was investigated.

The energy band gap value of Zinc Oxide was calculated to be 3.71 eV. Modified ZnO samples were mixed with acrylic resin in a ratio of 1 to 5 percent then the film was coated on glass and the UV sensitivities were examined. The films were visualized on an optical microscope. It has been identified that ZnO specimens were nanoscopic, UV-filtered and semi-conducting.

Keywords: Zinc oxide, nanoparticles, surface morphology, modification, UV-filtration

ÇİNKO OKSİT NANOPARTİKÜLLERİNİN HAZIRLANMASI, KARAKTERİZASYONU VE UYGULAMALARI

ÖZ

Çinko oksit iyi bilinen bir inorganik malzemedir ve endüstride fotokatalizör, güneş pilleri, ışık yayan cihazlar, gaz sensörleri, biyolojik problar ve antibakteriyel ajanlar gibi birçok kullanıma sahiptir. Bu çalışmada, çinko oksit nanopartikülleri farklı metotlar ve şartlar kullanılarak üretildi. Sentezlenen örnekler, Fourier Transform Infrared spektroskopisi(FTIR), X-ışını kırınım analizi (XRD), Taramalı electron mikroskobu (SEM) ve Termogravimetrik analizler (TG/DTG) ile karakterize edildi.

Çinko oksidin yüzeyi, (3-Aminopropil)trietoksisilan, Setil trimetil amonyum bromür ve Sodyum dodesil sulfat ile modifiye edilmiştir. Bu yüzey modifikasyonlarının etkileri, çinko oksit nanopartiküllerinin boyut, yapı, morfoloji ve optik özellikleri üzerinden incelenmiştir.

ZnO'in enerji band açıklığı değeri, 3,71 eV olarak hesaplanmıştır. Modifiye ZnO örnekleri, akrilik reçineye yüzde 1-5 olacak şekilde karıştırılarak cam üzerine film kaplanmış ve UV duyarlıkları incelenmiştir. Filmler, optic mikroskopta görüntülenmiştir. ZnO örneklerinin nanoboyutlu, UV-ışınlarını filter ettiği ve yarı iletken oldukları belirlenmiştir.

Anahtar Kelimeler: Çinko oksit, nanotanecik, yüzey morfolojisi, modifikasyon, UV-filtreleme

CONTENTS

Page

M.Sc THESIS EXAMINATION RESULT FORM ii
ACKNOWLEDGMENTS iii
ABSTRACT iv
ÖZ v
LIST OF FIGURES ix
LIST OF TABLES xiii

CHAPTER ONE - INTRODUCTION 1

1.1 General 1

CHAPTER TWO - THEORETICAL BACKGROUND 3

2.1 Synthesis Methods of Nano- and Micrometric Zinc Oxide 3
2.1.1 Metallurgical Process 4
2.1.2 Chemical Processes 4
2.2 Some recent articles related with Zinc Oxide in 2017 6
2.3 UV Sensitivity of ZnO naoparticles 12
2.4 The aim of the Thesis 13

CHAPTER THREE- MATERIALS AND METHODS 14

3.1 Materials 14
3.2 Preparation of the Zinc Oxide Nanoparticles 14
3.2.1 Effect of pH 15
3.2.2 Effect of Temperature 15
3.2.3 Effect of Concentration 16
3.2.4 Effect of Solvent Carbon Number 16

3.3 Characterization of ZnO Nanoparticles 17
3.3.1 Fourier Transform Infrared (FTIR) Spectra of the Samples 17
3.3.2 X-Ray Diffraction (XRD) Analysis 17
3.3.3 Scanning Electron Microscopy (SEM) Analysis 17
3.3.4 Thermogravimetric (TG/DTG) Analysis 17
3.3.5 Nanoparticle Size Distribution Analysis 17
3.4 Modification of ZnO Nanoparticles 18
3.4.1 Surface Modification with (3-Aminopropyl)triethoxysilane (APTES) 18
3.4.2 Surface Modification with Cetyl Trimethyl Ammonium Bromide(CTAB) 18
3.4.3 Surface Modification with sodium dodecylsulphate(SDS) 19
3.5 Application of ZnO Nanoparticles 19
3.6 Determination the Optical Properties of the Samples 20

CHAPTER FOUR - RESULTS AND DISCUSSIONS 21

4.1 Results of Characterization 21
4.1.1 Results of FTIR 21
4.1.2 XRD Analysis Results 24
4.1.3 Results of SEM Analysis 28
4.1.4 Results of TG/DTG Analysis 46
4.1.5 Particle Size Distribution Results 48
4.2 Results of Application of Modified ZnO Nano Particles 50
4.2.1 UV-Visible Spectroscopic Analysis of the Polymer composite films coated onto glass 50
4.2.2 OM Images of the Polymer composite films coated onto glass 55
4.2.3 SEM Images of the SDS, CTAB and APTES Modified ZnO 56
4.2.4 XRD Patterns of the SDS, CTAB and APTES Modifed ZnO (M) 59
4.2.5 ATR (Attenuated Total Reflection)-FTIR Characterization of the SDS, CTAB and APTES Modified ZnO (M) Polymer Coated Samples 62

4.2.6 UV-Visible Reflectance Spectrophotometric Analysis of the SDS, CTAB and APTES Modifed ZnO (M) Polymer Coated Samples..... 67

CHAPTER FIVE - CONCLUSIONS..... 70

REFERENCES..... 72

LIST OF FIGURES

Page

Figure 2.1 Examples of ZnO Structure: Flowers (a); rods (b); wires (c,d) 3

Figure 2.2 Sol-gel process of ZnO Nanoparticles 5

Figure 2.3 Graphical abstract of this study 13

Figure 3.1 Chemical formulas of APTES(A), CTAB(B) and SDS(C) 18

Figure 3.2 Molecules of CTAB surfactant 19

Figure 4.1 FTIR spectra of the samples, effects of pH and temperature 22

Figure 4.2 FTIR spectra of the samples, effects of precursor concentration 23

Figure 4.3 FTIR spectra of the samples, effects of solvent carbon number 23

Figure 4.4 XRD reference data of ZnO 24

Figure 4.5 XRD patterns of ZnO 25

Figure 4.6 XRD patterns of samples, pH and temperature effects 26

Figure 4.7 XRD patterns of samples before calcination concentration effects 26

Figure 4.8 XRD patterns of samples after calcination, effects of concentration 27

Figure 4.9 XRD patterns of samples, effects of solvent carbon number 27

Figure 4.10 SEM images of ZnO (Molumer) with 100 00 K x magnifications 28

Figure 4.11 SEM images of ZnO (Sigma-Aldrich) with 50 00 K x and 100 00 K x magnifications 29

Figure 4.12 SEM images of samples, effects of temperature and pH differences 30

Figure 4.13 SEM images of the ZnO samples (Synthesis 1a) after calcination 31

Figure 4.14 SEM images of the sample, concentration differences 32

Figure 4.15 SEM images of the ZnO sample (Synthesis 2a) after calcination 33

Figure 4.16 SEM images of the ZnO sample (Synhesis 2b) after calcination 34

Figure 4.17 SEM images of the ZnO samples (Synthesis 3a) before calcination..... 35

Figure 4.18 SEM images of the ZnO sample (Synthesis 3a) after calcination 36

Figure 4.19 SEM images of the ZnO sample (Synthesis 3b) before calcination 37

Figure 4.20 SEM images of the ZnO sample (Synthesis 3b) after calcination 38

Figure 4.21 SEM images of the ZnO sample (Synhesis 3c) before calcination 39

Figure 4.22 SEM images of the ZnO sample (Synthesis 3c) after calcination 40

Figure 4.23 SEM images of sample, effect of solvent carbon number differences ... 41

Figure 4.23m SEM images of sample (Methanol used as solvent, Synthesis C_1) 42

Figure 4.23e SEM images of the sample (Ethanol used as solvent, Synthesis C_2).... 43

Figure 4.23p SEM images of sample (Propanol used as solvent, Synthesis C_3) 44

Figure 4.23b SEM images of sample (Butanol used as solvent, Synthesis C_4) 45

Figure 4.24 TG/DTG thermogram of the sample, pH differences 46

Figure 4.25 TG/DTG thermogram of the samples, effect of concentration differences before calcination (BC) 46

Figure 4.26 TG/DTG thermogram of the samples, effect of concentration differences after calcination 47

Figure 4.27 TG/DTA thermogram of the samples, effects of solvent carbon number differences 47

Figure 4.28 Effect of pH on particle size distribution of the samples..... 48

Figure 4.29 Effect of temperature on the particle size distribution of the samples ... 48

Figure 4.30 Effect of concentration on the particle size distribution of the samples. 49

Figure 4.31 Effect of solvent carbon atom number on the particle size distribution of samples 49

Figure 4.32 The optical transmittance spectra of films 50

Figure 4.33 Tauc graph of the optical band gap energy calculation of ZnO 53

Figure 4.34 Direct methods for the calculation of the optical band gap energy 54

Figure 4.35 OM images of pure polymer doped with Zinc Oxide 55

Figure 4.36 SEM images of SDS modified ZnO sample 56

Figure 4.37 SEM images of CTAB modified ZnO sample 57

Figure 4.38 SEM images of APTES modified ZnO sample 58

Figure 4.39 XRD pattern of ZnO (M) 59

Figure 4.40 XRD pattern of SDS modified Zno (M) 60

Figure 4.41 XRD pattern of CTAB modified ZnO (M) 60

Figure 4.42 XRD pattern of APTES modified ZnO (M) 61

Figure 4.43 ATR-FTIR Spectrum of Acrylic Polymer Sample 63

Figure 4.44 ATR-FTIR Spectrum Search of Acrylic Polymer Sample 64

Figure 4.45 ATR-FTIR spectra of the TK0, TK1-3A, TK2-3A and TK4-3A 65

Figure 4.46 UV-Visible Reflectance Spectra of the TK0, TK1-3 and TK1-5 67

Figure 4.47 UV-Visible Reflectance Spectra of the TK0, TK2-1, TK2-3 and TK2-5 68

Figure 4.48 UV-Visible Reflectance Spectra of the TK0, TK3-1, TK3-3 and TK3-5 69

Figure 4.49 UV-Visible Reflectance Spectra of the TK0, TK4-1, TK4-3 and TK4-5 69

LIST OF TABLES

Page

Table 1.1 Various features of ZnO 1

Table 2.1 UV-visible classification of electromagnetic radiation 12

Table 3.1 Effects, chemical reagents, conditions and sample codes used in the experiments 16

Table 4.1 FTIR band assignments of O-H vibration 22

Table 4.2 The XRD data of ZnO 25

Table 4.3 Definition of the samples used in the application with polymer 52

Table 4.4 Average crystallite size of the ZnO samples 62

Table 4.5 FTIR band assignments of APTES 66

CHAPTER ONE
INTRODUCTION

1.1 General

ZnO is an inorganic multifunctional material which has wide range applications in industry because of having high chemical stability, high electrochemical coupling coefficient, broad range of radiation absorption and high photo stability (Segets et al., 2009; Lou, 1991).

The piezo- and pyroelectric properties of ZnO mean that it can be used as a sensor, converter, energy generator and photocatalyst in hydrogen production (Wang, 2008; Chaari & Matoussi, 2012).

In materials science, ZnO is classified as a semiconductor in group II-VI. A broad energy band (3.37 eV), high bond energy (60 meV) and high thermal and mechanical stability at room temperature make it attractive for potential use in electronics, optoelectronics and laser technology (Bacaksiz et al., 2008; Wang et al.2005).

Table 1.1 Various features of ZnO

Density	5.606 g/cm^3
Melting point	1975 °C
Boiling point	2360 °C
Band gap	3.3 eV
Refractive index	20.041
Crystal structure	Wurtzite
Weave parameters at 300 K A C a/c	 0.32495 nm 0.52069 nm 1.602
Static Dielectric Constant	8.656

ZnO is used in the ceramics industry because of its hardness, rigidity and piezoelectric constant. Its low toxicity, biocompatibility and biodegradability make

ZnO a material of interest for biomedicine and in pro-ecological systems as pigment and UV cut filter (Özgür et al., 2005; Bhattacharyya & Gedanken, 2007; Ludi & Niederberger, 2013).

A new recent report about the zinc oxide as a commercial product is presented below.

“Nano Zinc Oxide Market to Reach $7,677 Million by 2022, Globally - Allied Market Research, PORTLAND, Oregon, Oct 17, 2016 (PR Newswire Europe via COMTEX); a new report published by Allied Market Research titled, "*Nano Zinc Oxide Market by Application - Global Opportunity Analysis and Industry Forecast, 2014 - 2022*", projects that the world nano zinc oxide market was valued at $2,099 million in 2015 and is expected to reach $7,677 million by 2022, registering a CAGR of 20.4% from 2016 to 2022. Summary of the Nano Zinc Oxide Market Report can be accessed on the website” (Allied Market, 2017).

CHAPTER TWO
THEORETICAL BACKGROUND

2.1 Synthesis Methods of Nano- and Micrometric Zinc Oxide

Many techniques have been utilized to prepare ZnO powders, such as mechano chemical process, controlled precipitation, thermal evaporation, chemical vapor deposition, spray pyrolysis, sol-gel method, solvothermal and hydrothermal method, etc. (Zhou et al., 2017).

ZnO nanoparticles can be prepared from Zn-precursors as salts. The physicochemical properties of the particles such as size, shape and morphology will be different as far as the preparation methods concerned as shown below figures.

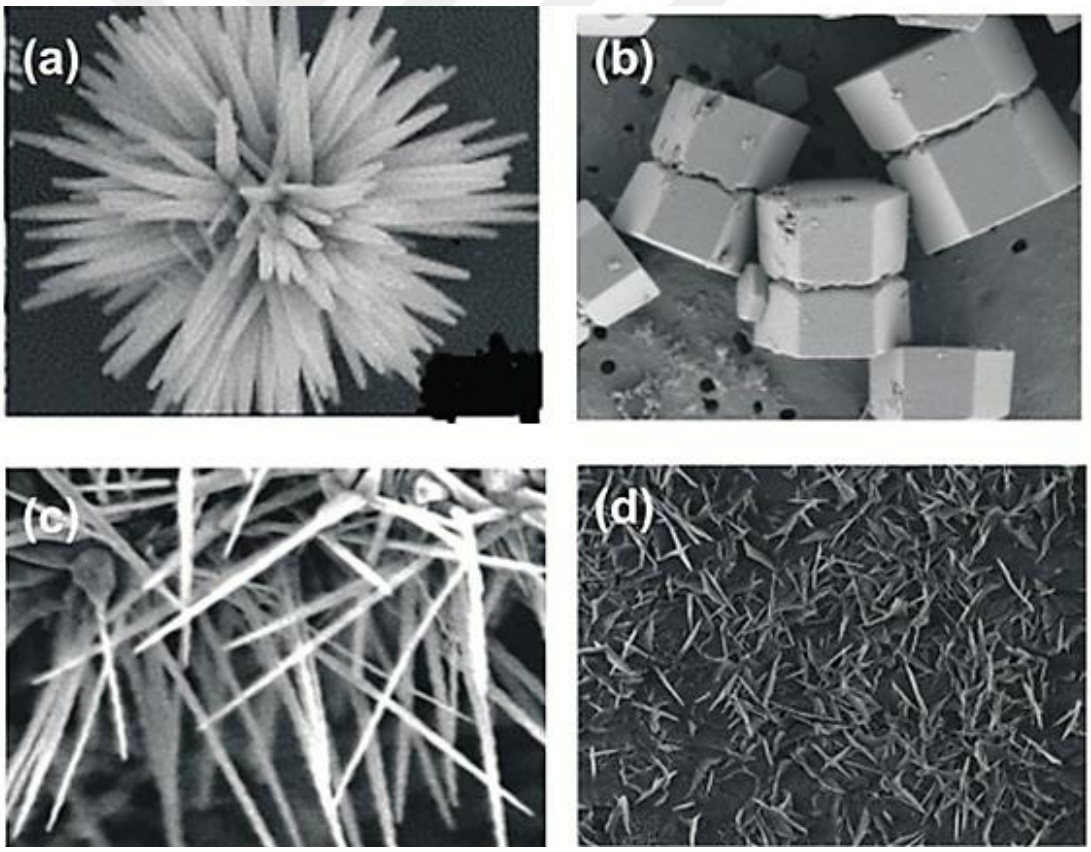


Figure 2.1 Examples of Zinc oxide structure: flower(a); rods (b); wires (c,d). (Radzimska and Jesonowski, 2014)

2.1.1 Metallurgical Process

The direct (American) process involves the reduction of zinc ore by heating with coal (such as anthracite), followed by the oxidation of zinc vapor in the same reactor, in a single production cycle (Pysklo, et al., 2007).

In the indirect (French) process, metallic zinc is melted in a furnace and vaporized at ca. 910°C. The immediate reaction of the zinc vapor with oxygen from the air produces ZnO. The particles of zinc oxide are transported via a cooling duct and are collected at a bag filter station (Mahmut et al., 2003).

2.1.2 Chemical Processes

2.1.2.1Mechano-chemical Process

It is a cheap and simple method of obtaining nanoparticles on a large scale. A "thinner" is added to the system in the form of a solid (usually NaCl), which acts as a reaction medium and separates the nanoparticles being formed.

The zinc oxide precursor formed as $ZnCO_3$and calcined at a temperature of 400–800 °C. The process as a whole involves the following reactions (2.1) and (2.2):

$$ZnCl_2 + Na_2CO_3 \rightarrow ZnCO_3 + 2NaCl \quad (2.1)$$

$$ZnCO_3 \rightarrow ZnO + CO_2 \quad (2.2)$$

2.1.2.2 Controlled Precipitation

This method is used widely. The method involves fast and spontaneous reduction of a solution of zinc salt using a reducing agent, to limit the growth of particles with specified dimensions, followed by precipitation of a precursor of ZnO from the solution.

At the next stage this precursor undergoes thermal treatment, followed by milling to remove impurities. The process is controlled by pH, temperature and time of precipitation. The resulting precipitate is calcined generally between 450 and 500°C for 3 h (Hong et al., 2006).

2.1.2.3 Sol-Gel Method

When the solution of precursors is hydrolyzed, a colloidal sol is created. We can coat the films by spin-coating or deep coating. When we condense the sol particles, a gel form appears, followed by evaporation of solvent. We get therefore xerogel particles. With heat treatment, dense ceramic is made. The production process was given below.

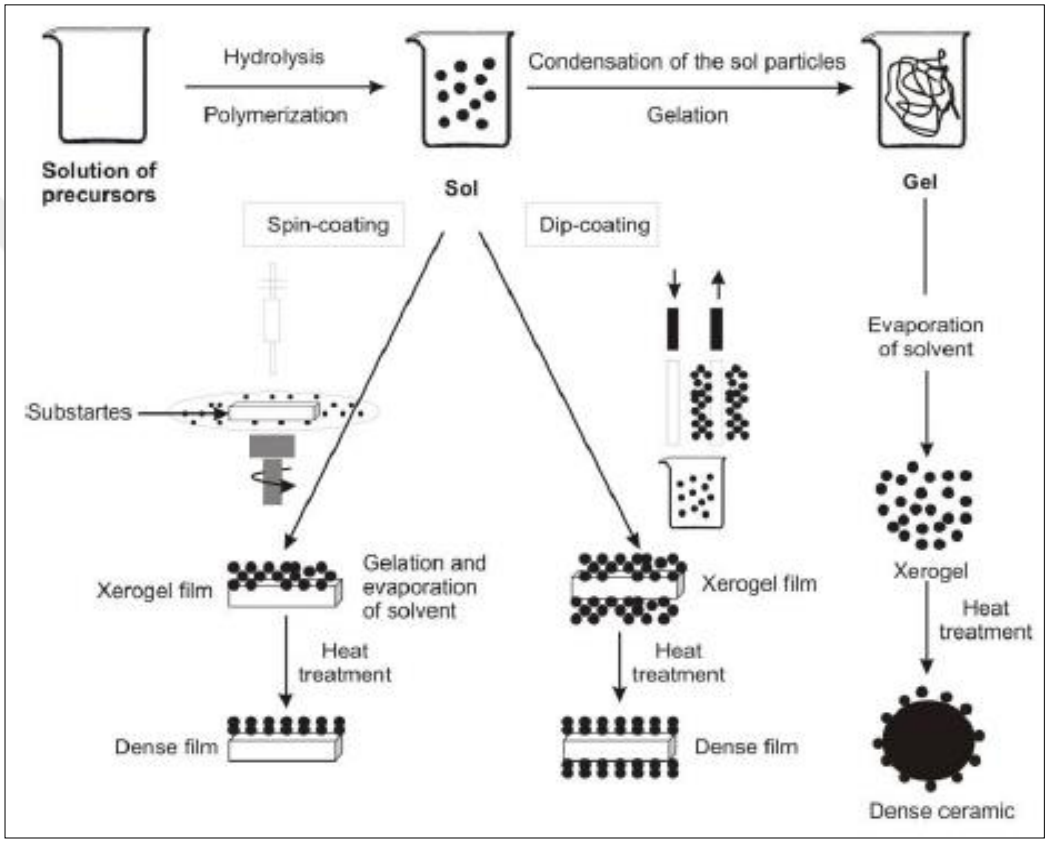


Figure 2.2 Sol-gel process of ZnO nanoparticles (Znaidi, 2010)

ZnO powder was prepared from zinc acetate dihydrate, oxalic acid, using ethanol as solvent. High-filling, uniform, ordered ZnO nanotubes have been prepared by sol-gel method into ultra-thin membrane (Ristic et al., 2005).

2.1.2.4 Hydrothermal Method

The hydrothermal method does not require the use of organic solvents or additional processing of the product (grinding and calcination), which makes it a simple and environmentally friendly technique.

Using the reagents Zinc chloride ($ZnCl_2$) and Sodium hydroxide (NaOH) in a ratio of 1:2, in an aqueous environment as in reaction (Chen at al., 2000) (2.3)

$$ZnCl_2 + 2NaOH \rightarrow Zn(OH)_2\downarrow + 2Na^+ + 2Cl^- \quad (2.3)$$

The white $Zn(OH)_2$ precipitate underwent filtration and washing, and then the pH was corrected to a value of 5–8 using HCl. The synthesis takes place in an autoclave, where the mixture of substrates is heated gradually to a temperature of 100–300 °C and left for several days. As a result of heating followed by cooling, crystal nuclei are formed, which then grow.

$$Zn(OH)_2 \rightarrow ZnO + H_2O \quad (2.4)$$

The pH affects the size and shape of the ZnO particles. The shape of the particles is also affected by the time and temperature of the hydrothermal process. With an increase in time, temperature and surfactant concentration, the size of the particles increases.

2.2 Some recent articles related with Zinc Oxide in 2017

In this section, some recent articles about the subject of the thesis related with zinc oxide were outlined. These articles cover the synthesis, characterization and applications of ZnO in 2017. There are also important applications related with the photocatalytic properties for dye degradation purposes in the waste water systems. Some gas sensor application of zinc oxide nanoparticles assembled systems was also investigated. From this part, the searched articles were outlined below.

Kaolin/ZnO composites was prepared by thermal decomposition of $Na_2Zn_3(CO_3)_4 \cdot 3H_2O$. Band gap energies and corresponding wavelengths of ZnO nanoparticles and the composites were determined as 3.29-3.31 eV and 377-375 nm,

respectively. The photocatalytic activity against discoloration of Acid Orange 7 was also studied and founded that ~39 mass% of ZnO contained composite exhibited the highest activity (Janíková, Tokarský, Kutláková, Kormunda, & Neuwirthová, 2017).

ZnO nanoparticles with an average particle size of 15.81 nm were synthesized using a hydrothermal method. It was found from XRD data that the ZnO nanoparticles had a single crystal wurtzite hexagonal structure. Solvent polarity was responsible for varying and controlling the size and morphology of the particles. In this respect, floral-like or wire-like belt sheet structures were observed in SEM images. The band gap energy was found to be 2.49 eV (Bharti, & Bharati, 2017).

ZnO nanoparticles, due to their biocompatible nature, have attracted the attention of the scientific community to explore and to understand their cytotoxicity, interactions with biomolecules such as proteins, nucleic acids, fats, cell membranes, tissues, biological fluids, etc., and bio-safety for proper utilization in biomedical applications. For these reasons, the preparation of ZnO nanomaterials with variable morphologies, factors influencing the growth, morphology and surface defects, and various laboratory methods to evaluate the antibacterial activities have reviewed. It was claimed that amine functionalization of ZnO nanoparticles showed better antibacterial and cytotoxical effects toward cancer cells (Kumar, Umar, Kumar, & Nalwa, 2017).

A super hydrophobic coating containing ZnO nanoparticles and copper stearate was developed. It has been observed that the coatings exhibited excellent floating characteristics and higher load bearing capacity (Suyambulingam et al., 2017)

ZnO nanoparticles were prepared in solvothermal method using zinc acetate and ethanol without any surfactant. Wurtzite type hexagonal ZnO nanoparticles were obtained. The crystalline size increased from 19 to 28 nm by increasing the temperature from 120 to 180 °C. Usage of LiOH decreased the crystalline size. Photoluminescence intensity increased with temperatures. LiOH addition was able to shift the peak from wavelength of 421 nm to 457 nm by excitation at wavelength of 250 nm (Widiyastuti et al., 2017).

ZnO nanocomposites based on carboxymethyl cellulose-chitosan-oleic acid were prepared. The morphological, mechanical, thermal, physical and antifungal properties of the composite films were investigated. Higher UV blocking and considerable antifungal properties against *Aspergillus niger* were observed (Noshirvani, Ghanbarzadeh, Mokarram, Hashemi, & Coma, 2017).

ZnO photocatalysts with controlled crystallite sizes, particle sizes, and morphologies were synthesized by thermal decarbonation of $ZnCO_3$ hydroxides. The catalysts had sizes and shapes varying from 80 ± 20 nm nonporous rhombohedral nanoparticles to 5 ± 0.5 μm porous particles, for a constant crystallite size of 64 ± 3 nm (Barhoum et al., 2017).

Ag doped ZnO visible nano photocatalyst was prepared for removing of methylene blue from aqueous solution. Degradation efficiency about 63% in visible-light illumination was observed. Doping of 0.5 percent of Ag enhanced the photocatalytic activity with a maximum efficiency of 98% for the degradation of methylene blue (Kakhki, Tayebee, & Ahsani, 2017).

Photonic properties of surface modified with imine type molecules of ZnO nanoparticles as an application in LEDs was reported. In this article, some improvements in the fluorescent intensity of ZnO were observed. The emission at 333 nm due to Mn^{2+} ion was achieved (Madhu, Kaur, & Kaur, 2017).

ZnO, Al and Ca-doped ZnO nanoparticles for sensor applications have been prepared by the sol–gel process. Al-doped ZnO sensor showed high response towards CO, while the Ca-doped sensor showed a good response to CO_2, operating temperatures of 300 and 450 °C, respectively (Hjiri et al., 2017).

In the synthesis of ZnO nanoparticles, effects of pH on the electrical, optical and photocatalytic properties were studied. From XRD data, ZnO nanoparticles had well crystalline, hexagonal wurtzite structure with average grain size in between 40–80nm. pH greatly effects on morphological and electrical properties. A sharp and strong band at about 487 cm^{-1} confirmed the XRD data. This ZnO photocatalyst

exhibited photocatalytic activity on degradation of direct red dye (Verma, Bhatia, & Bedi, 2017).

Hexagonal wurtzite structural ZnO photocatalysts with a grain size range of 20-100 nm were prepared by using sol-gel method. It was found that the band gap of ZnO nanoparticles narrowed to visible light region, i.e., ~ 2.69 eV, which increased with the calcination temperature. MB solution was decomposed within 30 min, and after 9 cycles, the catalyst maintains more than 95% photodegradation (Dong, Yu, Dong, Yang, & Wu, 2017).

The porous ZnO nanoparticles were synthesized by using thermal decomposition of hydrozincite, whereas the nanorods and nanowires were grown by hydrothermal and chemical vapor deposition methods, respectively. Gas-sensing properties of ZnO were also examined as a function of crystal growth orientation, crystal size, and porosity. It was found that ZnO porous nanoparticles exhibited the best sensitivity against ethanol (Quy et al., 2017).

The ZnO nanoparticles were synthesized via simple thermal oxidation. The nanoparticles exhibited an excellent near spherical shape with narrow size distribution and mean size of around 20 nm. Then, they modified with graphene oxide (GO) by a solvothermal method and used as photocatalysts in the photodegradation of azo-dyes such as neutral red, crystal violet, congo red and methyl orange under UV-light irradiation. The enhancement of photocatalytic performance was observed due to the synergistic effect between ZnO nanoparticles and GO layers (Atchudan, Edison, Perumal, Shanmugam, & Lee, 2017).

Usage of ZnO as an ingredient in sunscreens and its toxicology and risk assessment were examined. ZnO displayed no carcinogenic potential, and its skin penetration was low. A maximum systemic exposure dose (SED) and the lowest margin of safety (MOS) of ZnO for sunscreen were estimated to be 0.6 mg/kg/day and 448.2, respectively. It has been estimated that ZnO may be used safely in cosmetic products within the current regulatory limits of 25% in Korea (Kim et al., 2017).

Nanoparticles of TiO_2, ZnO and nanocomposite ZnO/TiO_2 with 11-43 nm crystallite sizes were prepared via a co-precipitation method. The XRD patterns of ZnO/TiO_2 powder showed two phases of anatase and wurtzite. TEM images showed three types of particles as fine TiO_2 particles, and submicron ellipsoidal and rod-like particles of ZnO. The energy gap (E_g) of the samples found to be in the range of 3.15-3.60 eV. Photodegradation efficiencies of the samples for methyl orange were evaluated and results showed that nanocomposite ZnO/TiO_2 calcined at 400 °C exhibited the highest apparent rate constant (k), and a higher capacity for methyl orange removal than TiO_2 and ZnO nanoparticles (Lachom, Poolcharuansin, & Laokul, 2017).

Large scale hydrothermal synthesis of ZnO nanostructures was performed at 115 °C and 2 or 6 h in an autoclave. Plate- and needle-like nanoparticles were obtained, characterized and found to be antibacterial active against *Staphylococcus aureus* (Ghasaban, Atai, & Imani, 2017).

Mesoporous ZnO nanospheres were synthesized by thermal decomposition of zinc hydroxide carbonate hydrate in the presence of diethylene glycol and polyvinyl pyrrolidone. The nanospheres exhibited a large specific surface area (43.4 m^2/g), uniform pore size (6.2 nm) and good dispersibility in water. The in vitro Doxorubicin hydrochloride release experiments demonstrated that ZnO exhibited a pH-triggered release behavior (Tian, Liu, Zhang, Li, & Wang, 2017).

The different morphologies of ZnO flowers, including spindle-based, flake-based and rod-based, were synthesized by adjusting the $[Zn^{2+}]$ in alkaline solution. The photocatalytic activities of the flake-based ZnO displayed better in catalytic degradation of dyes. It has been demonstrated that the enhancement of photocatalytic activity could be possible by controlling the shape of the flake-based ZnO flowers (Cao et al., 2017).

ZnO/graphene composite thin films were prepared by using sol-gel method. The crystal structure was characterized by XRD and found that the presence of graphene did not destroy the crystal structure of ZnO. The introduction of graphene into ZnO

did not bring obvious effects on the optical properties (Gu, Yu, Wang, Yao, & Chen, 2017).

ZnO was synthesized by using the sol-gel, the precipitation and solvent evaporation methods. The degree of crystallinity, particle size, porosity, band gap energy, types of defect sites and photocatalytic activity against Rhodamine B were determined. It was found that the preparation method influenced on the ZnO morphology. The highest photocatalytic activity was observed for ZnO prepared by the precipitation method (Wolski, Whitten, Sobczak, & Ziolek, 2017).

Microwave assisted ZnO nanoparticles and their photocatalytic activities for the degradation of Rhodamine B were studied. The highest photocataytic efficiency was obtained as 92% efficiency and rate constant of 0.042 min^{-1} (Thankachan et al., 2017).

ZnO nanostructures were prepared by using the microwave-assisted hydrothermal method. The effect of pH on the particle morphology was evaluated. The gas sensing performances against methane, carbon monoxide, and ammonia and hydrogen gases at 250°C were investigated. It was found that ZnO sensors displayed comparable responses to these gases related with morphology, surface area and porosity as well as defects induced by an increase in pH (Shingange et al., 2017).

The synthesis of ZnO nanostructures such as nano-bullets, nanorods, and nanospheres by modified polyol method without using surfactants were reported. It was found that nano-bullets were obtained at 160°C with Zinc acetate dihydrate concentration of 0.6 M, whereas at 0.8 M nanorods were observed while at 1.0 M only nanospheres appeared (Guzmán-Carrillo et al., 2017).

ZnO nanoparticles were synthesized by sol-gel method. It was found that ZnO annealed at a temperature of 600 °C have the greatest crystalinity and crystal size. Agglomeration and increase in grain size with increasing annealed temperature were observed from SEM images. The optical properties of ZnO increased with increasing annealed temperature (Ramelan, Wahyuningsih, Munawaroh, & Narayan, 2017).

ZnO nanoparticles were synthesized by using soft and solvothermal methods. Luminescence properties and solvent effect on the particles were reported (Multian et al., 2017).

Au nanoparticles coupled ZnO nanorod based photodetector for operation in the visible spectral range was developed and characterized in details specially the points of wiev of ZnO nanorods in nanotechnology. This can be used as a commercial sensitive photodetector (Choi, Hansen, Van Keuren, & Hahm, 2017).

Usage of ZnO nanoparticles as an adsorbent for the removal of Cr^{6+} from aqueous solution was investigated. The conditions were determined as 4 g L^{-1} of ZnO nanoparticles, the initial metal concentration of 9 mg L^{-1}, pH=2, 50 °C and the contact time of 90 min. A Langmuir adsorption isotherm model was applied to the adsorption data. Adsorption kinetics was also investigated and found that pseudo second order kinetics was followed. Thermodynamic study also revealed that the adsorption process was endothermic and spontaneous (Pandey, & Tripathi, 2017).

2.3 UV Sensitivity of ZnO naoparticles

Ultraviolet (UV) is an electromagnetic radiation with a wavelength from 10 nm to 400 nm and can be subdivided into a number of ranges recommended by the ISO standard ISO-21348 as given below as in Table 2.1.

Table 2.1 UV-visible classification of electromagnetic radiation

Name	Abbreviation	Wavelength/nm	Photon energy/eV
Ultraviolet A	UVA	315–400	3.10–3.94
Ultraviolet B	UVB	280–315	3.94–4.43
Ultraviolet C	UVC	100–280	4.43–12.4

Optical properties of ZnO nanoparticles were characterized based on UV transmission spectra. By using the photon enegy, it can be possible to determine the optical properties of the materials.

2.4 The aim of the Thesis

Zinc oxide is an important metal oxide used in various areas for several different purposes such as semiconductor, insulator, photocatalyst, sensor, sunscreen reactant and an adsorbent. For these reasons, there are several methods to synthesize zinc oxide nanoparticles. The products have different morphologies, shapes and sizes dependent upon the preparation methods.

Hypothesis 1: Synthesized products show different properties related with their physical structures.

In this thesis, zinc oxide nanoparticles will be synthesized by using co-precipitation and solvothermal methods by using convenient zinc salts via formation of zinc hydroxide followed by thermal methods as calcinations at elevated temperatures. During the synthesis, the experiments will be carried out as a function of pH, time, temperature and initial precursor concentration to determine the optimum conditions. Effects of capping agents such as APTES, CTAB and SDS during the synthesis will also be investigated. The synthesized products will also be characterized by several methods such as FTIR, XRD, SEM, TG/DTG and UV-Vis Spectrophotometer. Optical band gap energies will be determined. Commercial ZnO products purchased from Sigma-Aldrich and Molumer will be compared with the synthesized products.

Hypothesis 2: Modification of ZnO nanoparticles with the surfactans affects the UV-absorption of applicated polymer.

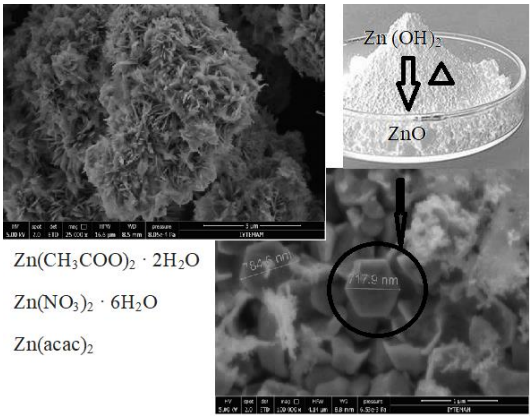


Figure 2.3 Graphical abstract of this study

CHAPTER THREE
MATERIALS AND METHODS

3.1 Materials

The chemicals that were used in the experiments: Zinc acetate dihydrate, $Zn(CH_3COO)_2 \cdot 2H_2O$ (Cat. No: Z0625); Sodium hydroxide, NaOH (Cat. No: 1064625000); Zinc nitrate hexahydrate, $Zn(NO_3)_2 \cdot 6H_2O$ (Cat. No: 10196-18-6); Zinc acetylacetonate, Bis(2,4-pentanedionato)zinc, $Zn(C_5H_7O_2)_2 \cdot xH_2O$ or $Zn(acac)_2$(Cat. No: 108503-47-5); Urea, NH_2CONH_2 (Cat. No: 208884); Methanol, CH_3OH (Cat. No: 534013); Ethanol, (Cat. No: 32221); Propanol, C_3H_8O (Cat. No: 82092, Fluka); Butanol, $C_4H_{10}O$ (Cat. No: 19430, Fluka). All the chemicals were purchased commercially from Sigma-Aldrich or Fluka.

ZnO Modification Materials: ZnO powder was provided by Molumer Chemical Industry/Izmir-Turkey as a commercial product. (3-Aminopropyl) triethoxysilane (APTES) (Cat No: 440140), Cetyltrimethylammonium bromide (CTAB) (Cat. No: 855820) and Sodium dodecyl sulfate (SDS) (Cat. No: 862010) were purchased from Aldrich Chemical Corporation and used without further purification.

3.2 Preparation of the Zinc Oxide Nanoparticles

Zinc acetate dihydrate and sodium hydroxide were used in zinc oxide synthesis in which temperature and pH change was taken into consideration. Heidolph model magnetic stirrer, pH meter, NÜVE model centrifuge and NÜVE model oven were used in the study.

The chemical reaction between zinc acetate and sodium hydroxide as in Eq. (3.1) and (3.2) was carried out in the Physical Chemistry Laboratories of Dokuz Eylul University.

$$Zn(CH_3COO)_2 + 2NaOH \rightarrow Zn(OH)_2 + 2CH_3COONa \quad (3.1)$$

The resulting precipitate of $Zn(OH)_2$ was washed with water several times, and then underwent thermal treatment in the autoclave.

$$Zn(OH)_2 \rightarrow ZnO + H_2O \quad (3.2)$$

Zinc nitrate hexahydrate and urea were used to measure the concentration effect in zinc oxide synthesis. ROCKER 300 model vacuum pumps, NÜVE model oven and ash furnace were used.

Zinc acetyl acetonate as zinc oxide precursor and methanol, ethanol, propanol, butanol as solvents and sodium hydroxide were used to measure the effects of solvent carbon number.

3.2.1 Effect of pH

0.02 M zinc acetate dihydrate and 2.0 M sodium hydroxide are prepared by dissolving in 50 ml of distilled water. Sodium hydroxide is added dropwise to the zinc acetate dihydrate mixing on the magnetic stirrer. The final pH was set to 9 and 12. At the end of the reaction, the resulting white precipitate was separated by centrifugation at 7000 rpm for 5 minutes. The impurities were removed by first washing with water and then with ethanol. The precipitates were allowed to dry overnight at 60 °C.

3.2.2 Effect of Temperature

0.02 M zinc acetate dihydrate and 2.0 M sodium hydroxide are prepared by dissolving in 50 ml of distilled water. Sodium hydroxide is added dropwise to the zinc acetate dihydrate mixing on the magnetic stirrer. The final pH is set to 12. After the reaction was complete, the solution was separated into two tubes. The precipitates are separated by centrifugation at 7000 rpm for 5 minutes. The impurities were removed by first washing with water and then with ethanol. One of the tubes was dried at 80 °C, the other at 60 °C overnight.

3.2.3 Effect of Concentration

Zinc nitrate in different concentrations (0.1-0.3-1.0 M) was dissolved in 50 mL of distilled water when urea in different concentrations (0.2-0.6-2 M) was dissolved in 50 mL of purified water. Zinc nitrate and urea solution were mixed together in the flask. The temperature was fixed at 95 °C with water bath. Closed flask was stirred at 95 °C under a vapor pressure for 2.5 hours to form precipitates. The solution was filtered under vacuum and then left to dry at 25 °C for 48 hours. After the settling process, calcination was carried out at 500 °C for 10 minutes in the ash furnace.

3.2.4 Effect of Solvent Carbon Number

2.13 g of zinc acetylacetonate (8.1 mmol) is dissolved by heating and stirring with 100 mL of different alcohols (Methanol, Ethanol, Propanol, Butanol). 0.88 g of sodium hydroxide was dissolved in 50 mL of ethanol and added to the flask. It was stirred at 80 °C for 6 hours. After 6 hours, it was allowed to cooling. The resulting precipitates were separated by centrifugation at 4500 rpm for 7 minutes. The precipitates are washed with ethanol to remove impurities. The precipitate was allowed to dry at 25 °C for 24 hours.

Table 3.1 Effects, chemical reagents, conditions and sample codes used in the experiments

Type	Used chemicals reagents and their Formulas	Different conditions	Sample Codes
Temperature and pH Effect	Zinc acetate dihidrate, $Zn(CH_3COO)_2.2H_2O$ Sodium hydroxide, NaOH	pH=9, 60°C pH=12, 60°C pH=12, 80°C	Synthesis 1a Synthesis 1b Synthesis 1c
Concentration Effect	Zinc nitrate heptahydrate, $Zn(NO_3)_2.7H_2O$ Urea, $CO(NH_2)_2$	0.1 M 0.3 M 1 M	Synthesis 2c Synthesis 2b Synthesis 2c
Solvent Carbon Number Effect	Zinc acetylacetonate, $Zn(C_5H_7O_2)_2$ Methanol, CH_3OH Ethanol, C_2H_6O Propanol, C_3H_8O Butanol, $C_4H_{10}O$	 C_1 C_2 C_3 C_4	 Synthesis 3a Synthesis 3b Synthesis 3c Synthesis 3d

3.3 Characterization of ZnO Nanoparticles

The characterization of synthesized zinc oxide samples was done by FTIR, TG/ DTG, Nano Particle Size Distribution, SEM and XRD analysis methods.

3.3.1 Fourier Transform Infrared (FTIR) Spectra of the Samples

For FTIR analysis, a Perkin-Elmer Spectrum BX-II Model FTIR spectrophotometer was used. 0.001 g of zinc oxide pellets prepared with 0.1 g of potassium bromide (KBr) were analyzed by FTIR spectroscopy at a range of 4000-400 cm^{-1} and at a resolution of 2 cm^{-1}.

3.3.2 X-Ray Diffraction (XRD) Analysis

The XRD patterns of the specimens were taken in the Cu K_α radiation (λ = 1.5415 Å), at a scanning speed of 4°/ min and in the range of 2θ = 20-80 ° with the Rigaku-Rint 2200/PC (Ultima 3) model XRD instrument in Metallurgical and Materials Engineering Department of Engineering Faculty of Dokuz Eylul University.

3.3.3 Scanning Electron Microscopy (SEM) Analysis

SEM images were taken at various magnifications at 5 kV on JEOL JSM 60 model SEM at IYTE MAM Research Center and Katip Çelebi University.

3.3.4 Thermogravimetric (TG/DTG) Analysis

TGA analyzes of ZnO samples were performed with a Perkin-Elmer Diamond TG /DTG analyzer to investigate the thermal stabilities of the samples. Analyzes were performed in platinum vessels under nitrogen gas atmosphere at a temperature range of 30-1000 °C and a heating rate of 10 °C/min.

3.3.5 Nanoparticle Size Distribution Analysis

Malvern brand Zeta Sizer Nano S device was used in Chemistry Department of Science Faculty of Dokuz Eylul University.

3.4 Modification of ZnO Nanoparticles

ZnO Modification Materials: ZnO powder was provided by Molumer Chemical Industry/Izmir-Turkey. APTES (A), CTAB (B) and SDS (C) were used without further purification. Chemical formulas of the compounds were given in Figure 3.1.

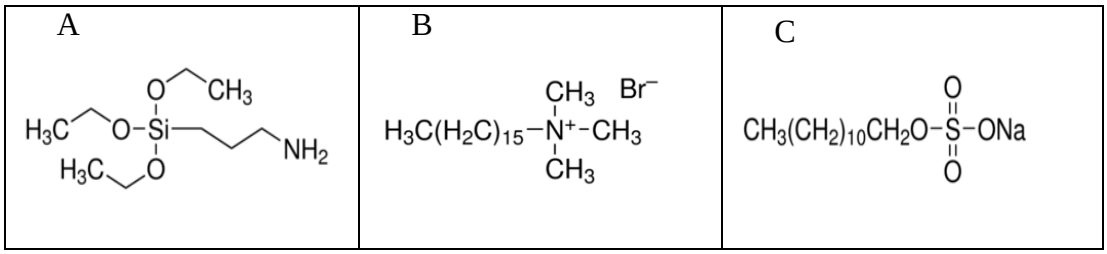


Figure 3.1 Chemical formulas of APTES (A), CTAB (B) and SDS (C)

3.4.1 Surface Modification with (3-Aminopropyl)triethoxysilane (APTES)

The grafted APTES in acidic condition (or basic condition) was prepared following this process: 30 g of zinc oxide was dispersed into distilled water (600 mL, pH=6.0-6.5), the initial pH was adjusted to 6.5 with 2 M HNO_3 solution. The suspension was stirred for a further 1 h and 20 mL of APTES was added. The reaction mixture was stirred for a further 24 h then excess APTES was removed by filtration and washing with alcohol and acetone. The powder was dried at 60 °C under vacuum.

3.4.2 Surface Modification with Cetyl Trimethyl Ammonium Bromide(CTAB)

30 g of ZnO powder dissolved in 500 mL of distilled water. The solution was stirred until homogeneous was obtained and then 3 g of CTAB was (dissolved in acetone) added to this ZnO solution. The mixture was stirred at room temperature for 24 hours. Furthermore, the mixture was centrifuged and the precipitate was washed with distilled water, ethanol and acetone for the removal of excess amounts of CTAB and dried in an oven for 1 day at 60°C.

CTAB is a surfactant. CTAB in the solution will be ionized into $CTA^+$and Br^-. Hydrophilic head is often referred to as the ammonium group and the hydrophobic as the tail is composed of a hydrocarbon chain cetyl group as in Figure 3. 2.

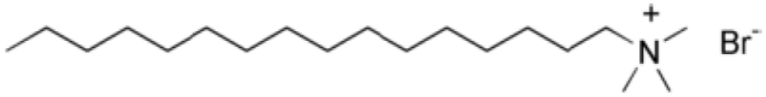


Figure 3.2 Molecules of CTAB surfactant

ZnO is reacted with CTAB where Zn ions in the form of $[Zn(OH)_4]^{2-}$ is negatively charged , while the positively charged CTA^+ with tetrahedral heads and hydrophobic tails. Through the ion pair formed hydrothermal process, CTA^+-$[Zn(OH)_4]^{2-}$ is formed by electrostatic interactions initially. CTAB molecules could accelerate ionization $[Zn(OH)_4]^2$. Ion pair formed a combination and ZnO CTAB, CTAB collected between ZnO crystallites during the hydrothermal crystallization and washed with distilled water to form ZnO powder.

3.4.3 Surface Modification with sodium dodecylsulphate(SDS)

30 g of ZnO powder was suspended in 500 mL of distilled water. 3 g of SDS was added to this suspension and stirred at room temperature for 24 hours. The colloidal solution was formed and allowed to rest to precipitate. Upper part of the colloidal suspension was taken with the aid of a pipette and then the precipitate deposited on the bottom part of the beaker is separated and washed with ethanol and acetone several times. Rest of the suspension was stored for further experiments. The white precipate was then dried at 60°C for 4 hours in an etuve.

3.5 Application of ZnO Nanoparticles

We first integrated the ZnO and then the modified ZnO specimens in different proportions (1%, 3% and 5%) into the acrylic based, mere, varnish polymer. Because of the insufficient of magnetic stirrer, each sample was first mixed with 2 mL solvent in an ultrasonic bath. After mixing with the solvent, 10 mL of base varnish was added into it and then mixed again in an ultrasonic bath to make it homogeneous.

The final blend samples were applied in equal thickness to the glass lamellas and allowed to air dry for 1 day. Dry films were analyzed in a UV-visible spectrophotometer to determine band gap energy values of the samples.

3.6 Determination the Optical Properties of the Samples

Optical properties of the synthesized ZnO nanoparticles coated on a glass substrate as films were characterized based on UV transmission/reflection spectra.

The sample was sonicated for uniform dispersion and the aqueous component was subsequently coated onto glass substrate at room temperature for optical band gap (Eg) using UV–Vis spectrophotometer (Thermoscientific Evolution 600 UV-Vis Labsphere) over a wavelength range of 200-400 nm.

The optical band gap of a direct-semiconductor can be obtained by analyzing the absorption edge and applying the Tauc model (Tauc, Grigorovici, & Vancu, 1966; Tauc, 1968; Dolgonos, Mason, & Poeppelmeier, 2016).

$$(\alpha h\nu) = A(h\nu - E_g)^{1/2} \tag{3.3}$$

where α is the absorption coefficient, hν is the photon energy, A is a constant and E_g is the optical band gap. The absorption coefficient (α) is directly related to the transmittance (T) and film thickness (d), which can be calculated using the following formula,

$$T = B \exp(-\alpha d) \tag{3.4}$$

where the constant B is approximately unity. The optical bandgap of the samples was determined by extrapolating the straight section for the plot of $(\alpha h\nu)^2$ versus the photo energy.

On the other hand**,** optical band gap energy values can also be calculated directly from the UV-Visible Transmittance/Reflectance Spectrum by using the general equation of (3.5) (Dharma, Pisal, & Shelton, 2009).

$$E = \frac{hC}{\lambda} \tag{3.5}$$

Where E is band gap energy in eV. h is Plank constant with a value of 6.626×10^{-34} Js. C is speed of light, 3.0×10^8 m/s and λ is cut off wavelength found from the UV-Visible spectrum of the material. In this calculation, $1eV=1.6 \times 10^{-19}$ Joules as conversion factor.

CHAPTER FOUR
RESULTS AND DISCUSSIONS

4.1 Results of Characterization

4.1.1 Results of FTIR

In order to estimate drying/calcination temperature of the prepared ZnO samples, FTIR spectrum of the samples were recorded and the area under the –OH stretching vibration band was evaluated. The FTIR spectra of the synthesized zinc oxide samples are shown in Figure 4.1, Figure 4.2 and Figure 4.3. The Zn-O characteristic vibration of the zinc oxide was observed at 453-506 cm^{-1}. OH stretching band was observed between 3389 and 3412 cm^{-1}. The area shrinkage of the -OH band has been investigated with drying of the resulting Zn $(OH)_2$ compound.

Infrared absorption band frequencies of zinc hydroxy compounds were reported The bands occurring in the 3600-3260 $cm\text{-}^{1}$ region are generally attributed to the fundamental OH stretching mode. The very broad band at 3260 cm^{-1} is due to $Zn(OH)_2$ (Srivastava, & Secco, 1967).

The characteristic frequencies of oxides of 52 metals have been studied in the region 700-240 cm^{-1} (McDevitt, & Baun, 1964).

In the evaluation of the FTIR spectra, absorbance maximum of the band(intensity) and the area under the band must be considered. Hydroxyl group vibrational frequencies of alcohol and water are given in Table 4.1.

Table 4.1 FTIR band assignments of O-H vibration (Socrates, 2001)

Functional Group	Type of Vibration	Characteristic Absorptions (cm^{-1})	Intensity
Alcohol			
O-H	(stretch, H-bonded)	3200-3600	strong, broad
O-H	(stretch, free)	3500-3700	strong, sharp
Water			
O-H	(symmetric stretch)	3700-3100	strong, broad
O-H	(asymmetric stretch)	3490	strong, broad
O-H	(bending)	1645	strong, broad

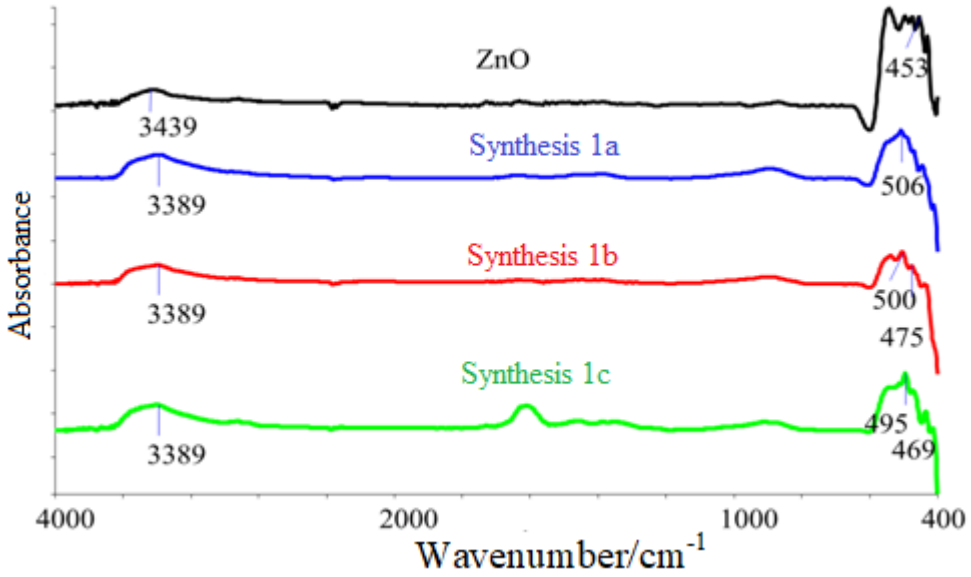


Figure 4.1 FTIR spectra of the samples, effects of pH and temperature

Experimental results of Synthesis 1a and 1b inform us that ZnO yield decreased with increasing the molarity of the precursor in the solution. Likewise, calcinations at 60°C gives better results than calcinations at 80°C. On the other hand, From FTIR spectra of the samples for Synthesis 1a, 1b and 1c, the yield of ZnO product was increased when the concentration of Zn^{2+} in solution was decreased.

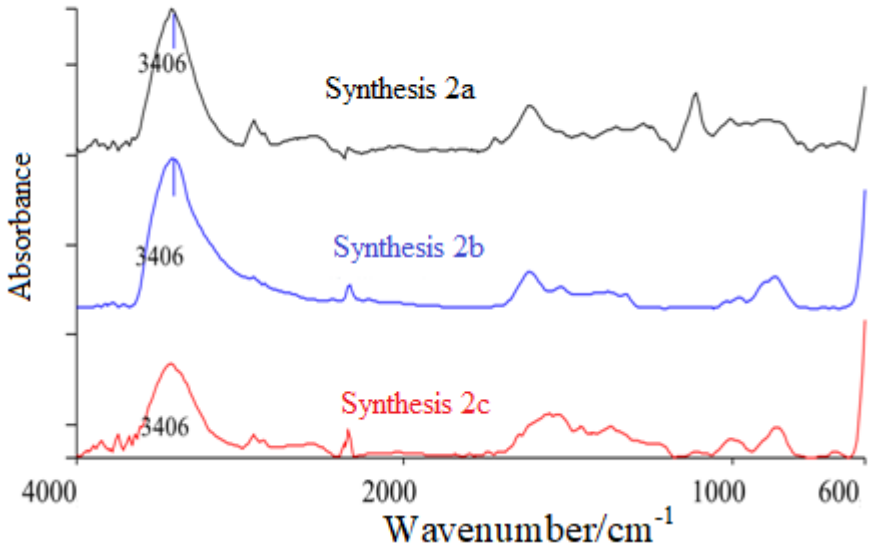


Figure 4.2 FTIR spectra of the samples, effects of precursor concentration

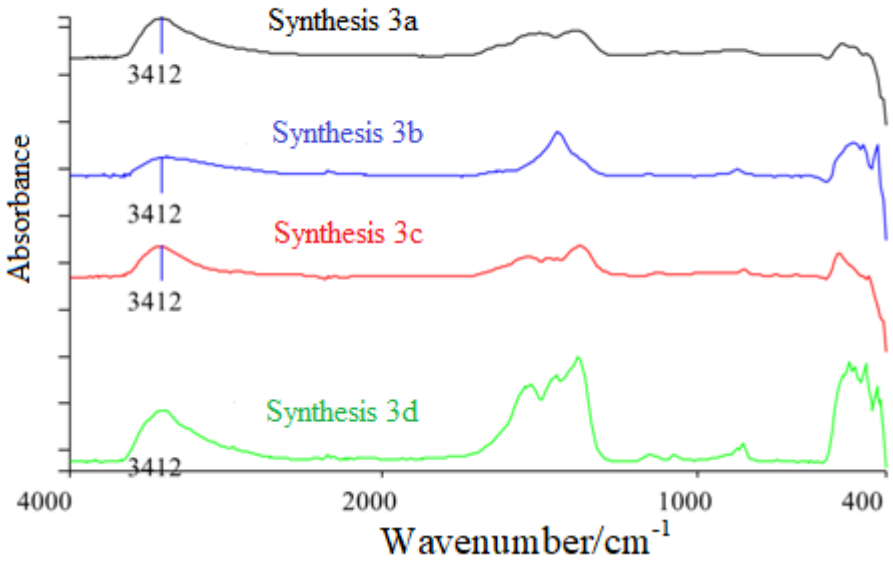


Figure 4.3 FTIR spectra of the samples effects of solvent carbon number

In the FTIR spectra, as can be seen from Figure 4.2 and 4.3, the bands related with the presence of –OH groups on the surface of the $Zn(OH)_2$ which turns to ZnO after calcination were observed at about 3406 and 3412 cm^{-1}. Due to the solvent effect (C_1, C_2, C_3 and C_4, alcohols), the band shifted by approximately 6 cm^{-1}. Similar shifts were also observed at 1630 cm^{-1} (-OH bending vibration band) and the bands below 500 cm^{-1} which are generally due to the Zn-O (M-O band).

4.1.2 XRD Analysis Results

The reference XRD data (JCPDS 36-1451) of ZnO was presented in Figure 4.4.

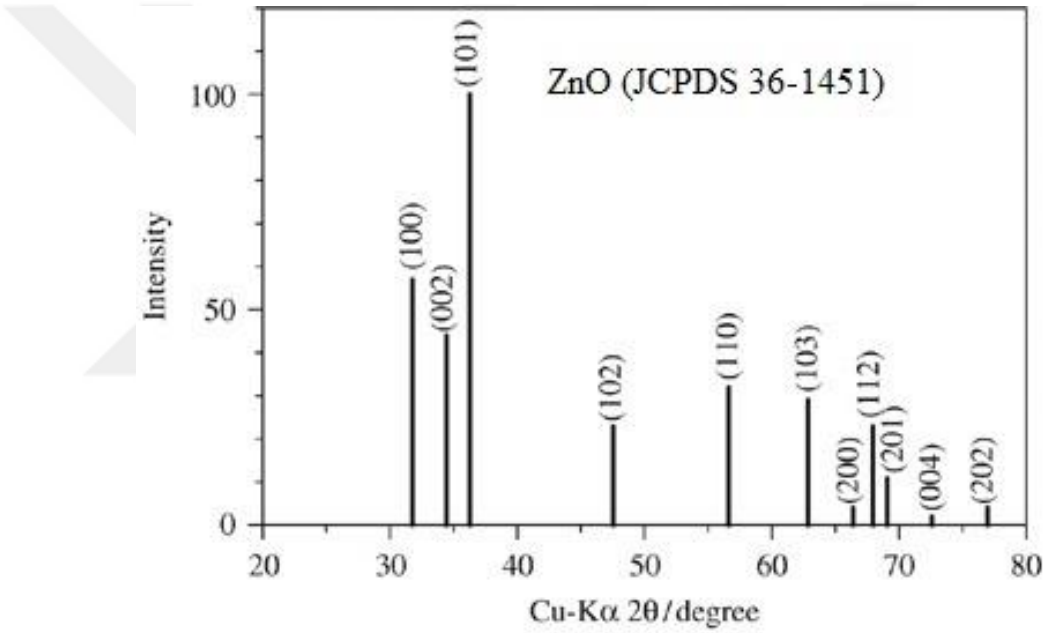


Figure 4.4 XRD reference data of ZnO (Bel Hadj Tahar, et al., 2008; Li, et al., 2013)

ZnO, Sigma-Aldrich (Cat. No. 205532) was purchased as commercial product and XRD patterns are given in Figure 4.5. When the XRD patterns of ZnO were examined, the following data was obtained. These data are given in Table 4.2.

Table 4.2 The XRD data of ZnO

2θ/°	**Intensity**		**d/Å**	**(hkl)**
31.86	4954	63	2.8066	(100)
34.5	3323	42	2.5976	(002)
36.34	**7850**	**100**	**2.4702**	**(101)**
47.16	1697	21.6	1.9066	(102)
56.7	2552	32.5	1.6222	(110)
62.94	2186	27.8	1.4755	(103)
66.44	399	5.08	1.4060	(200)
68.04	1880	23.9	1.3768	(112)
69.16	940	11.9	1.3572	(201)
72.66	173	2.20	1.3002	-
77.02	311	3.96	1.2371	(202)

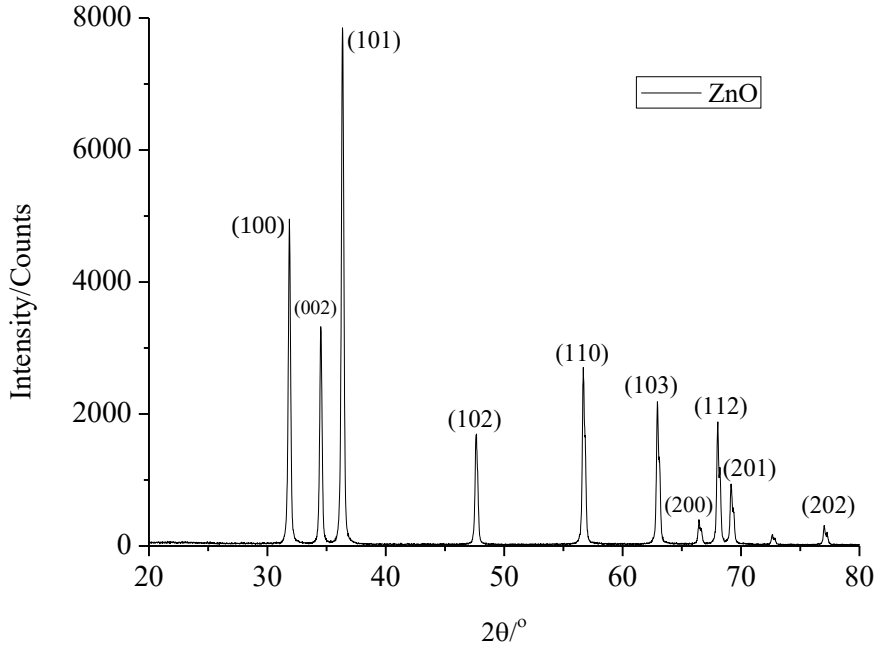


Figure 4.5 XRD patterns of ZnO

The XRD patterns of the synthesized zinc oxide samples and the standard ZnO from Molumer Company are shown in Figure 4.6, Figure 4.7, Figure 4.8 and Figure 4.9, respectively.

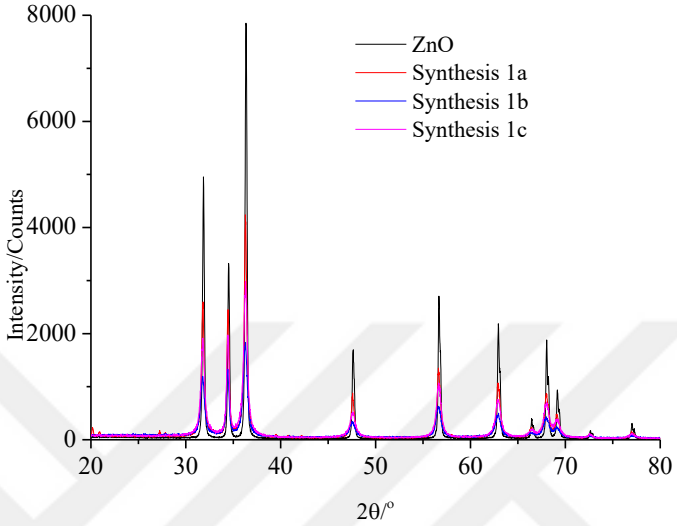


Figure 4.6 XRD patterns of the samples and pH, temperature effects

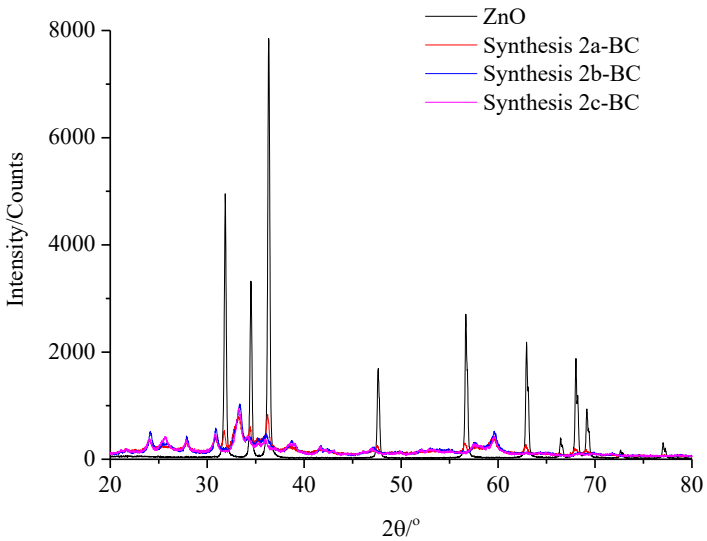


Figure 4.7 XRD patterns of the samples before calcination and concentration effects

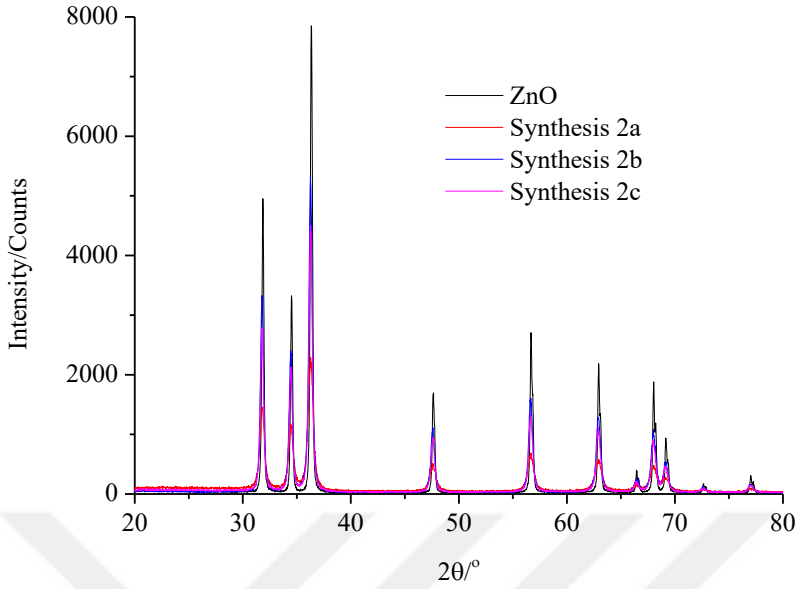


Figure 4.8 XRD patterns of the samples after calcination, effects of concentration

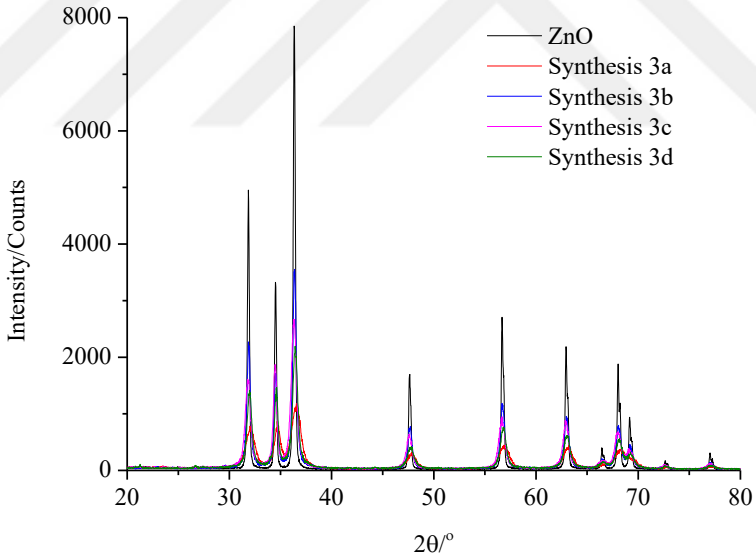


Figure 4.9 XRD patterns of the samples, effects of solvent carbon number

When the data of the synthesized ZnO samples were compared with the data of commercial ZnO in Figure 4.4 and Figure 4.5, it was determined that all of the samples prepared were ZnO. However, it has been observed that the intensity of the signals is different with the 2θ values of the formed surfaces being the same. The

peak of surface (101) at 2θ= 36.34° is seen in all samples. The peak intensities of the other surfaces vary.

Differences were observed in the peaks originating from $Zn(OH)_2$ before the calcination. However, due to water extraction after calcination, ZnO patterns were found to be harmonious.

4.1.3 Results of SEM Analysis

SEM Images of ZnO (M) (Molumer) and ZnO (Sigma-Aldrich, Cat. No: 205532) (SA) were given in Figure 4.10 and Figure 4.11, respectively. These SEM images were used as standards for the comparison of the prepared ZnO samples. From Figure 4.10 and 4.11, non-homogeneous or non-uniform hexagonal rod-shaped ZnO particles with various sizes were observed. The particle size for ZnO (SA) was smaller than ZnO (M) which has the particle size of 128 nm.

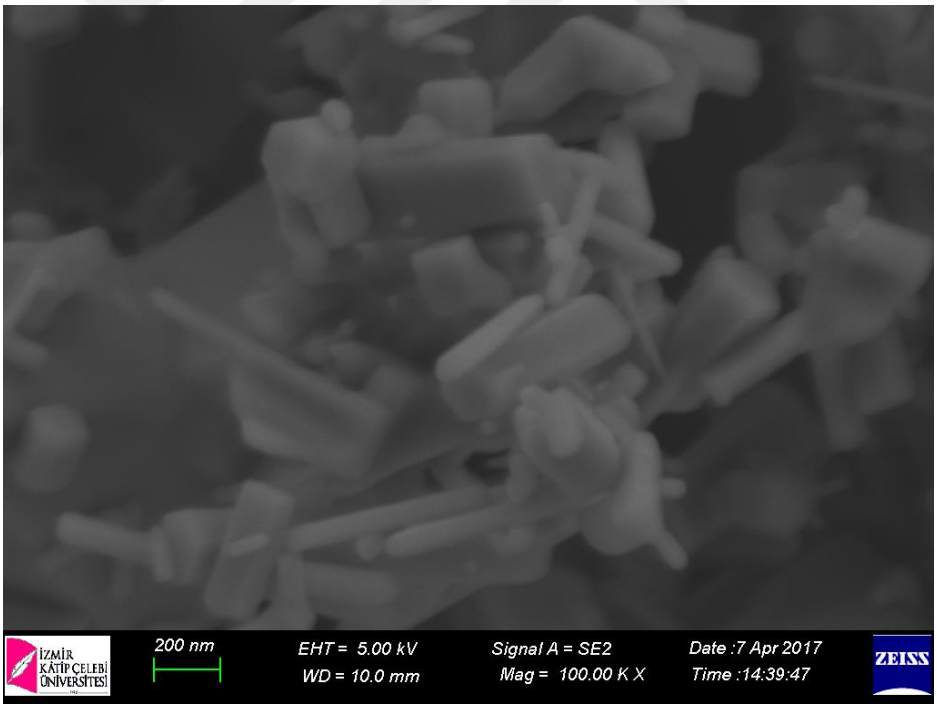


Figure 4.10 SEM Images of ZnO (Molumer) with 100 00 K× magnifications

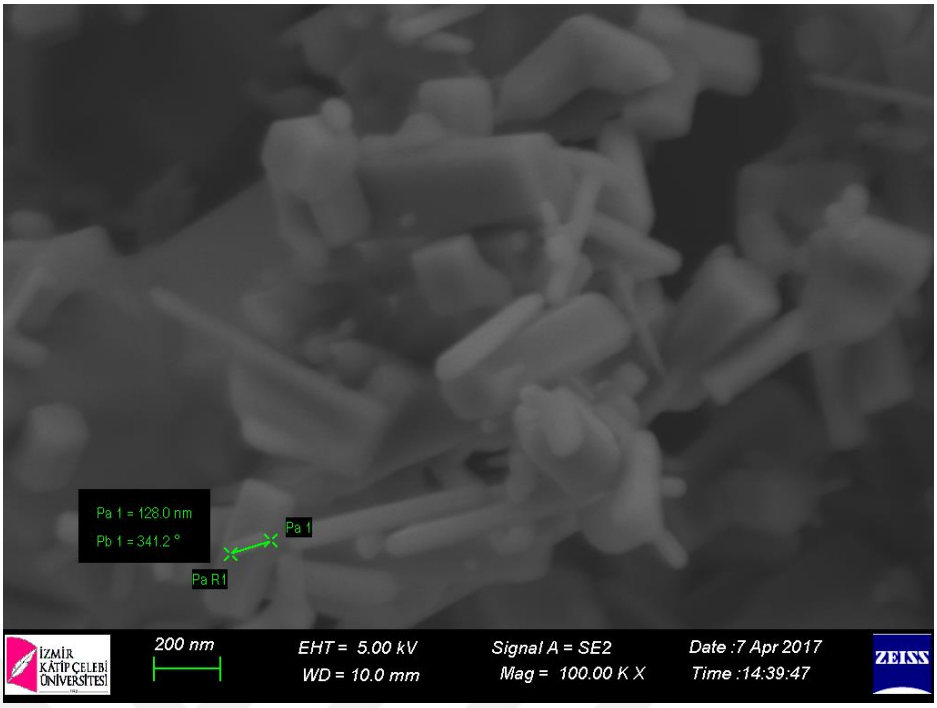


Figure 4. 10 continues

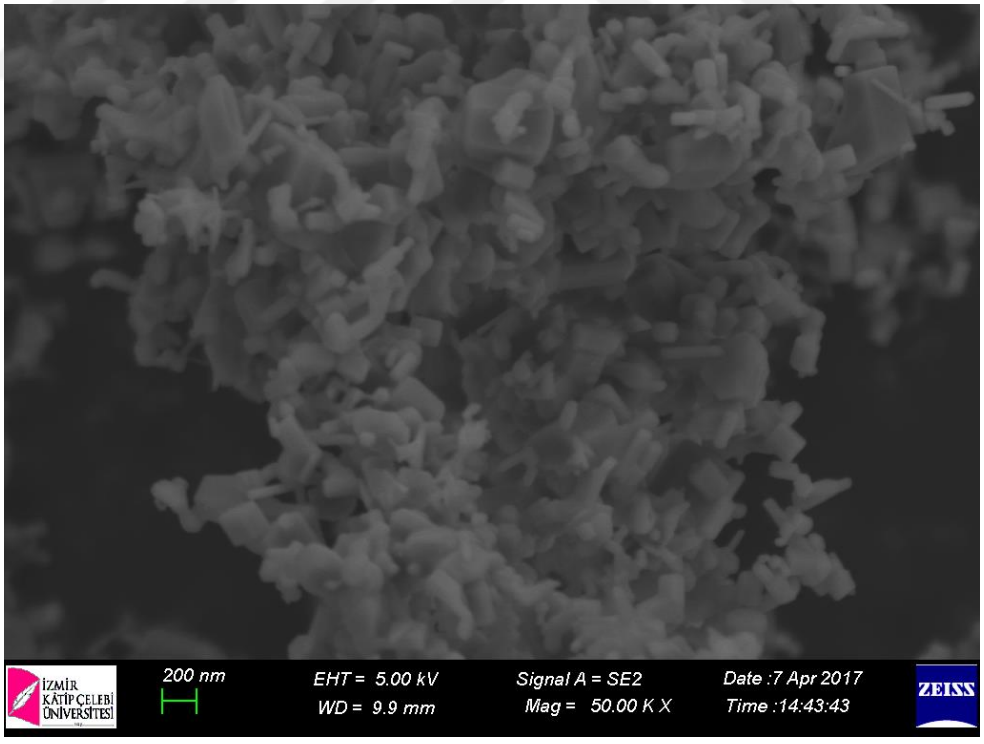


Figure 4.11 SEM Images of ZnO (Sigma-Aldrich) with 50 00K× and 100 00 K× magnifications

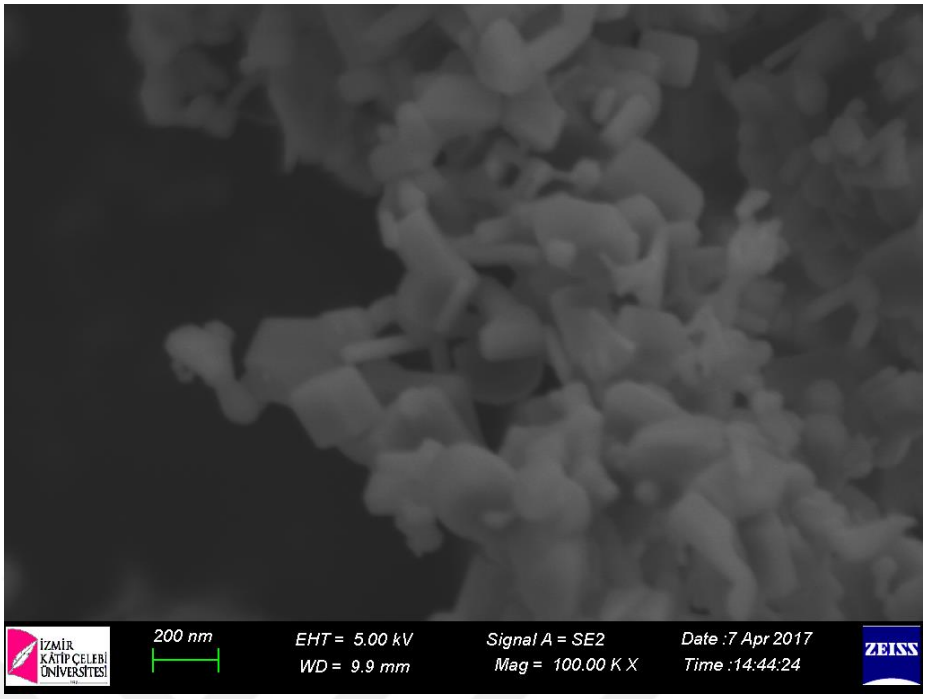


Figure 4.11 continues

SEM images of the synthesized zinc oxide samples were shown in Figure 4.12 (Synthesis 1a, 1b and 1c); Figure 4.13 (Synthesis 2a, 2b and 2c) and Figure 4.14 (3a, 3b, 3c). Morphological structure analysis of the surfaces was made by enlarging the composition of zinc oxide, 25000 and 50000 times by electron microscopy.

Synthesis 1a Synthesis 1b Synthesis 1c

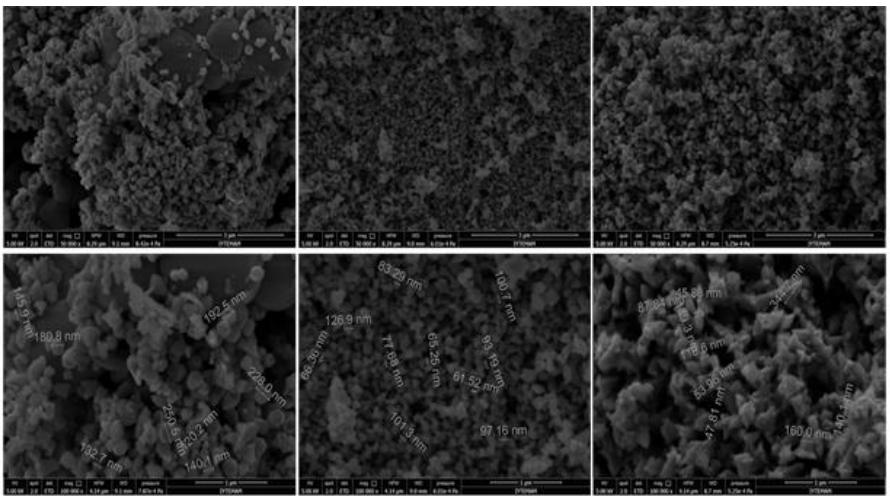


Figure 4.12 SEM images of the samples, effects of temperature and pH differences

In Figure 4.12, spongy formed and blunt triangular structures were observed at pH=9 and 60 °C for the ZnO nanoparticles of the sample, Synthesis 1a. On the other hand, at pH=12 and 60 °C conditioned sample, Synthesis 1b, the spongy bodies were removed from the center. Only triangular structures stay. At pH=12 and 80^{o}C in Synthesis 1c, the corners of triangular structures were sharpened. In Figure 4.13 SEM Images of the ZnO sample (Synthesis 1a) after calcination were shown.

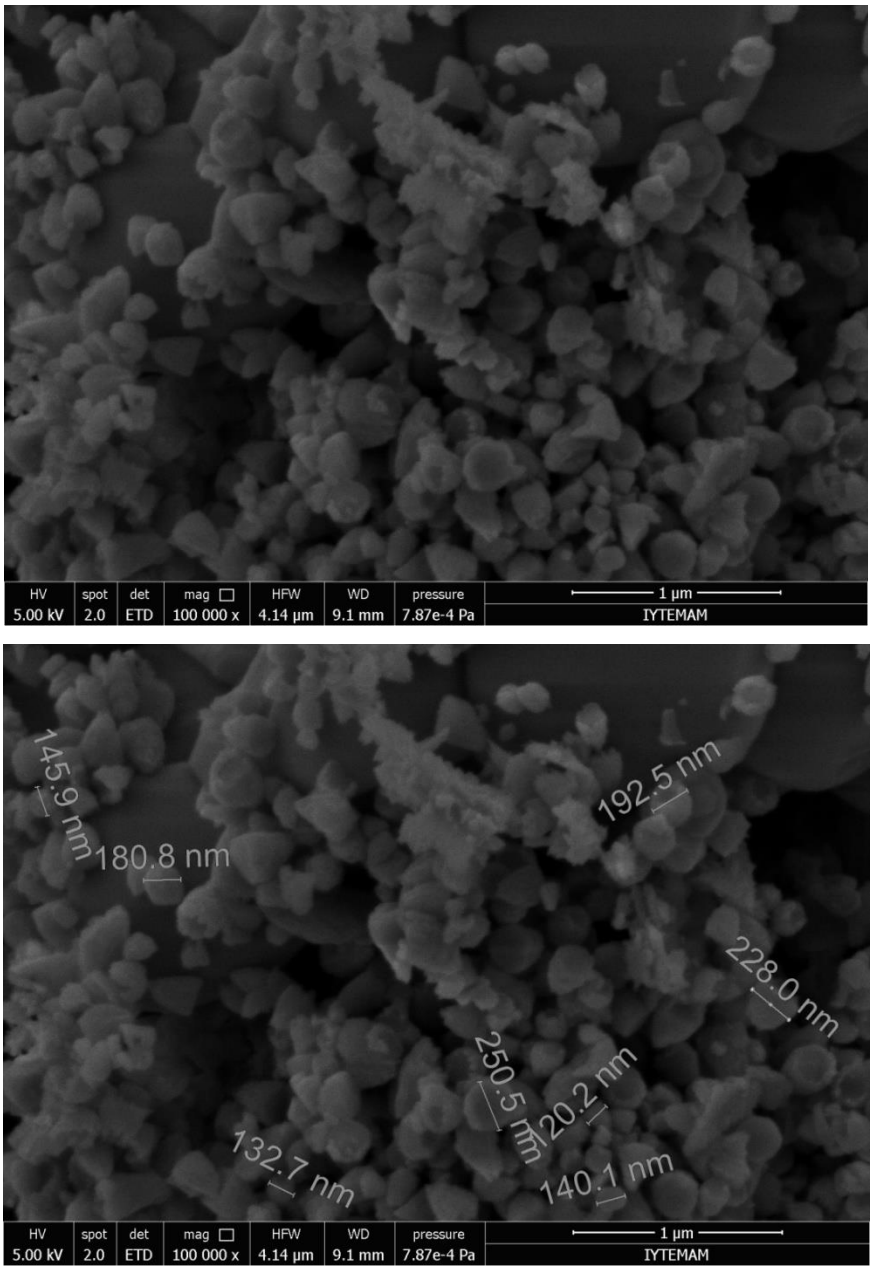


Figure 4.13 SEM Images of the ZnO sample (Synthesis 1a) after calcination

Synthesis 2a Synthesis 2b Synthesis 2c

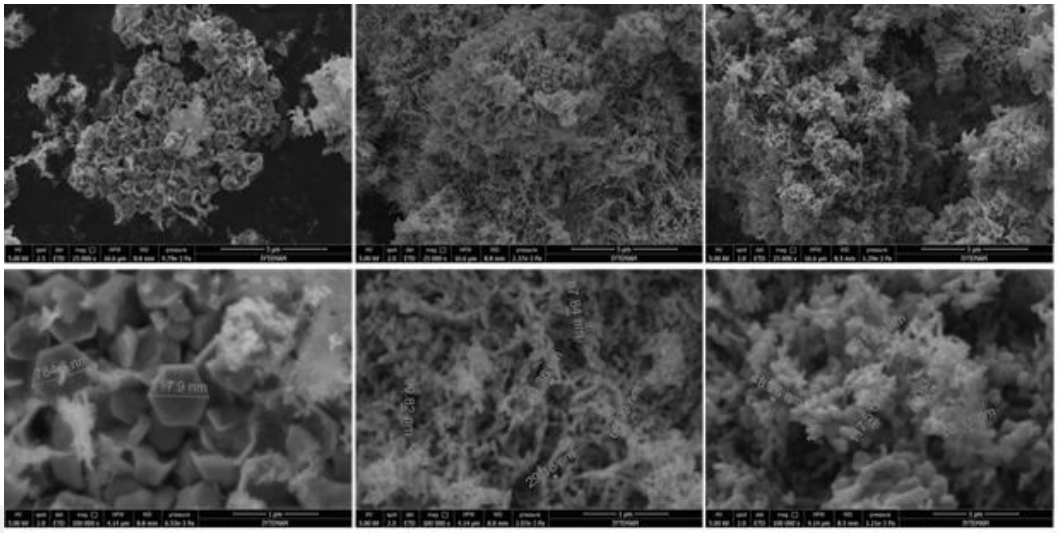


Figure 4.14 SEM images of the samples, concentration differences

In Figure 4.14, it was observed that the structures of the zinc oxide compound synthesized from 0.2 M urea with 0.1 M $Zn(NO)_3$ in Synthesis 2a were hexagonal. In the sturcture of zinc oxide complexes synthesized from 0.3 M $Zn(NO)_3$ and 0.6 M urea in 2b, the hexagonal shape was removed from the center, and thread like structures were observed. In the structure of ZnO compound synthesized with 1.0 M $Zn(NO)_3$ and 2.0 M urea in Synthesis 2c, the filamentous structures left the particles in place. SEM Images of the ZnO sample (Synthesis 2a) after calcination were presented in Figure 4.15. In these Figure, the different sized particles less than about 100 nm were observed. In Figure 4.16, SEM Images of the ZnO sample (Synthesis 2b) after calcination were presented. The particle shape and sizes can be seen clearly from the Figure.

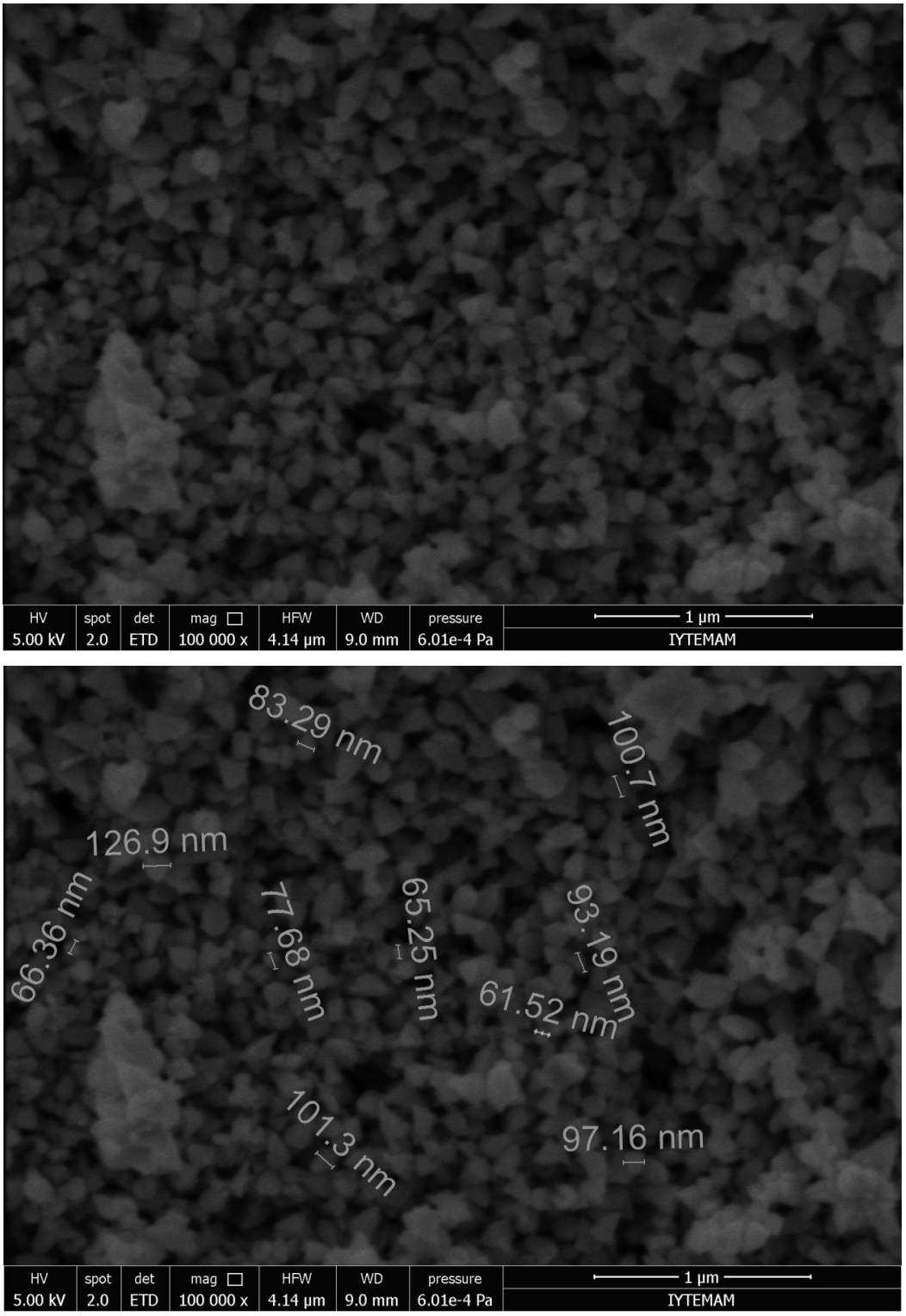
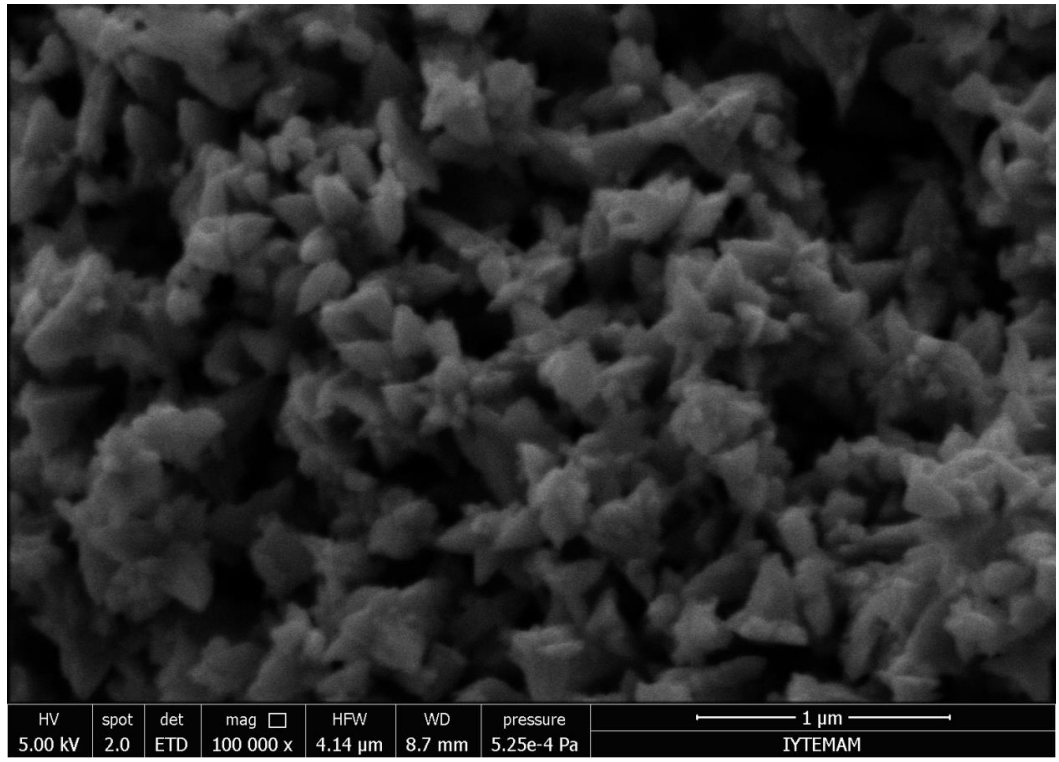


Figure 4.15 SEM Images of the ZnO sample (Synthesis 2a) after calcination



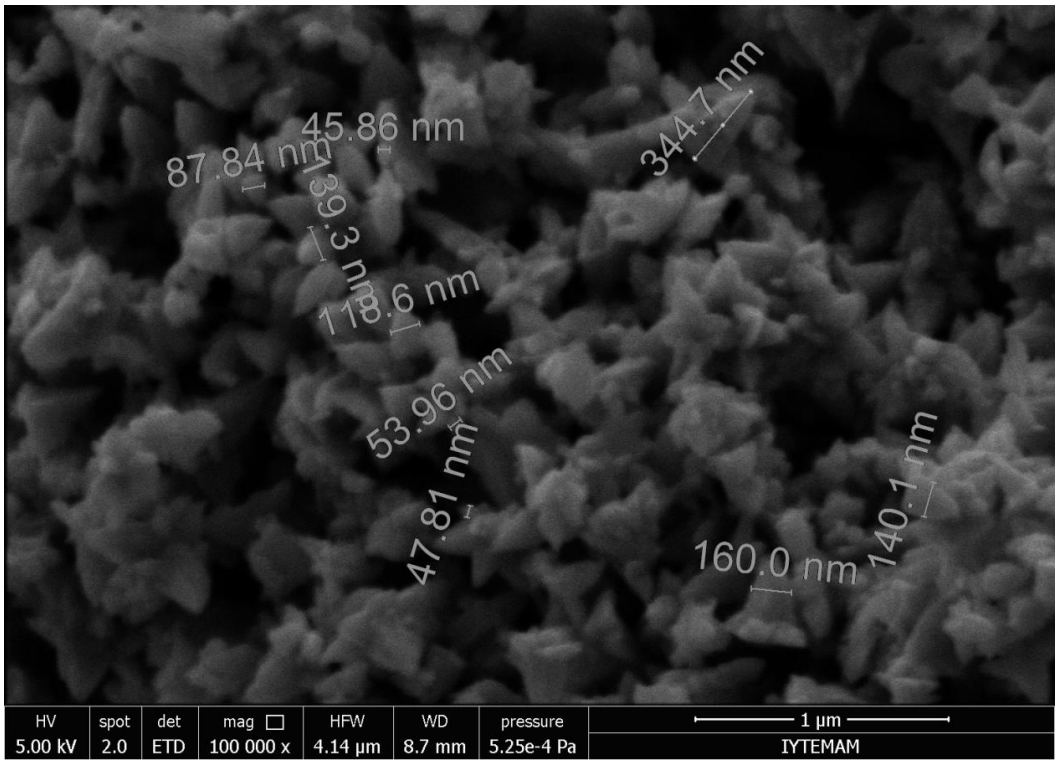
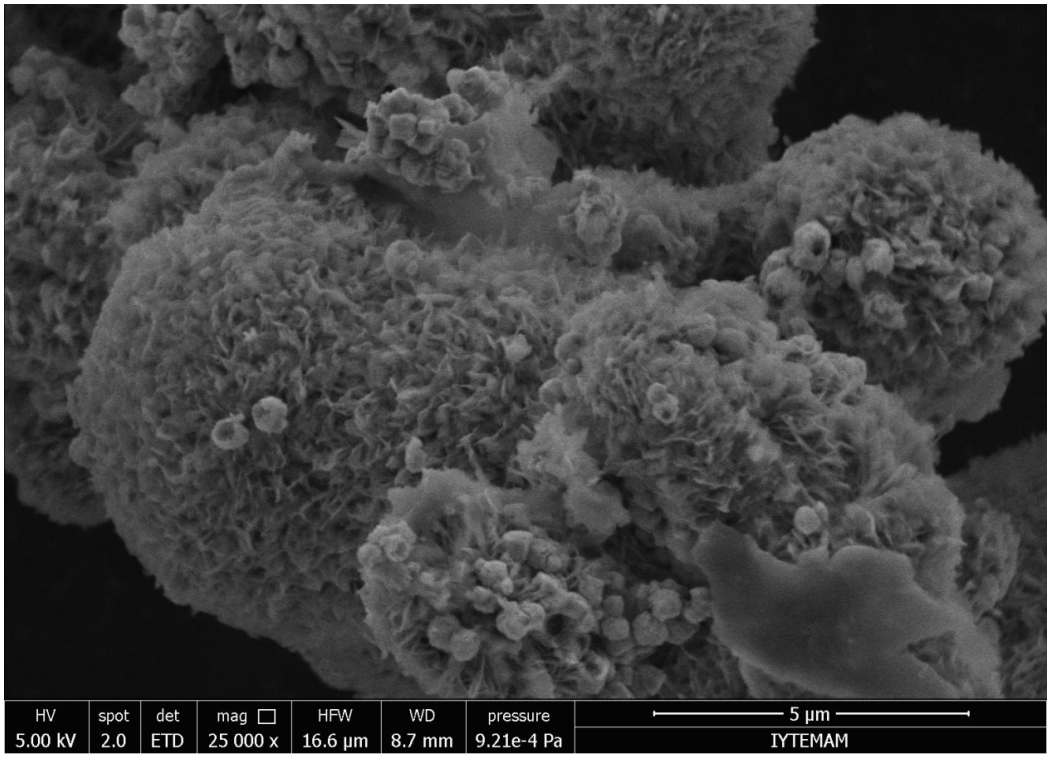


Figure 4.16 SEM Images of the ZnO sample (Synthesis 2b) after calcination



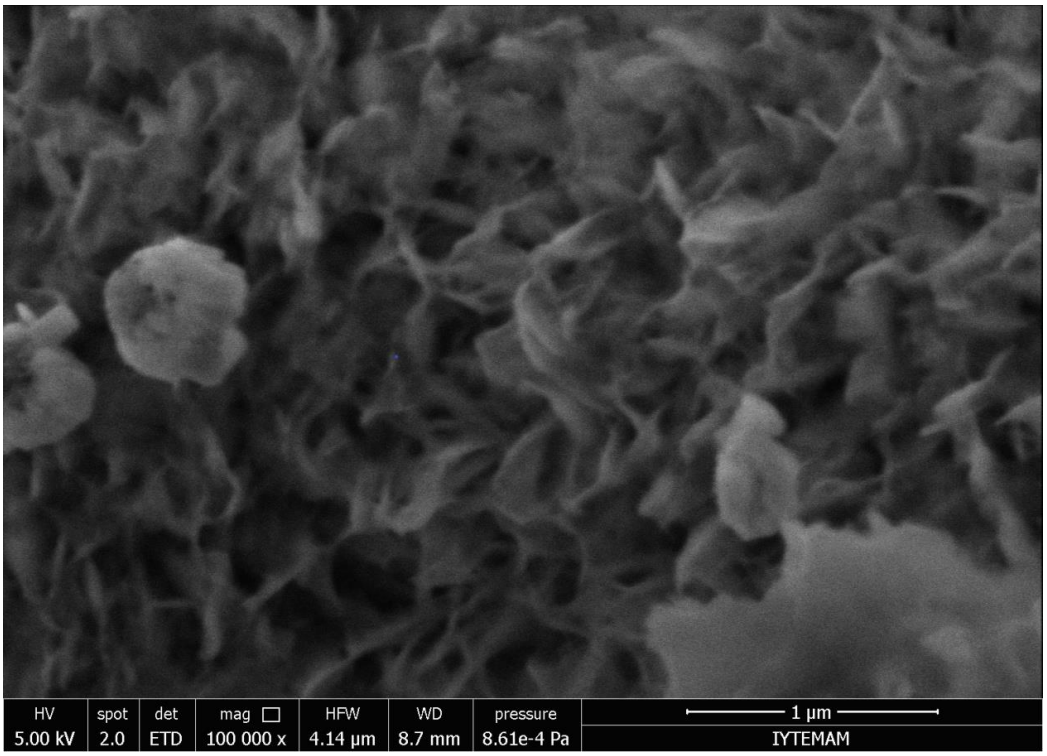
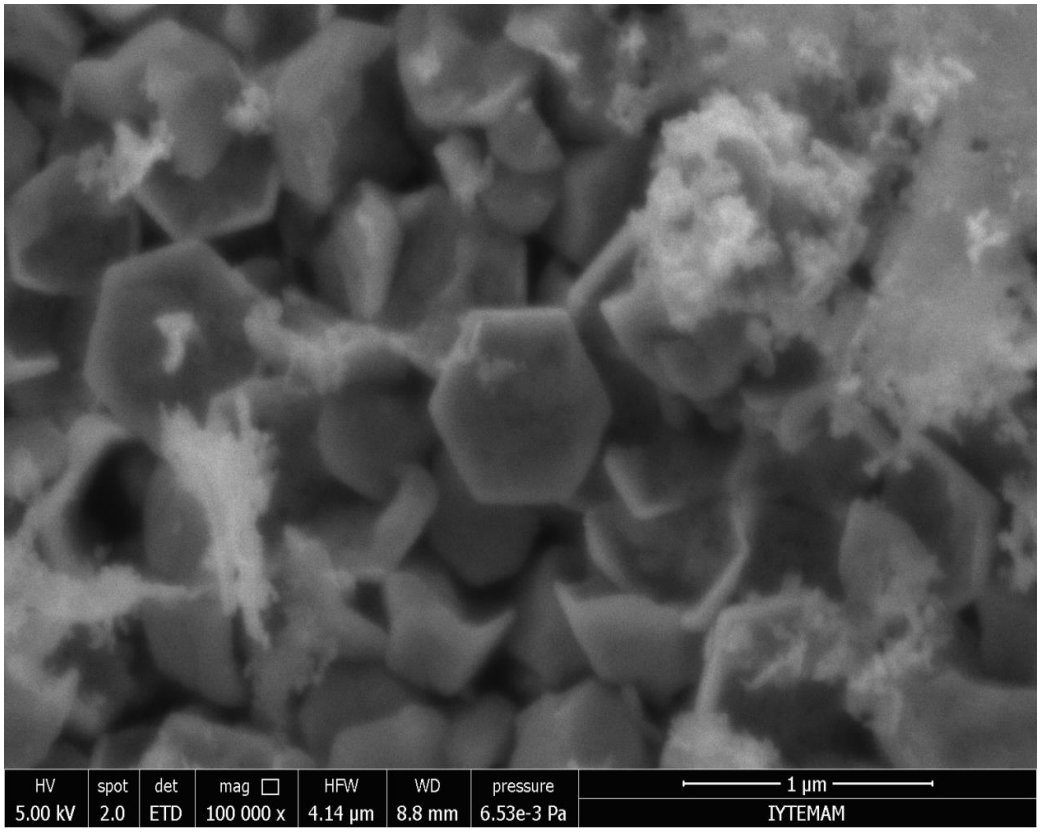


Figure 4.17 SEM Images of the ZnO sample (Synthesis 3a) before calcination



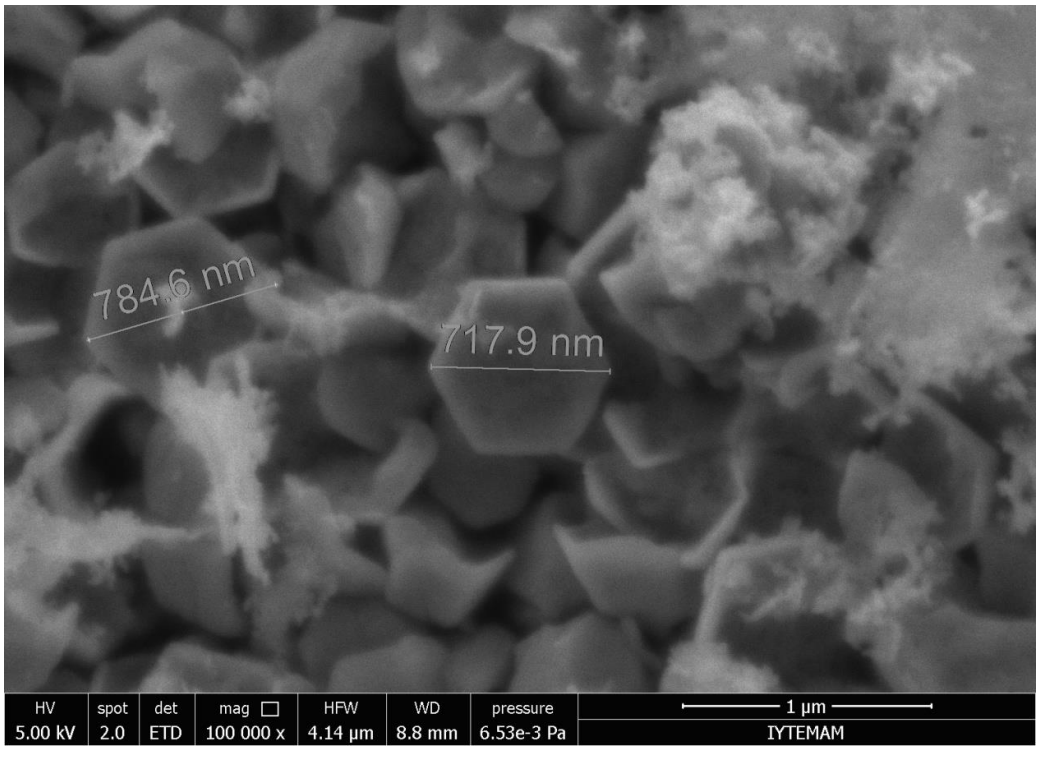


Figure 4.18 SEM Images of the ZnO sample (Synthesis 3a) after calcination

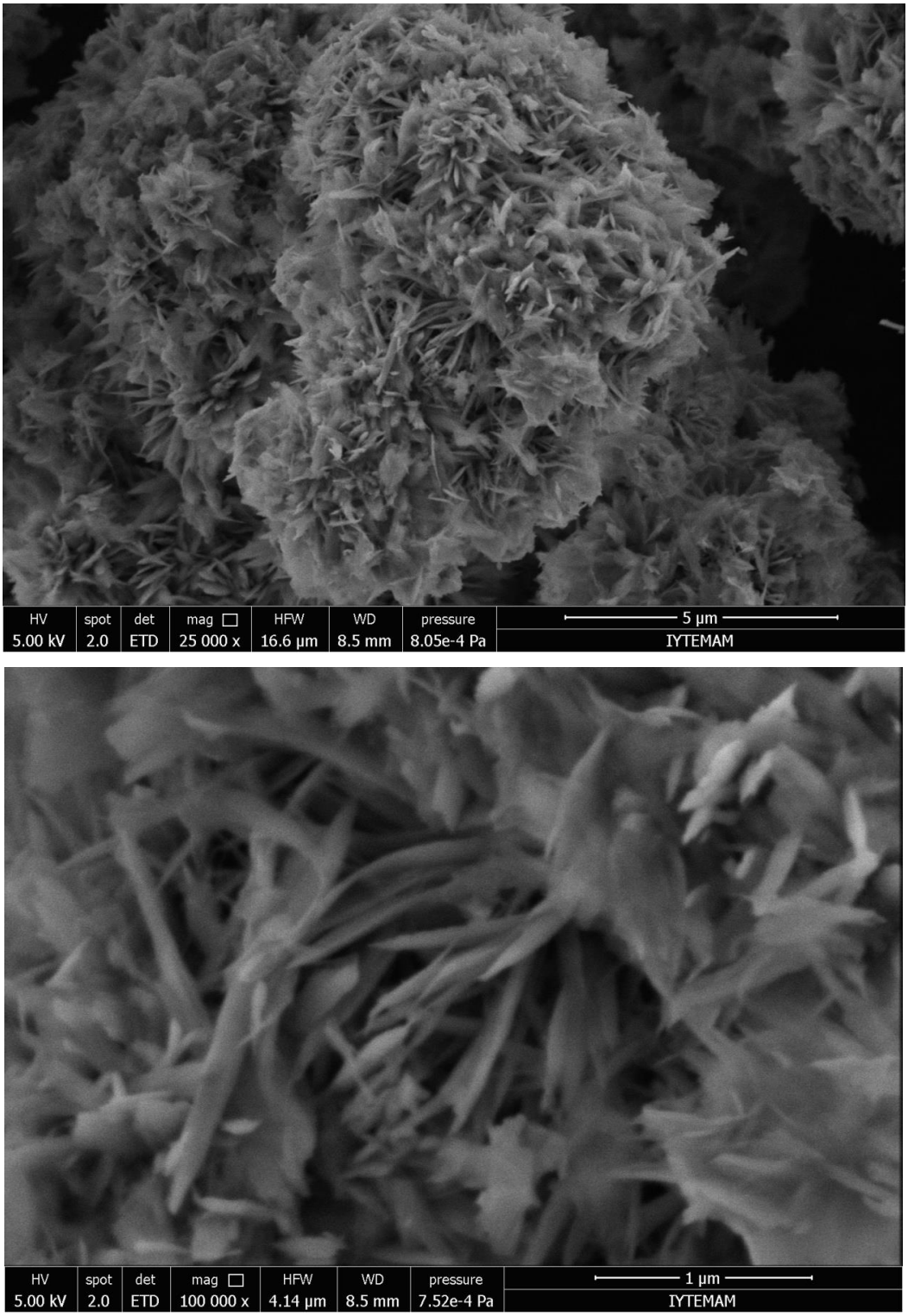


Figure 4.19 SEM Images of the ZnO sample (Synthesis 3b) before calcination

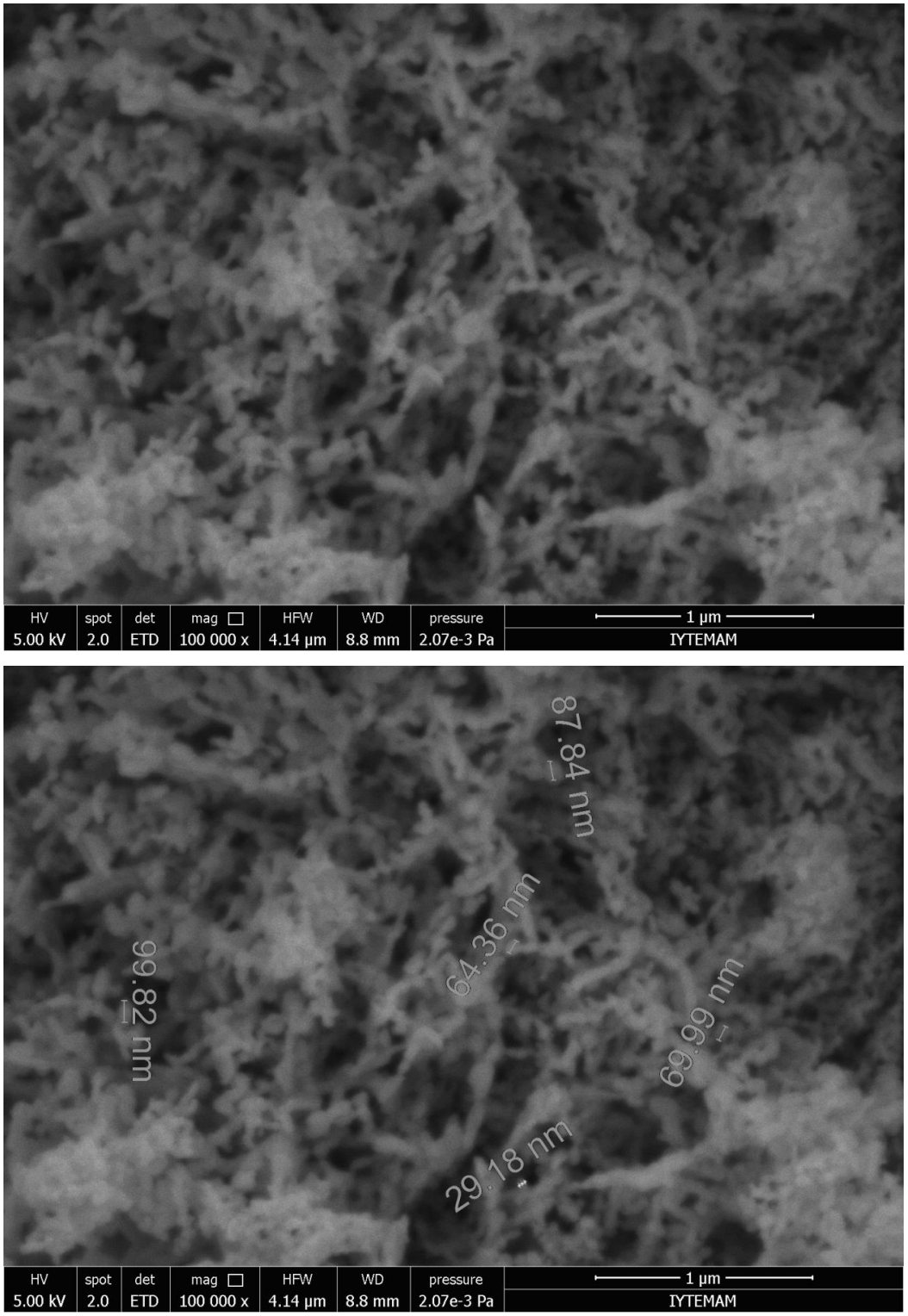


Figure 4.20 SEM Images of the ZnO sample (Synthesis 3b) after calcination

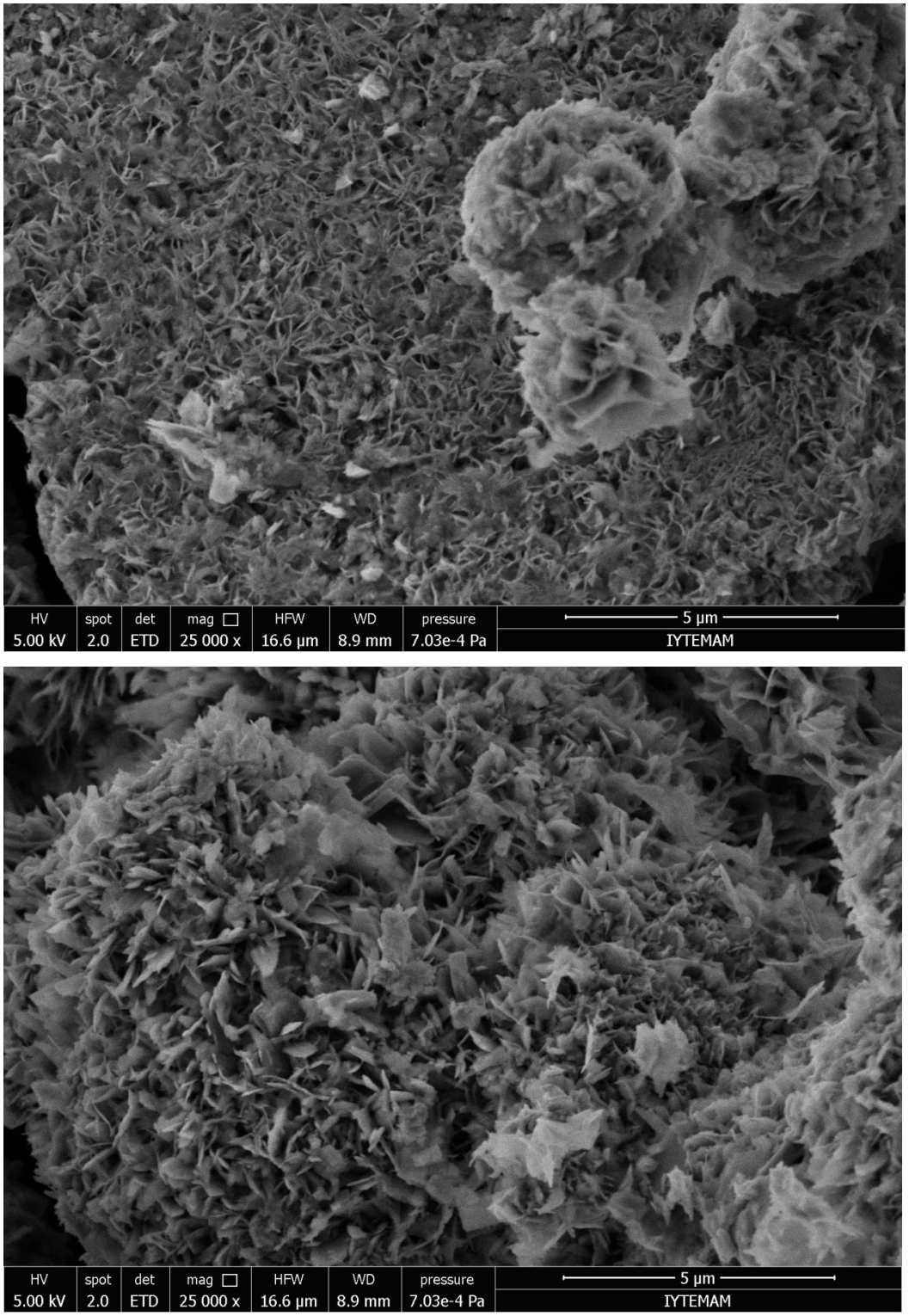


Figure 4.21 SEM Images of the ZnO sample (Synthesis 3c) before calcination

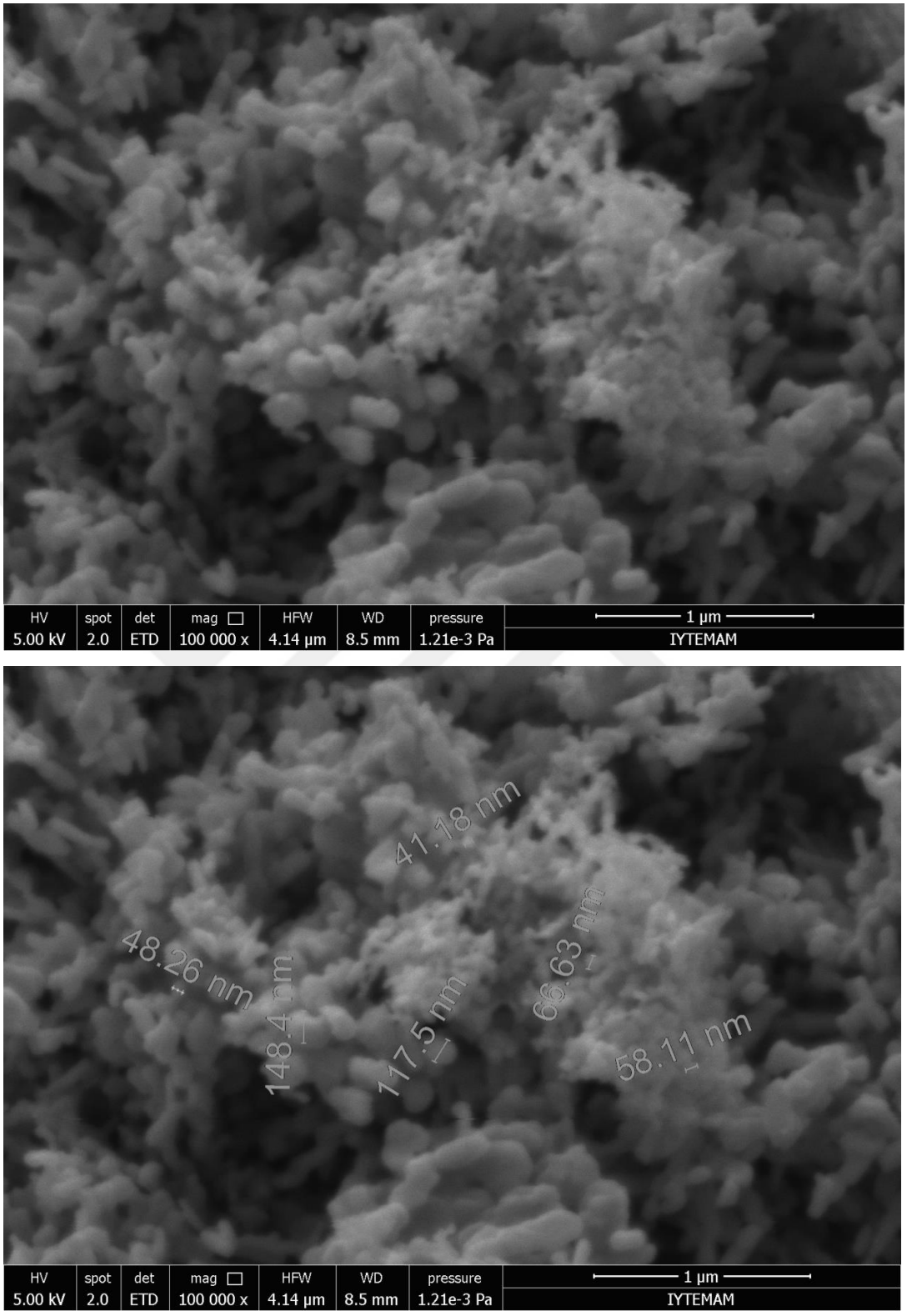


Figure 4.22 SEM Images of the ZnO sample (Synthesis 3c) after calcination

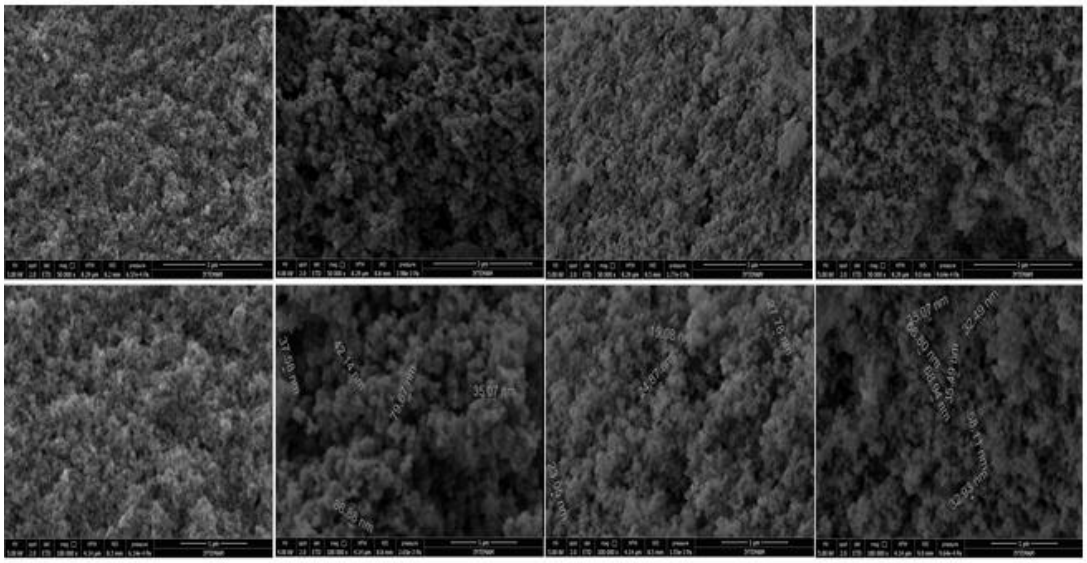


Figure 4.23 SEM images of the samples, effect of solvent carbon number differences

In Figure 4.23, in Synthesis 3, SEM images of all of the samples were given together to investigate the effect of solvent carbon number differences. For this purpose, Methanol, Ethanol, Propanol and Butanol were used as solvents in the synthesis as the number of carbon atoms of C_1, C_2, C_3 and C_4. In Figures 4.23m, e, p and b, one can see easily the effects of solvent carbon atom number. As the number of carbon atom increased from C_1, C_2, C_3 and to C_4, the particles become more pronounced and the particle size becomes smaller.

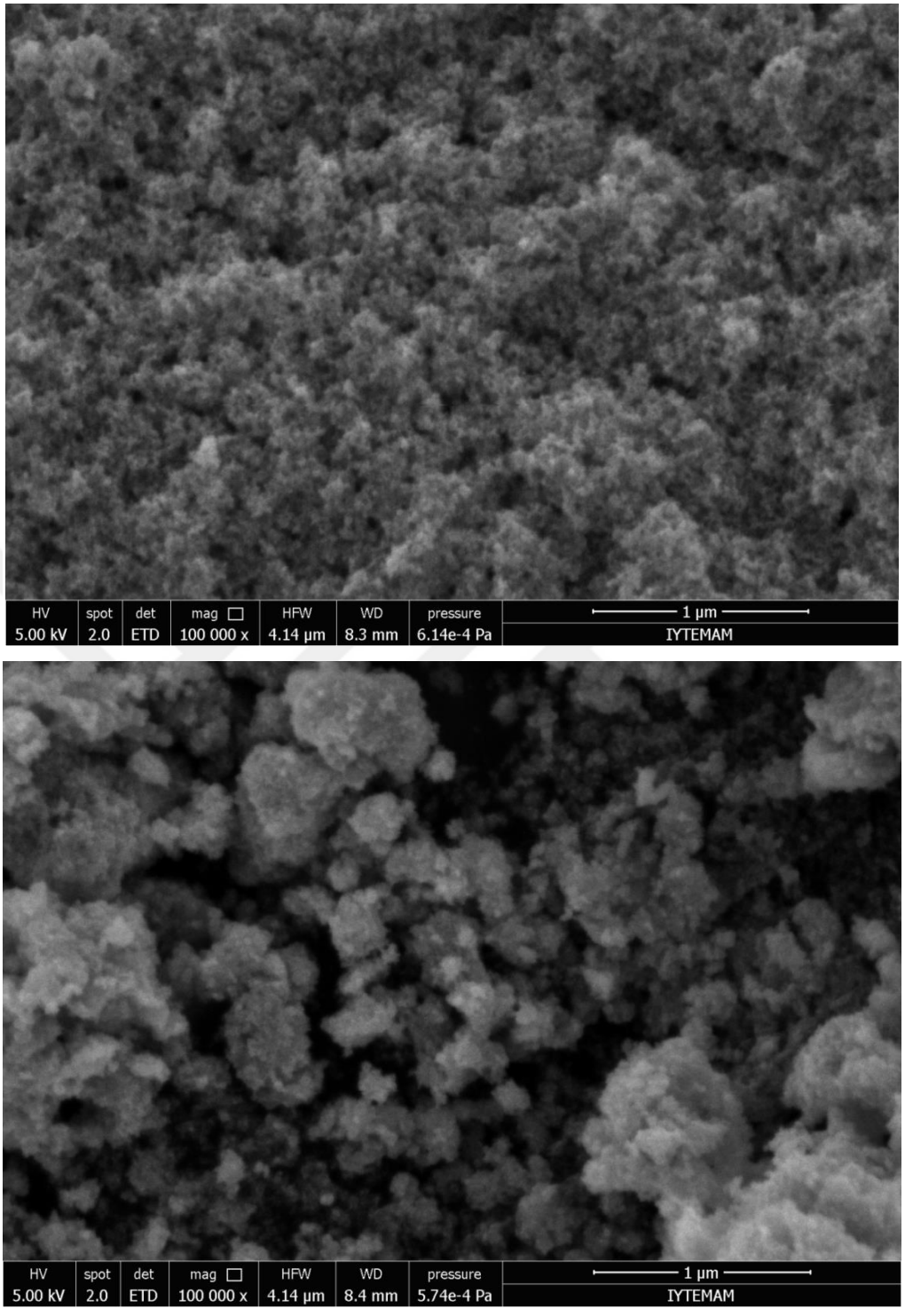
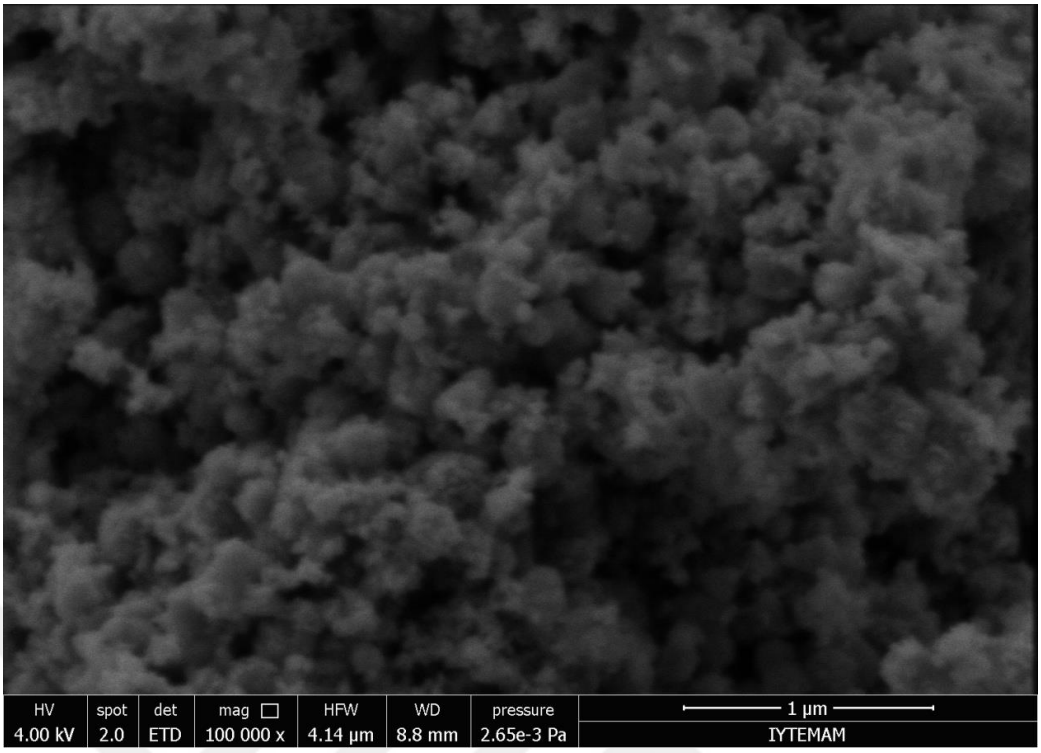


Figure 4.23m SEM Images of the Sample (Methanol used as solvent, Synthesis C_1)



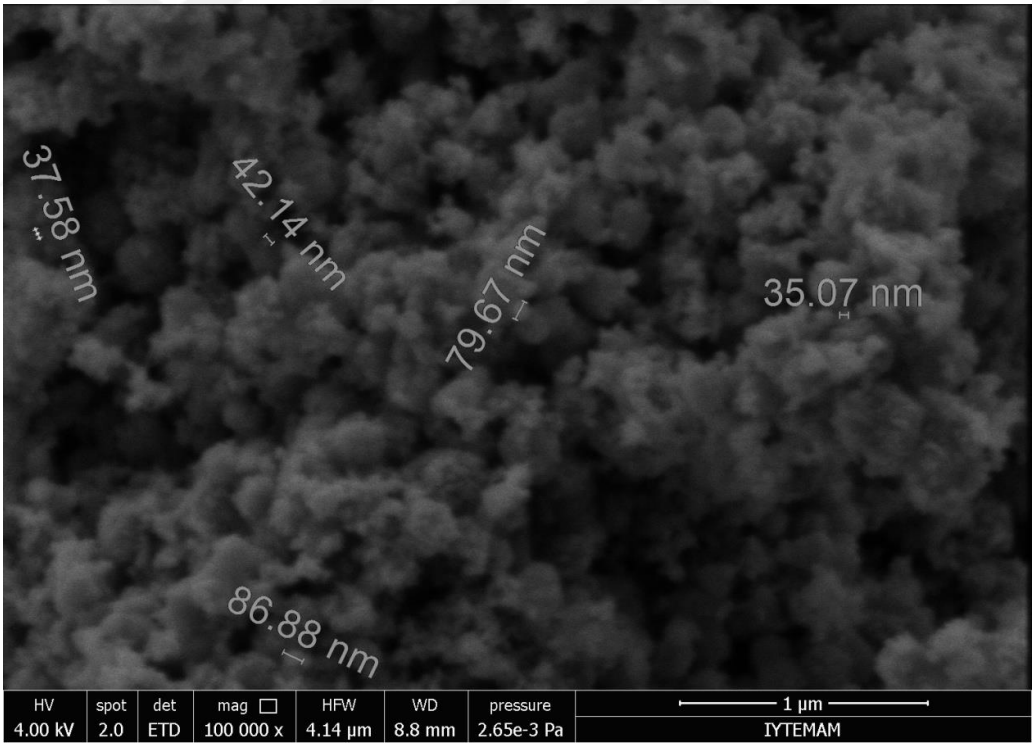
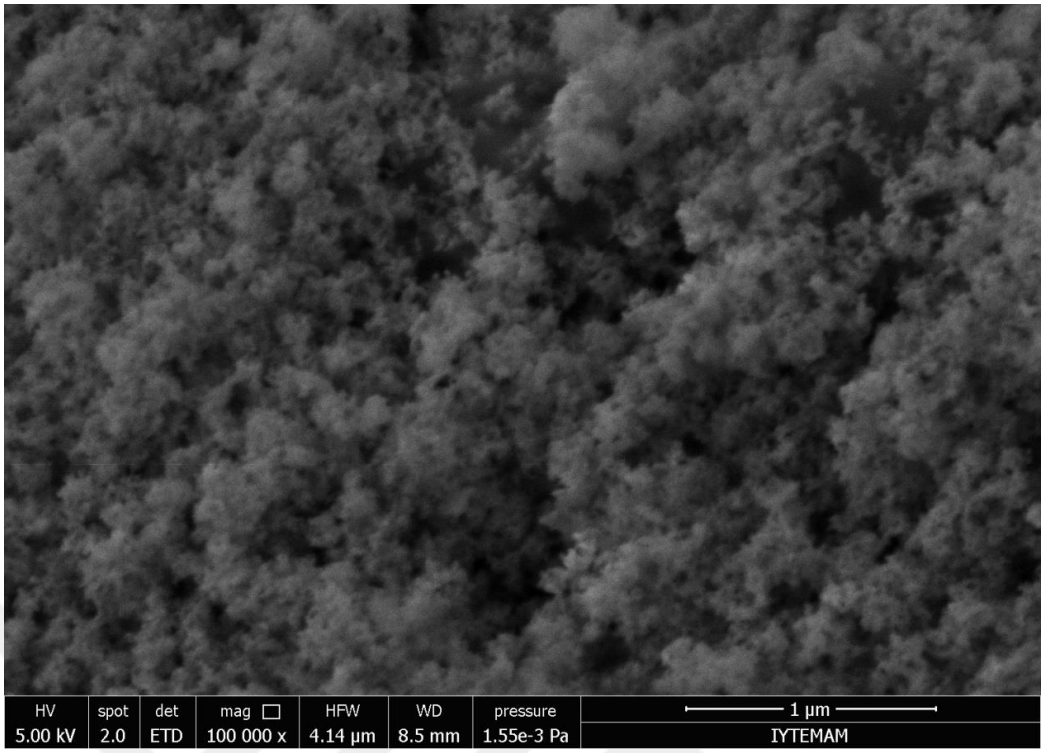


Figure 4.23e SEM Images of the Sample (Ethanol used as solvent, Synthesis C_2)



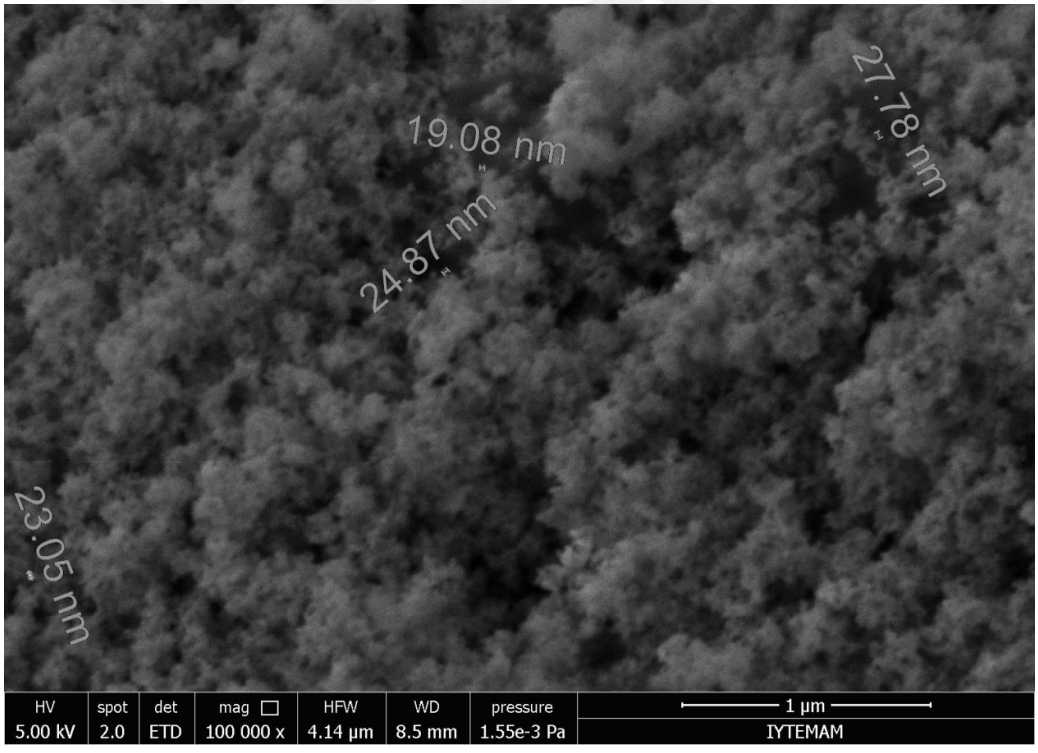


Figure 4.23p SEM Images of the Sample (Propanol used as solvent, Synthesis C_3)

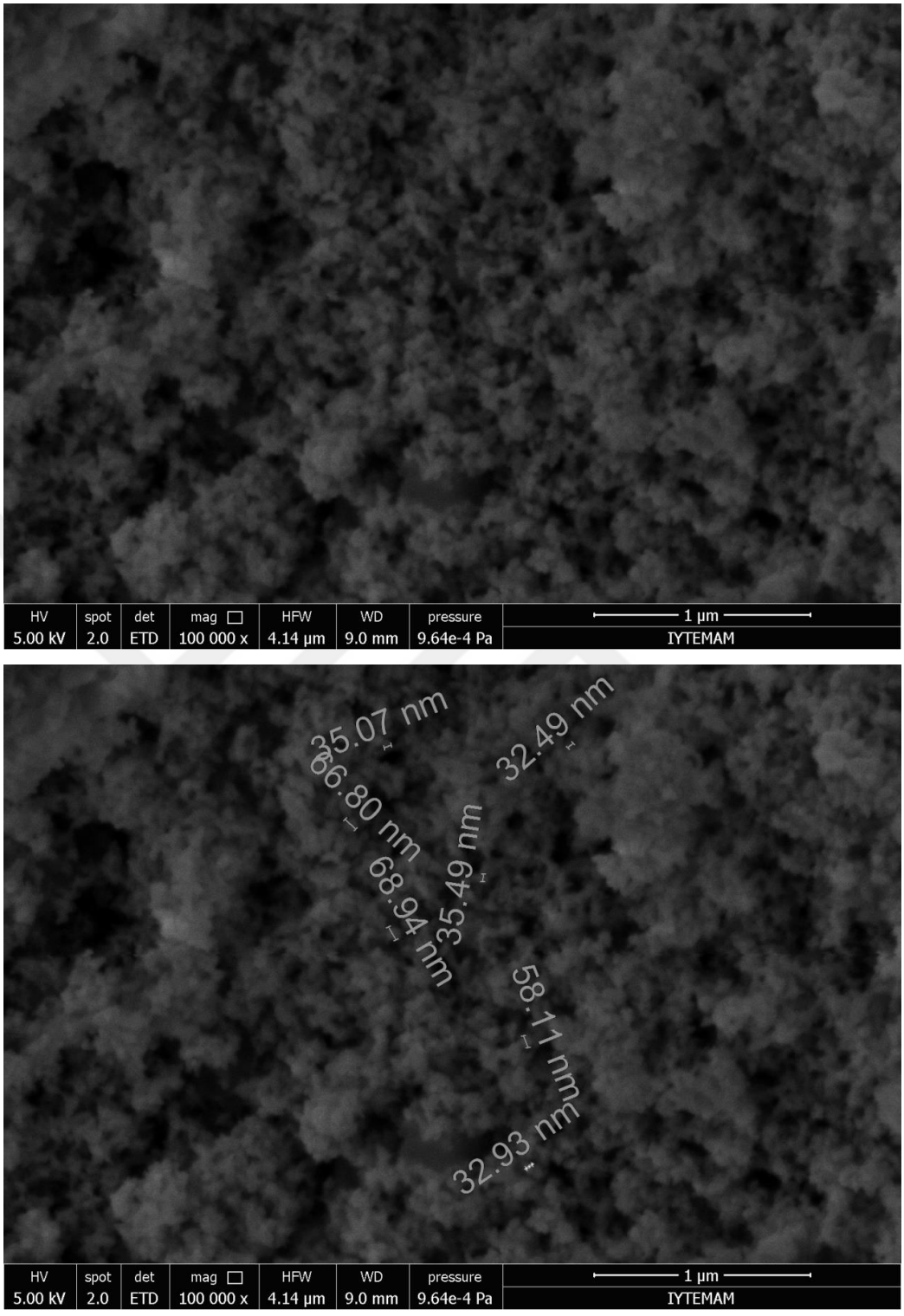


Figure 4.23b SEM Images of the Sample (Butanol used as solvent, Synthesis C_4)

4.1.4 Results of TG/DTG Analysis

TG/DTG thermograms of prepared ZnO samples are shown in Figure 4.24, Figure 4.25, Figure 4.26, and Figure 4.27.

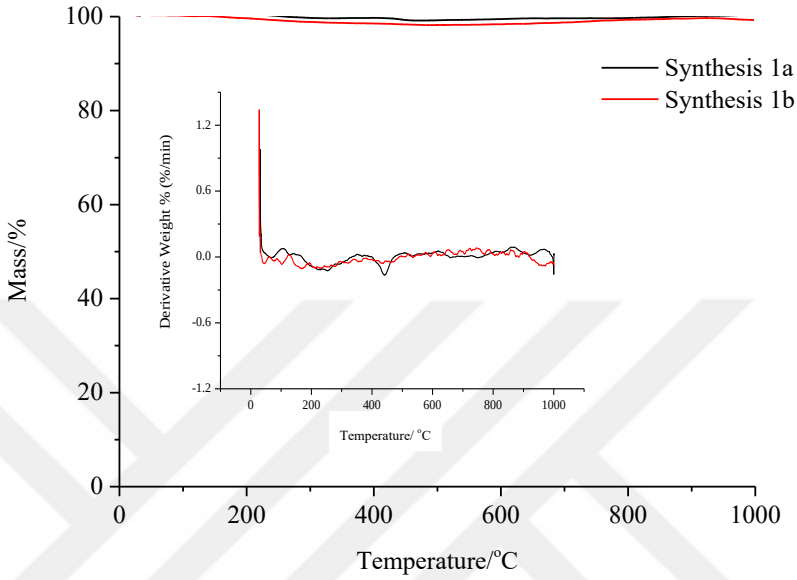


Figure 4.24 TG/DTG thermogram of the samples, pH differences

No clear and significant mass loss was observed in the metal oxide compound in the working temperature ranges of 30-100°C.

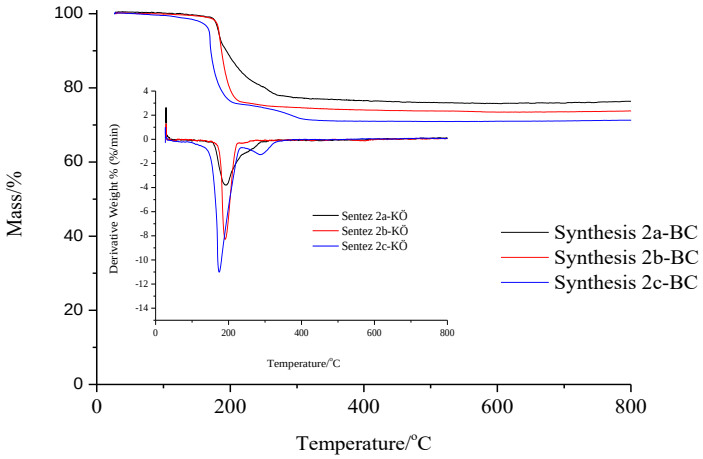


Figure 4.25 TG/DTG thermogram of the samples, effects of concentration differences before calcination (BC)

However, mass loss was observed in the pre-calcination thermograms of the zinc hydroxide compound formed in Figure 4.25. The observed mass loss is due to dehydration of water from $Zn(OH)_2$.

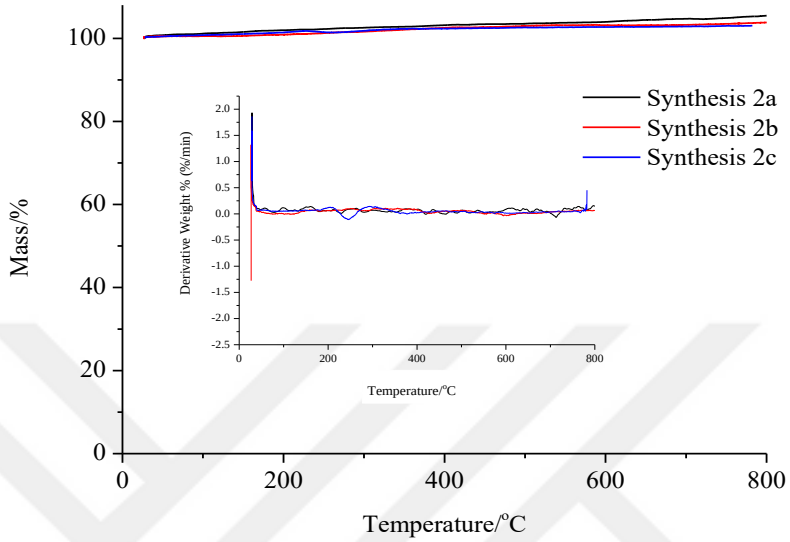


Figure 4.26 TG/DTG thermogram of the samples, effects of concentration differences after calcination

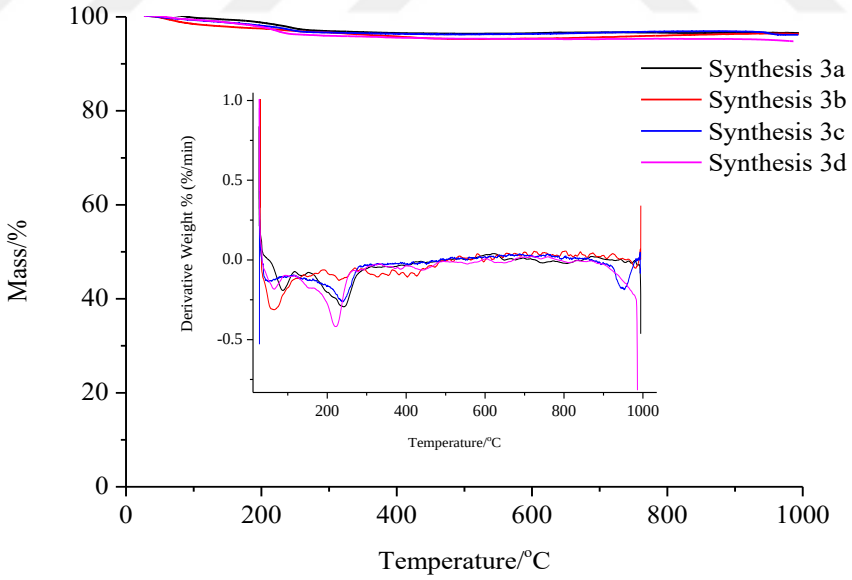


Figure 4.27 TG/DTG thermograms of the samples, effects of solvent carbon number differences

Figure 4.27 shows the mass losses of the samples due to the solvents (i.e. alcohols) which cannot be removed from the medium.

4.1.5 Particle Size Distribution Results

The pH-, temperature-, concentration-, and solvent-particle size plots of zinc oxide samples are shown in Figure 4.28, Figure 4.29, Figure 4.30, and Figure 4.31, respectively.

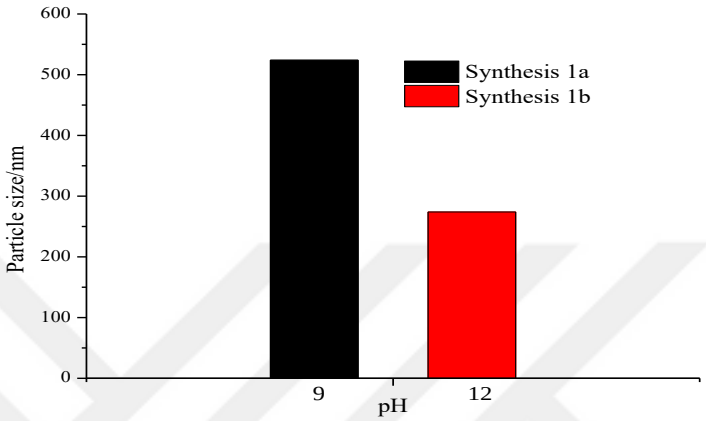


Figure 4.28 Effect of pH on particle size distribution of the samples

As the pH is increased, the particle sizes are decreasing. A difference was also observed between the nanoscale dimensions of the two zinc oxide complexes synthesized at different temperatures.

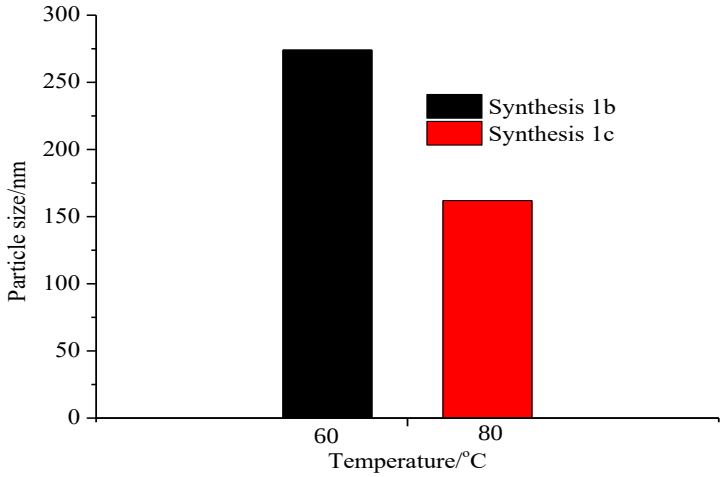


Figure 4.29 Effect of Temperature on the particle size distribution of the samples

As the temperature increases, the nano size decreases. On the other hand, in Figure 4.29, the nanoscale effect of the zinc oxide compound synthesized at different concentrations was observed. As the concentration increased, the nano size decreased.

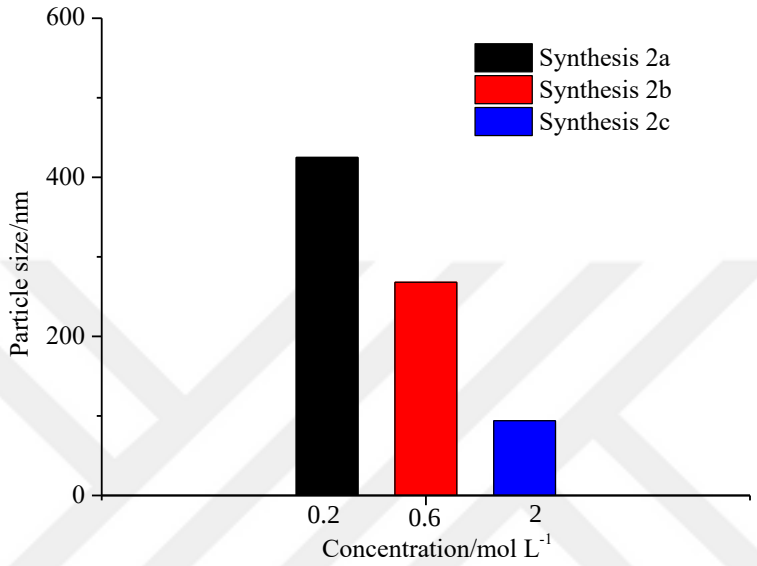


Figure 4.30 Effects of concentration on particle size distribution of the samples

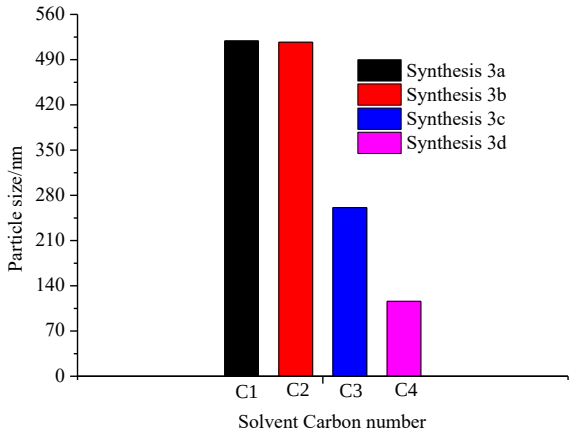


Figure 4.31 Effects of solvent carbon atom number on the particle size distribution of the samples

In Figure 4.31, the effect of different solvents on the particle size of the nanoparticles was observed. As the carbon number of the solvent increased, the size

of the ZnO nanoparticles decreased. Here, usage of Butanol as a solvent was found to be more effective on particle sizes of the samples.

4.2 Results of Application of Modified ZnO Nano Particles

Ultraviolet (UV) is an electromagnetic radiation with a wavelength from 10 nm to 400 nm and can be subdivided into a number of ranges recommended by the ISO standard ISO-21348 as given Table 2.1.

The samples applied onto the glass cover slips were dried and then analyzed on a UV-VIS Spectrophotometer. The decrease in the intensity of the reflected light on the sample indicates that absorption increases. The graphs below show how much the samples absorb the light.

4.2.1 UV-Visible Spectroscopic Analysis of the Polymer composite films coated onto glass

As a characterization and an application of the synthesized ZnO samples, UV Transmittance spectra of the polymer composite films were shown in Figure 4. 32. In Table 4.3, definition of the samples used in the application with polymer was given.

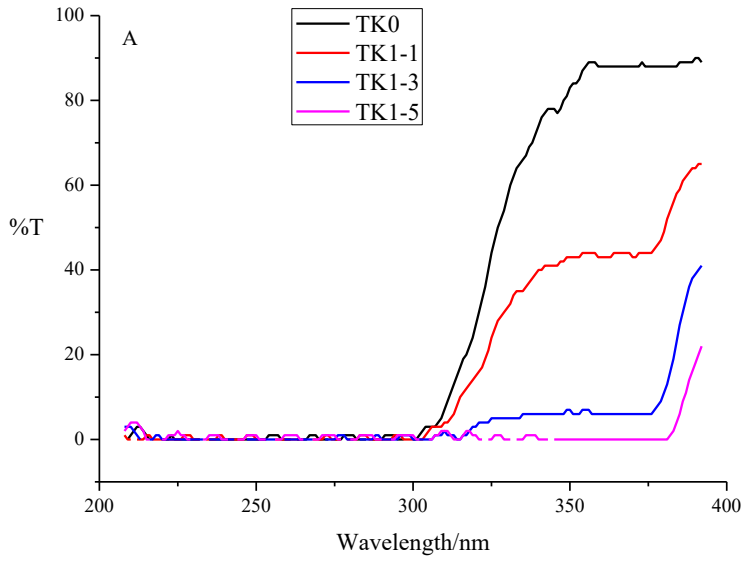


Figure 4.32 The optical transmittance spectra of films

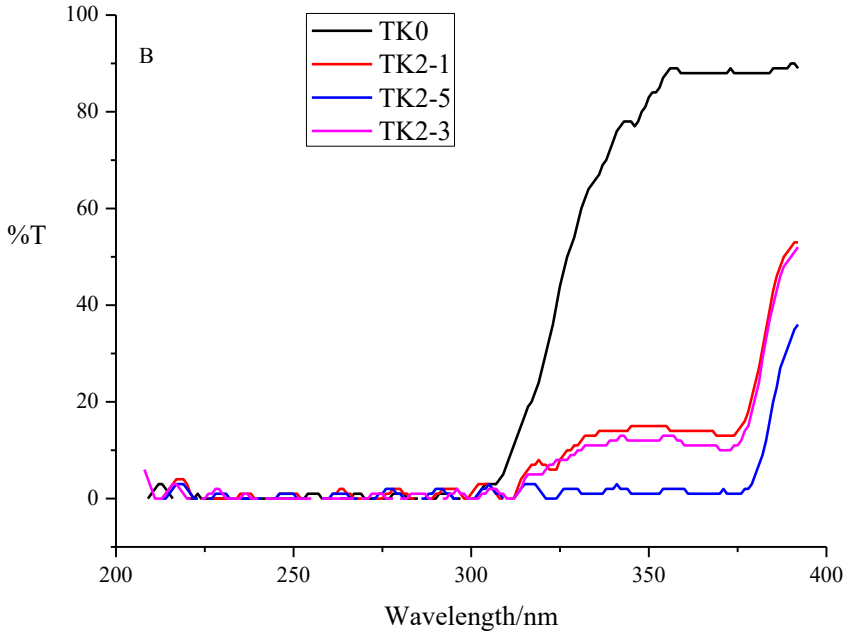


Figure 4.32 continues

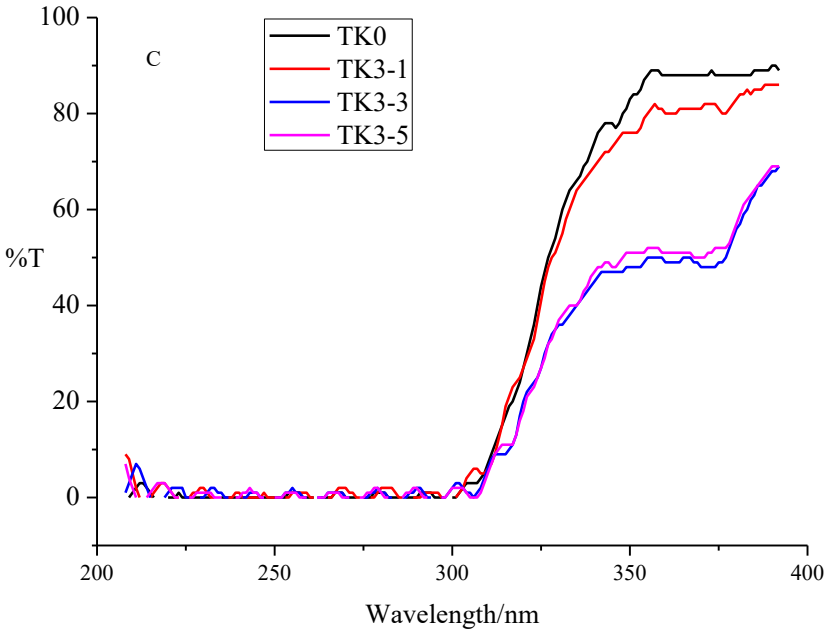


Figure 4.32 continues

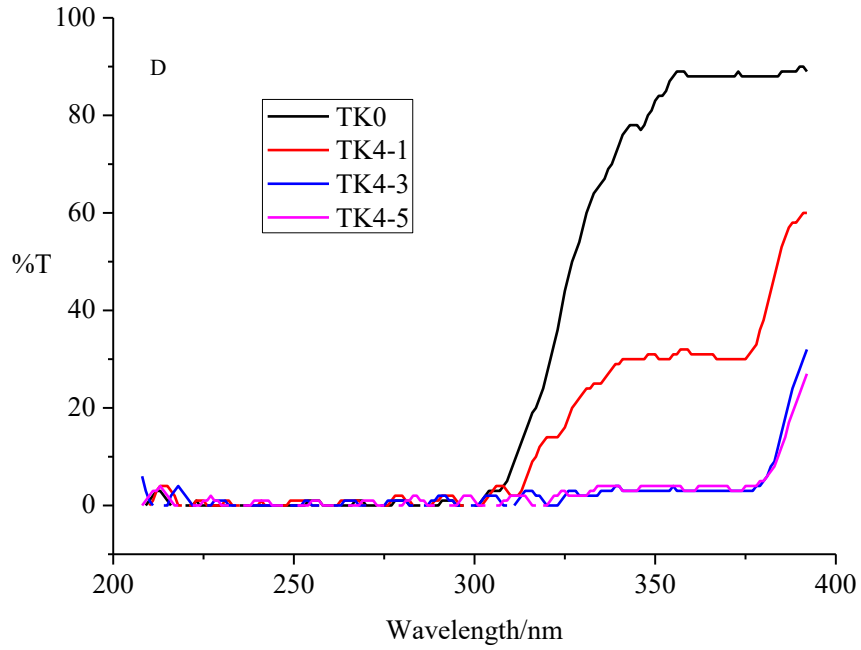


Figure 4.32 continues

Table 4.3 Definition of the samples used in the application with polymer

Graphic included	Sample code	Compound mixed with polymer	Addition quantity of ZnO as %
A	TK1-1	ZnO	1
	TK1-3	ZnO	3
	TK1-5	ZnO	5
B	TK2-1	ZnO + CTAB	1
	TK2-3	ZnO + CTAB	3
	TK2-5	ZnO + CTAB	5
C	TK3-1	ZnO+ APTES	1
	TK3-3	ZnO + APTES	3
	TK3-5	ZnO + APTES	5
D	TK4-1	ZnO + SDS	1
	TK4-3	ZnO + SDS	3
	TK4-5	ZnO + SDS	5

When the charts A, B, C and D are examined with the Figure 4.32, it was observed that the performance of the pure polymer (TKO) between 300 - 400 nm was very low. The presence of ZnO ensures that the polymer absorbs light better. As the amount of ZnO increases, the amount of absorbed light also increases. Optimum result for plain ZnO and ZnO+CTAB samples was obtained with 5% attendance while ZnO+APTES did not give the desired result. The optimum value for ZnO+SDS is 3%. An example that provides the best result at 1% participation is the inclusion of the ZnO+CTAB compound.

By using the data obtained from Figure 4.32, optical band gap energy value of the ZnO(M) can be calculated by using the Tauc equations defined in Chapter 3. In Figure 4.33, Tauc graph of the optical band gap energy calculation of ZnO was presented. The calculated energy band gap value of ZnO from this graph is 3.788 eV.

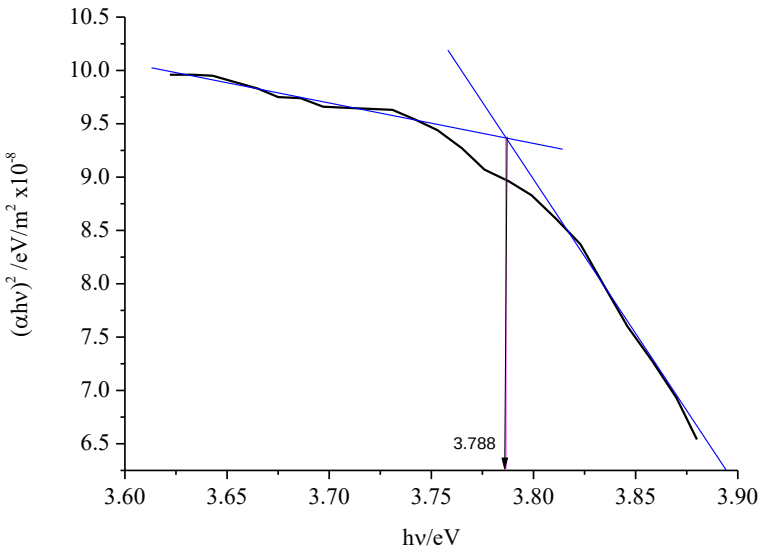


Figure 4.33 Tauc graph of the optical band gap energy calculation of ZnO

In order to calculate directly the band gap energy value of the ZnO samples from the UV Spectrum, first of all, the cut-off wavelength value can be estimated by taking advantage of the cut-off point of the tangents on the plot as indicated below in Figure 4.34.

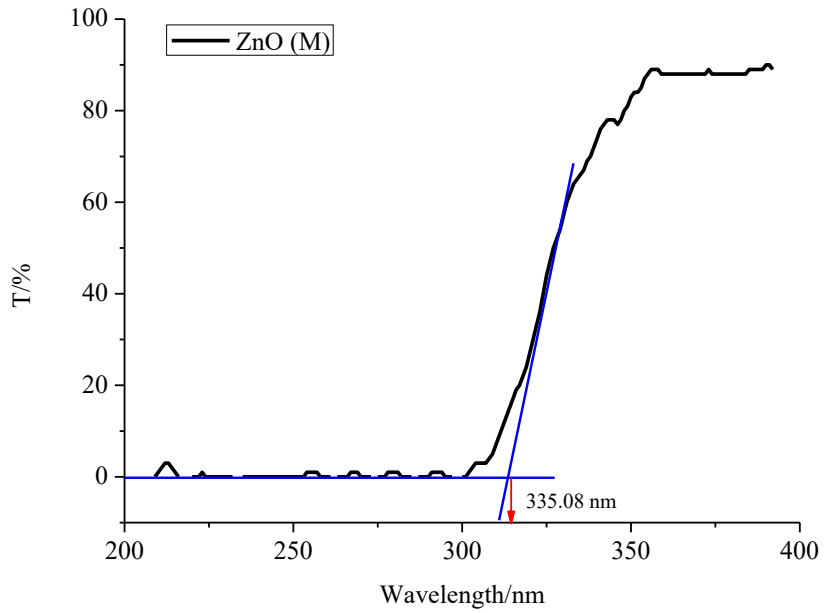


Figure 4.34 Direct methods for the calculation of the optical band gap energy

The estimated value from the plot is 335.08 nm. By using Equation (3.5) in Chapter 3 as below;

$$E = \frac{hC}{\lambda} \tag{3.5}$$

The band gap energy in eV can be calculated. h is Planks constant with a value of 6.626×10^{-34} Js. C is speed of light, 3.0×10^{8} m/s and λ is cut off wavelength found from the UV-Visible spectrum of the material. Here wavelength is 308.82 nm. In this calculation, $1eV=1.6 \times 10^{-19}$ Joules as conversion factor.

$$E = \frac{6.626 \times 10^{-34} Js \times 3.0 \times 10^{8} ms^{-1}}{335.08\, nm \times 10^{-9} \frac{m}{nm}} = 5.932 \times 10^{-19} J$$

This value is easily converted to eV by using the conversion factor.

$$E = \frac{5.932 \times 10^{-19} J}{1.6 \times 10^{-19} \frac{J}{eV}} = 3.71\ eV$$

or

$$E_g = \frac{1239.8}{\lambda_{cut-off}} = \frac{1239.8}{335.08\ nm} = 3.71\ eV$$

The difference by these two methods comes from the determination of the cut-off wavelength.

4.2.2 OM Images of the Polymer composite films coated onto glass

To investigate the effectiveness of the modification of the surfaces of ZnO particles, SEM images were recorded. SEM images of SDS modified ZnO, CTAB modified ZnO and APTES modified ZnO were shown in Figure 4.36, Figure 4.37 and Figure 4.38, respectively.

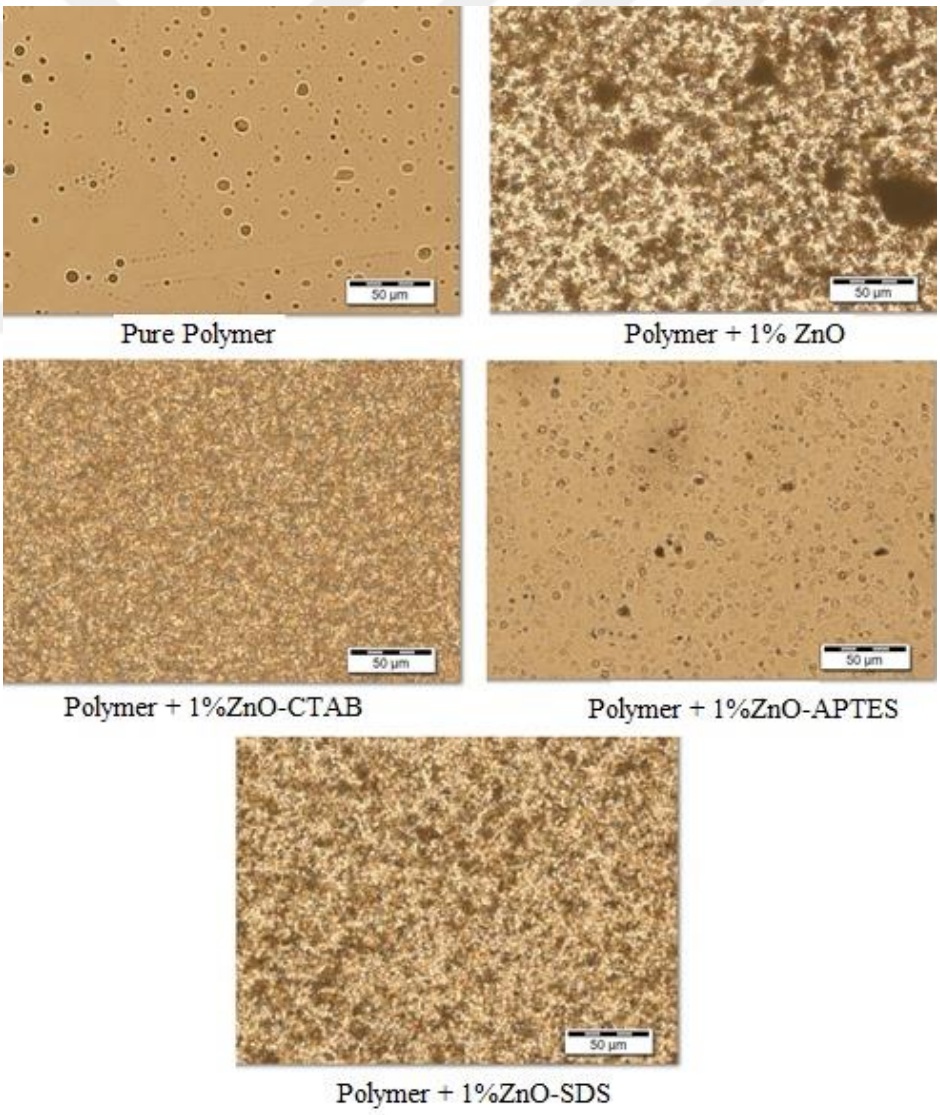


Figure 4.35 OM images of pure polymer and polymers doped with zinc oxide

4.2.3 SEM Images of the SDS, CTAB and APTES Modified ZnO

To investigate the effectiveness of the modification of the surfaces of ZnO particles, SEM images were recorded. SEM images of SDS modified ZnO, CTAB modified ZnO and APTES modified ZnO were shown in Figure 4.36, Figure 4.37 and Figure 4.38, respectively.

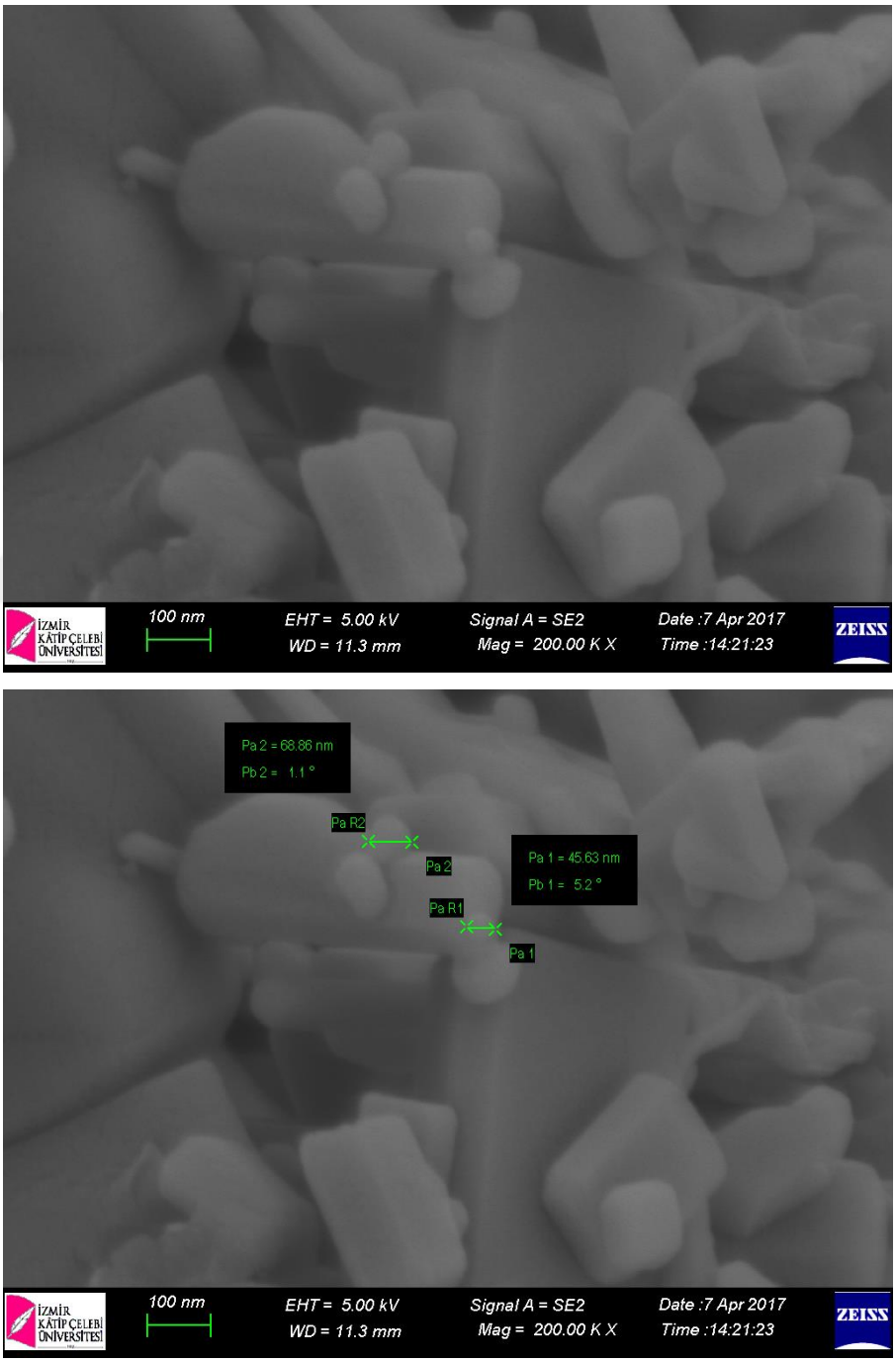


Figure 4.36 SEM Images of SDS modified ZnO sample

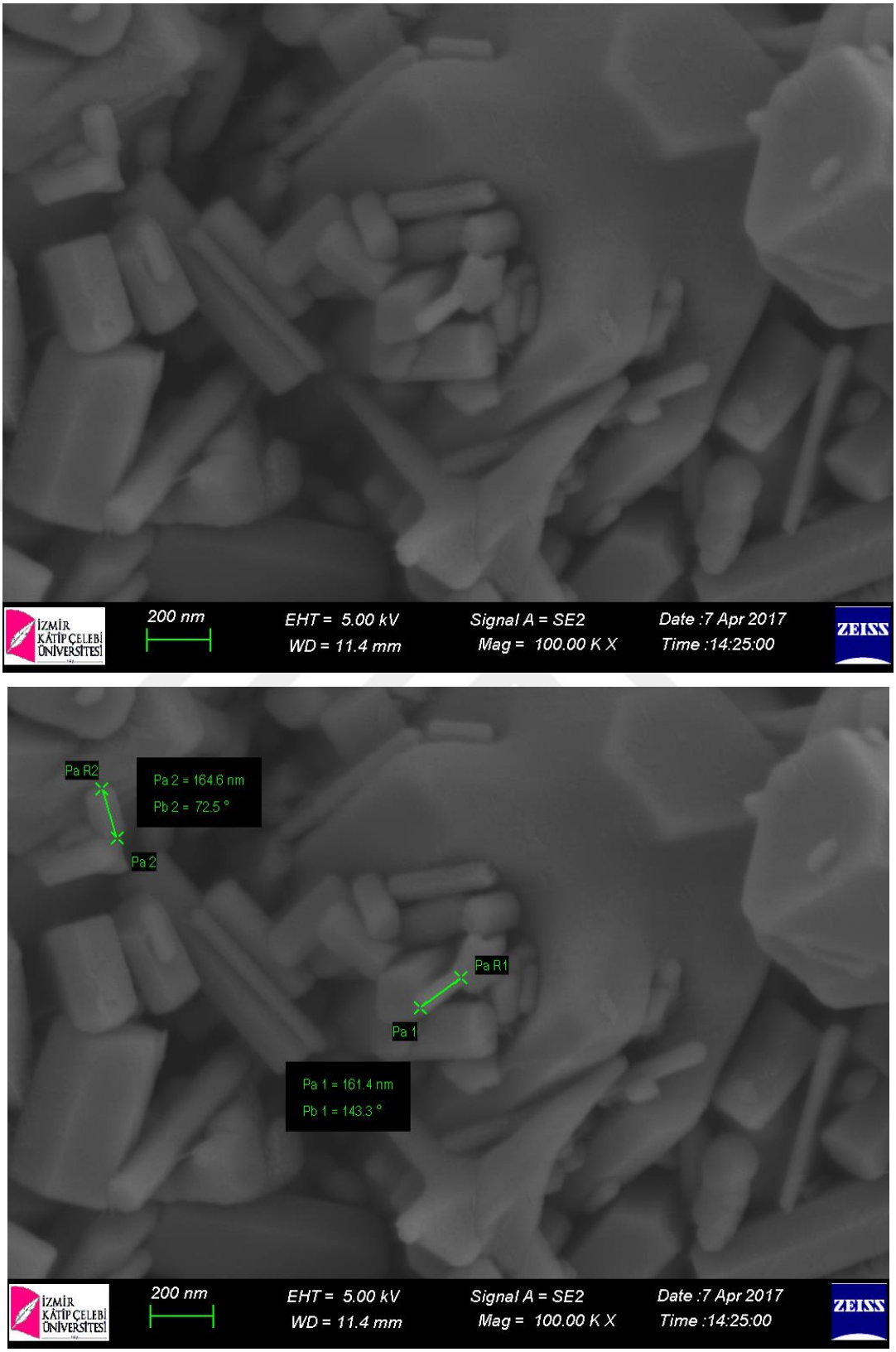


Figure 4.37 SEM Images of CTAB modified ZnO sample

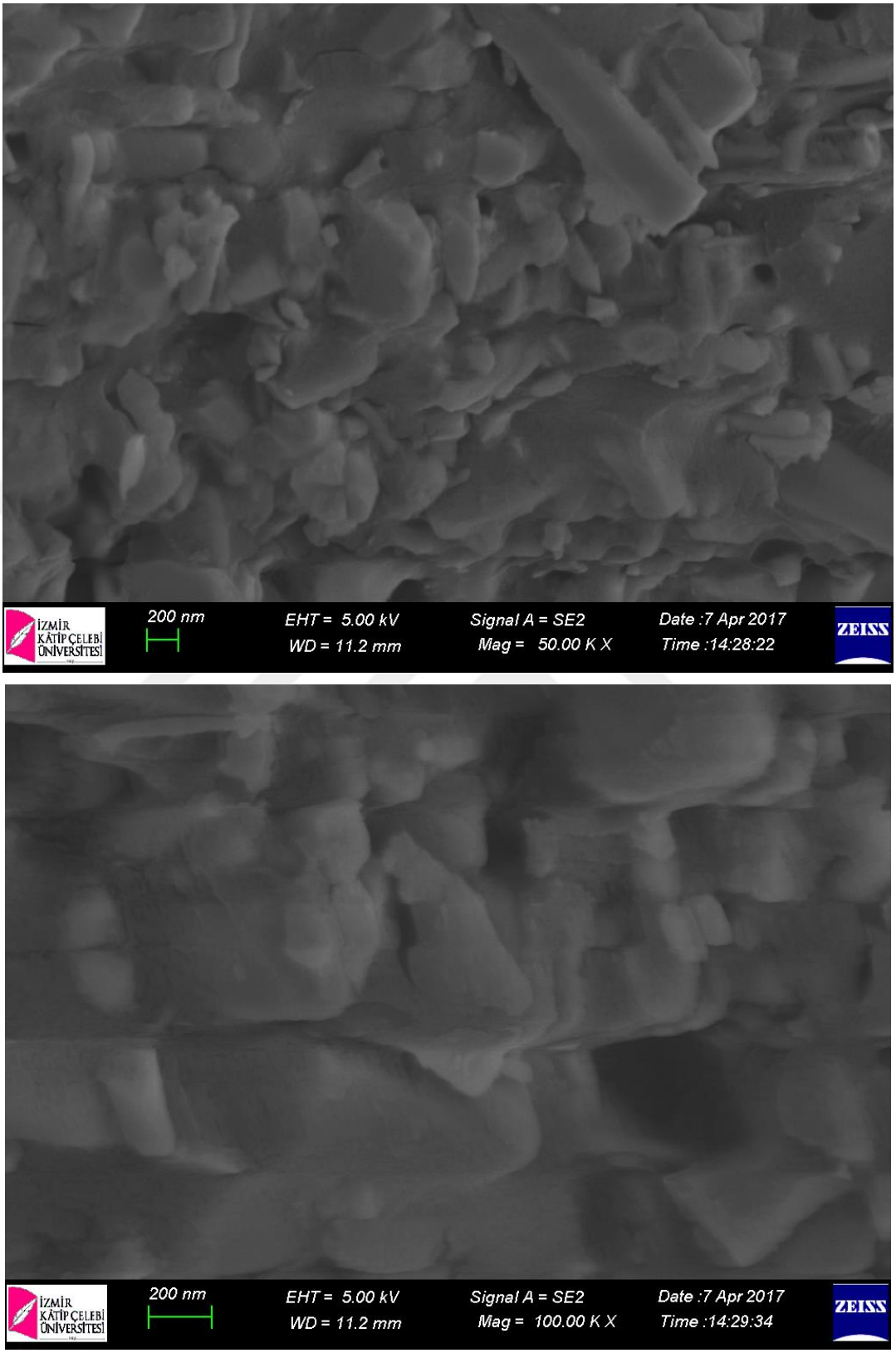


Figure 4.38 SEM Images of APTES modified ZnO sample

In Figures 4.36-4.38, it can be seen that modification of the surfaces of ZnO nanoparticles with SDS, CTAB and APTES were very effective. In Figure 4.10 and 4.11, it has been estimated that non-homogeneous or non-uniform hexagonal rod-shaped ZnO particles with various sizes were observed. After modification the shapes of the particles were conserved. Especially, modification of ZnO surface with APTES in Figure 4.38 was clearly seen. There was a chemical reaction between –OH functional groups of the surface of ZnO nanoparticles and amine ($-NH_2$) groups of APTES which was as expected.

4.2.4 XRD Patterns of the SDS, CTAB and APTES Modifed ZnO (M)

In order to investigate the effects of SDS, CTAB and APTES modifications of the surfaces of ZnO onto crystal structure, XRD patterns of the modified samples were obtained and average crystallite sizes of the particles calculated by using Scherrer's equation. The XRD patterns of the samples were given in Figure 4.39 for ZnO (M), Figure 4.40 for SDS modified ZnO, Figure 4.41 for CTAB modified ZnO and 4.42 for APTES modified ZnO, respectively.

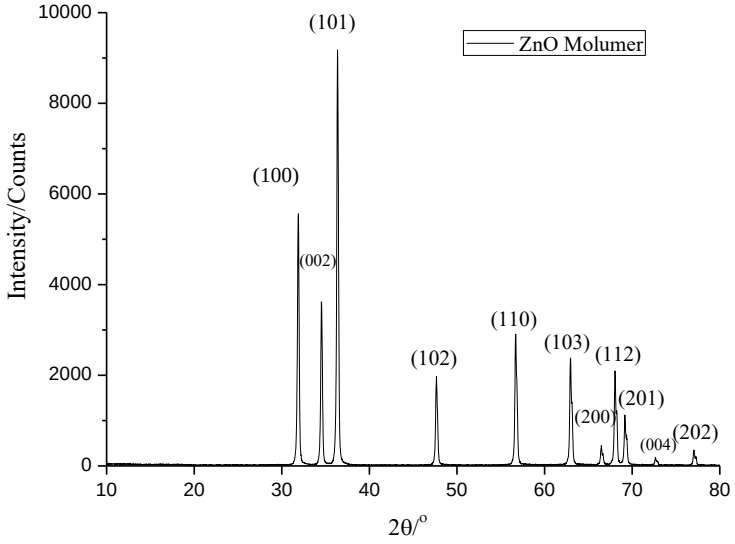


Figure 4.39 XRD Pattern of ZnO (M)

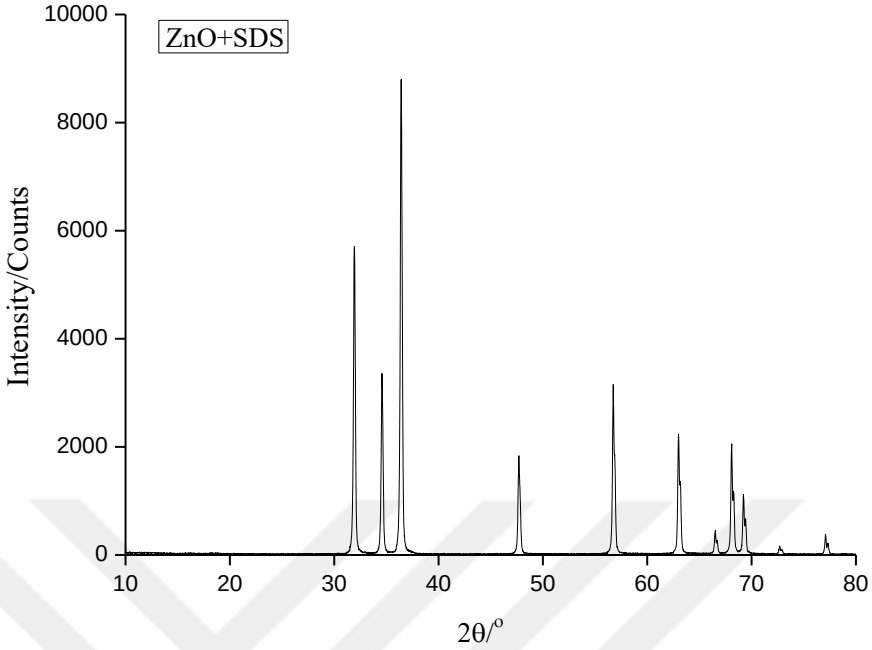


Figure 4.40 XRD Pattern of SDS Modified ZnO (M)

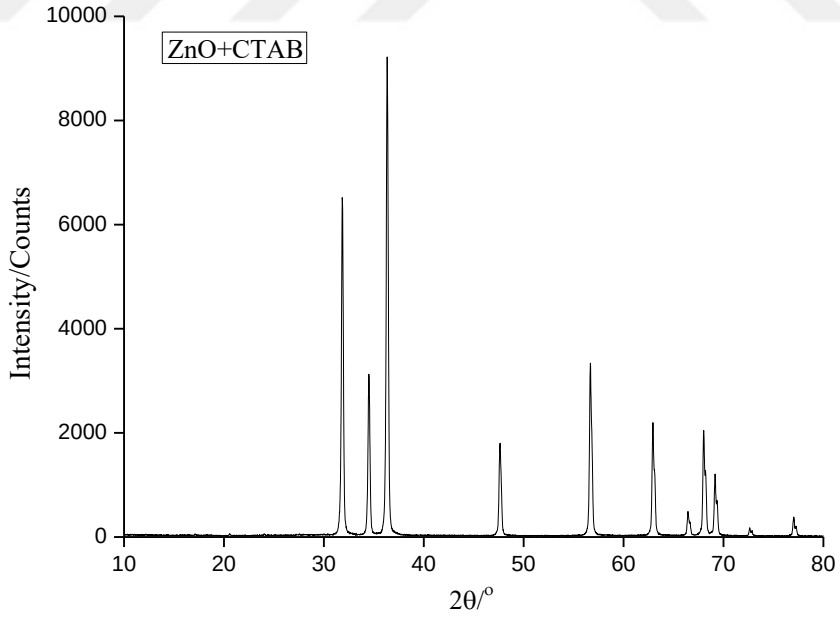


Figure 4.41 XRD Pattern of CTAB Modified ZnO (M)

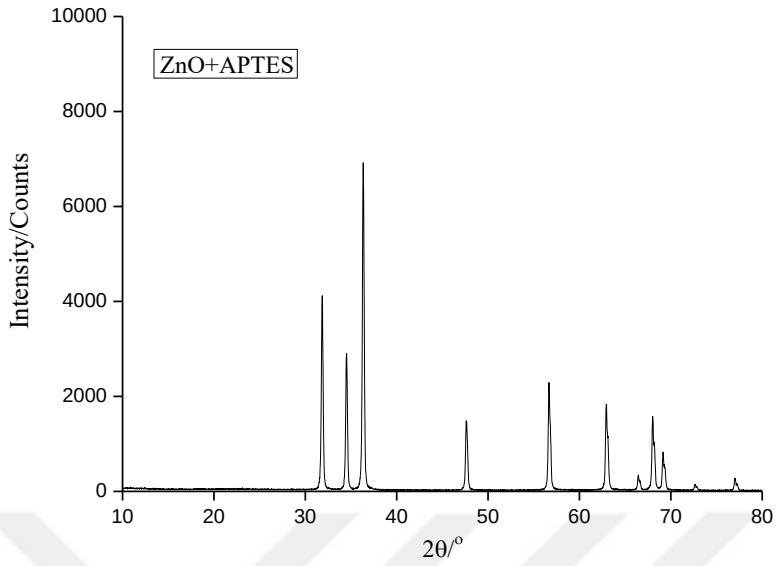


Figure 4.42 XRD Pattern of APTES Modified ZnO (M)

It can be said that the XRD patterns of the ZnO samples revealed good crystallinity and phase purity. The diffraction peaks could be indexed to the hexagonal wurtzite structure of ZnO. No other peaks were observed either from the precursor or from the SDS, CTAB and APTES.

A most intense peak at 2θ=36.67° is obtained along (101) orientation. The sharpness, strong intensity and narrow width of ZnO diffraction peaks in the XRD pattern indicate that the synthesized ZnO sample is well crystallized.

The average crystallite size D was calculated by the Debye-Sherrer Formula ($D = K\lambda/\beta\cos\theta$) where K is the Sherrer constant, λ is the X-ray wavelength, β is the peak width at half-maximum, θ is the Bragg diffraction angle. On substituting the values K =0.90, λ=1.5418Å, β=0.05, and cosθ=0.94 in the formula, the crystallite diameter can be obtained. The average crystallite size, estimated by Scherrer's equation for the (100), (002), and (101) diffraction peaks. The calculated average crystallite sizes of the ZnO samples were given in Table 4.4.

Table 4.4 Average crystallite size of the ZnO Samples

Sample	Miller indices (hkl)			Average crystallite size (nm)
	100	002	101	
ZnO Sigma-Aldrich	38.69	38.35	36.41	37.81
ZnO Molumer	40.00	39.89	39.72	39.87
ZnO+CTAB	39.45	39.26	37.98	38.89
ZnO+ APTES	40.00	40.07	38.89	39.65
ZnO+ SDS	42.98	42.65	40.87	42.16

From Table 4.4, it can be said that the ZnO particles are nanoparticles with as average crystallite size of about 38 nm.

4.2.5 ATR (Attenuated Total Reflection)-FTIR Characterization of the SDS, CTAB and APTES Modified ZnO (M) Polymer Coated Samples

In this part of the study, the SDS, CTAB and APTES Modified ZnO (M) samples were added into acrylic type varnish obtained DYO AŞ/İzmir to form polymer composites. These composites were coated onto lamellar glass substrate and characterized by ATR-FTIR Spectroscopic Analysis. ATR-FTIR spectrum of the acrylic polymer sample and its Library Search spectra were given in Figure 4.43 and 4.44. As an example, ATR-FTIR spectra of the TK0, TK1 3A, TK2 3A and TK4 3A were also presented in Figure 4.45.

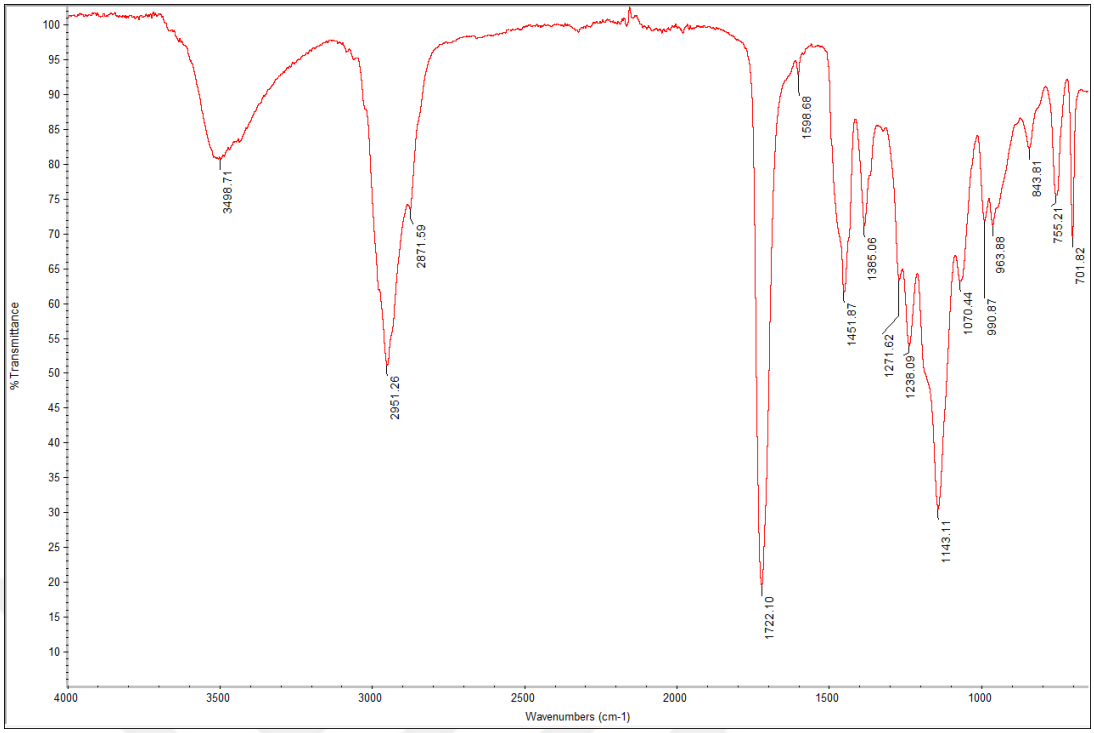
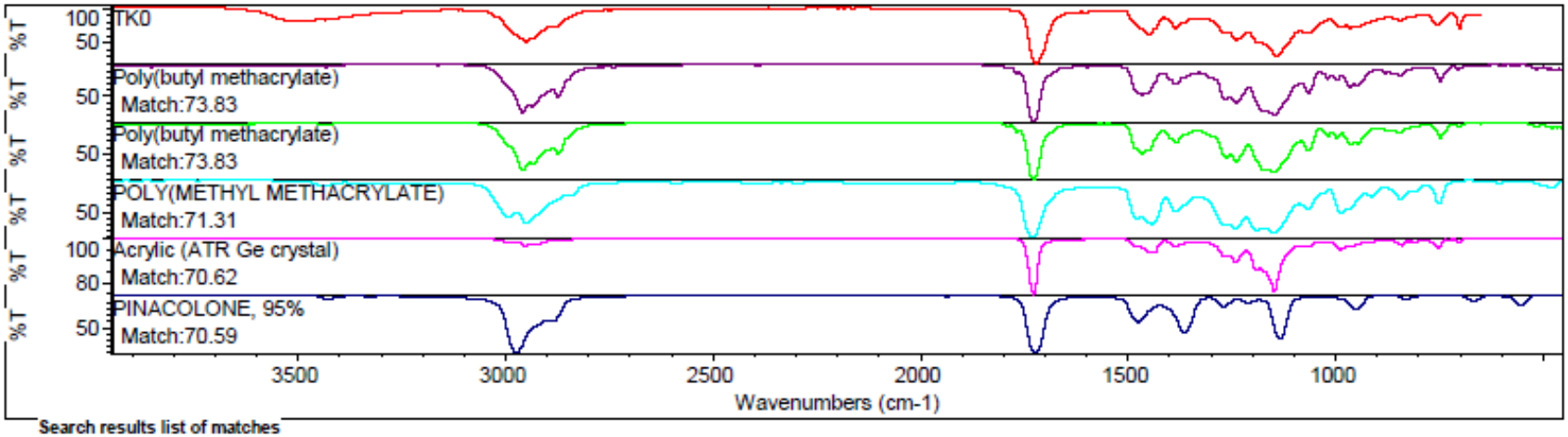


Figure 4.43 ATR-FTIR Spectrum of Acrylic Polymer Sample



Search results list of matches

	Index	Match	Compound Name	Library Name
1	819	73.83	Poly(butyl methacrylate)	HR Nicolet Sampler Library
2	760	73.83	Poly(butyl methacrylate)	HR Nicolet Sampler Library
3	30	71.31	POLY(METHYL METHACRYLATE)	Hummel Polymer Sample Library
4	16	70.62	Acrylic (ATR Ge crystal)	User Example Library
5	22	70.59	PINACOLONE, 95%	Aldrich Vapor Phase Sample Library
6	13	69.99	Acrylic (ATR Corrected)	User Example Library
7	653	69.54	Poly(2-hydroxyethyl methacrylate)	HR Nicolet Sampler Library
8	12	65.95	P-TOLUALDEHYDE, 97%	Aldrich Vapor Phase Sample Library
9	798	65.58	Poly(isobutyl methacrylate)	HR Nicolet Sampler Library
10	19	64.90	POLY(METHACRYLATE), W/OH GROUPS	Hummel Polymer Sample Library

Figure 4.44 ATR-FTIR Spectrum Search of Acrylic Polymer Sample

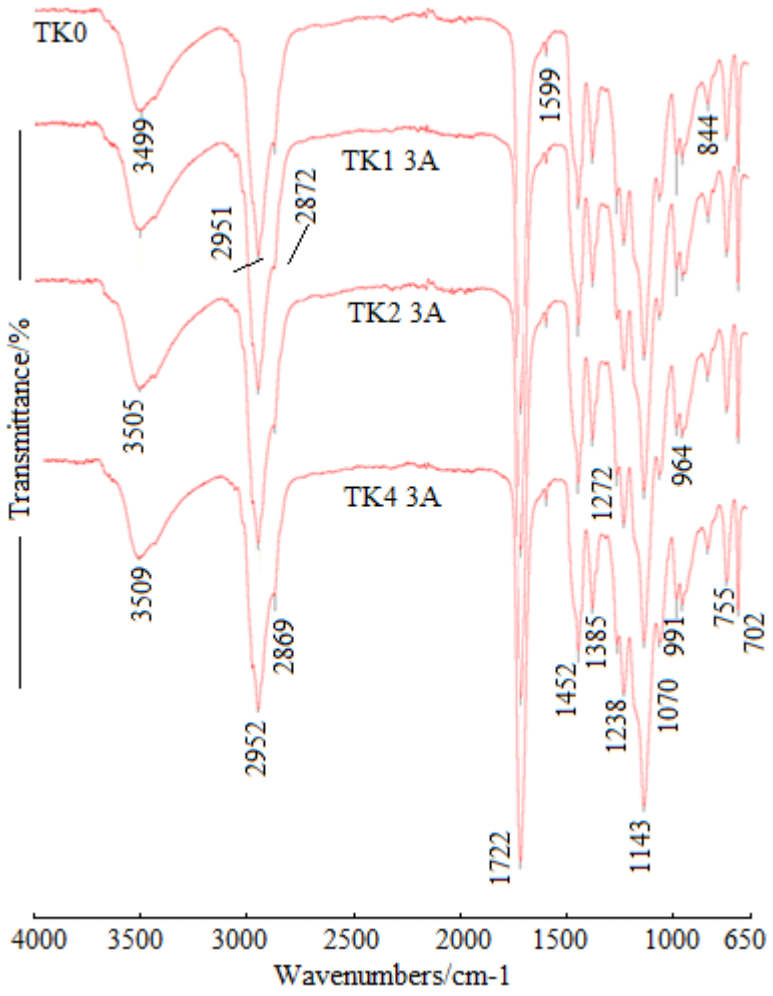


Figure 4.45 ATR-FTIR spectra of the TK0, TK1 3A, TK2 3A and TK4 3A

Figure 4.43 shows ATR-FTIR spectrum of Acrylic Polymer Resin (TK0). In the spectrum, the band at 3499 cm^{-1} indicates the presence of –OH. The absorption bands in the region 2800-3000 cm^{-1} correspond to the CH_2 and CH_3 group of the acrylic resin. The strong band at 1722 cm^{-1} is due to C=O stretching vibration. Corresponding C–O stretches are observed at 1143 and 1070 cm^{-1}. The strong absorption bands of 1452 cm^{-1} and 1385 cm^{-1} should belong to C=O of acrylates. On the other hand, we have used SDS, CTAB and APTES for the modification of the ZnO(M).

The FTIR band assignments of SDS are; the 3457 cm^{-1} band corresponding to H–OH stretching, 2943, 2915, 2848 and 1465 cm^{-1} bands corresponding to CH_2

stretching and bending modes which is characteristic of a polar environment, the 1220 cm^{-1} band corresponding to skeletal vibration involving the bridge S–O stretch (Reichardt, & Welton, 2011), the 1075 cm^{-1} band corresponding to C–C band stretching, 827 and 579 cm^{-1} bands corresponding to asymmetric C–H bending of the CH_2 group (Singh et al., 2011).

Assignments of FTIR vibrational frequencies of CTAB: 2959 cm^{-1}, -CH_3 anti-symmetrical stretching; 1462 cm^{-1} anti-symmetrical deformation; 2870 cm^{-1} symmetrical stretching; 1395 cm^{-1} symmetrical deformation; 2916 cm^{-1}-(CH_2)- anti-symmetrical stretching; 1462 cm^{-1} in-plane deformation; 2848 cm^{-1} symmetrical stretching; 1303 cm^{-1} torsional; 1300-1000 out-plane swinging; 720, 728 cm^{-1} in-plane swinging (Li, 2004).

FTIR spectrum of APTES was given in below Table 4.5 (Majoul, Aouida, & Bessaïs, 2015) and elsewhere (Chiang, Ishida, & Koenig, 1980; Culler, Ishida, & Koenig, 1985; Pena-Alonso, Rubio, Rubio, & Oteo, 2007).

Table 4.5 FTIR band assignments of APTES

Vibrational features	Pure APTES solution (cm^{-1})
ν_{as} (Si—OH)	–
ν_{as} (N—H)	3370
ν_s (N—H)	3295
ν_{as} (CH_3)	2975
ν_{as} (CH_2)	2928
ν_s (CH_2)	2870
δ (Si—CH_2)	1411
δ (NH_2)	1600
δ (NH_2)	–
δ (NH_2)	–
ν_{as} (Si—O—C)	1104
ν_s (C—O)	1089

After FTIR the assignments of Acrylic resin, SDS, CTAB and APTES, we can discuss the Figure 4.45 in the following manner. When we look at the ATR-FTIR spectra of the TK0, TK1 3A, TK2 3A and TK4 3A, the major and strong bands the acrylic resin were dominant due to the matrix effect. However, some wave number shifts (from 3499 to 3505 and 3509 cm^{-1}) was also observed for –OH band region.

This is due to the interaction of the surfactants mainly through –OH bands. The mechanism of the interaction of the surfactants with ZnO and acrylic resins should be investigated in details for the future studies.

4.2.6 UV-Visible Reflectance Spectrophotometric Analysis of the SDS, CTAB and APTES Modifed ZnO (M) Polymer Coated Samples

UV-Visible Reflectance Spectra of the Samples were given below for TK0, TK1.3 and TK1.5 in Figure 4.46, for TK0, TK2-1, TK2-3 and TK2-5 in Figure 4.47, for TK0, TK3-1, TK3-3 and TK3-5 in Figure 4.48 and for TK0, TK4-1, TK4-3 and TK4-5 in Figure 4.49. In these Figures, TK0 (Acrylic Resin) was given for comparison as a reference. In these Figures, TK0 showed only about 10% reflectance in the region of 300-600 nm.

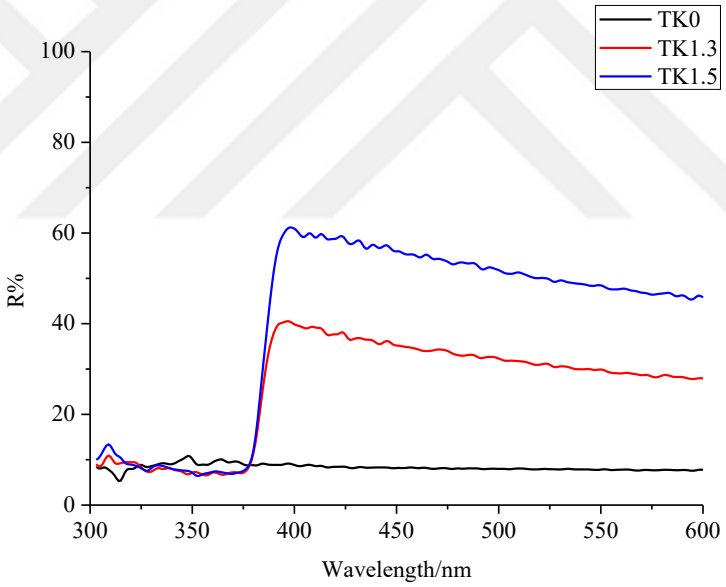


Figure 4.46 UV-Visible Reflectance Spectra of the TK0, TK1.3 and TK1.5

In this Figure, decays from 375 nm to 600 nm with a cut-off wavelength of about 378 nm was observed for TK1-3 and TK1-5 (Acrylic resin+%3 and %5 ZnO) with reflectance of 30 and 50%, respectively. Addition of ZnO in the acrylic resin increased the optical reflectance of the films which reflects directly the UV absorber properties of ZnO.

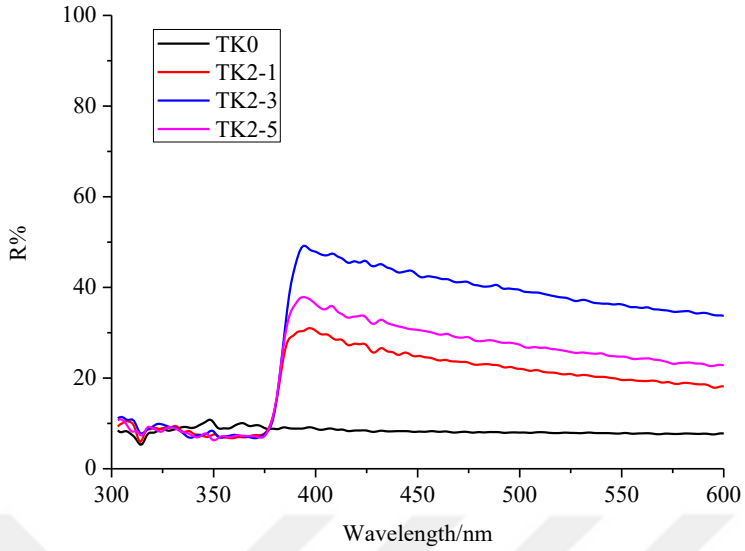


Figure 4.47 UV-Visible Reflectance Spectra of the TK0, TK2-1, TK2-3 and TK2-5

In this Figure, decays from 375 nm to 600 nm with a cut-off wavelength of about 378 nm was observed for TK1-3 and TK1-5 (Acrylic resin+ %1, %3 and %5 CTAB modified ZnO) with reflectance of 20, 35 and 25%, respectively. In this case, addition of CTAB modified ZnO in the acrylic resin increased the optical reflectance of the films which reflects the UV absorber properties of ZnO but the amounts of 3% CTAB modified ZnO was enough, then a decrease was observed. When we remember, CTAB is a quaternary ammonium salt, a cationic surfactant which was effective here.

In Figure 4.48, addition of APTES modified ZnO in acrylic resin was not very effective as compared with the CTAB and SDS modified ZnO samples. This may be due to the weak modification of the surface of the ZnO. In general, APTES interacts with surface –OH groups over $–NH_2$ functional groups in its structure.

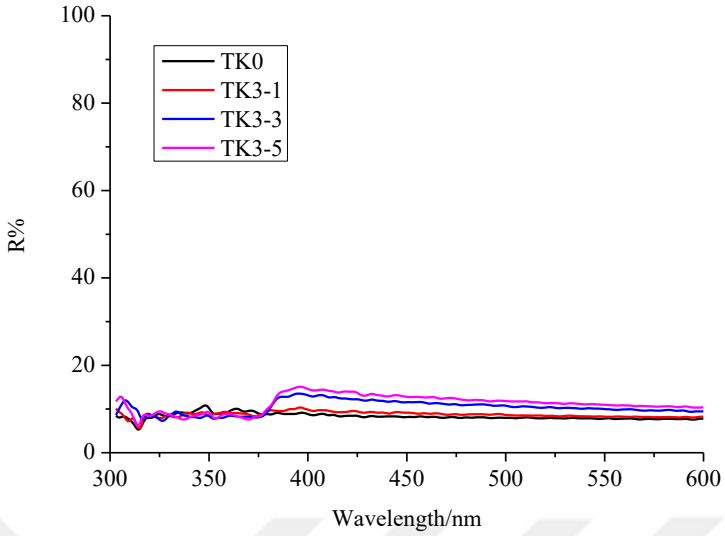


Figure 4.48 UV-Visible Reflectance Spectra of the TK0, TK3-1, TK3-3 and TK3-5

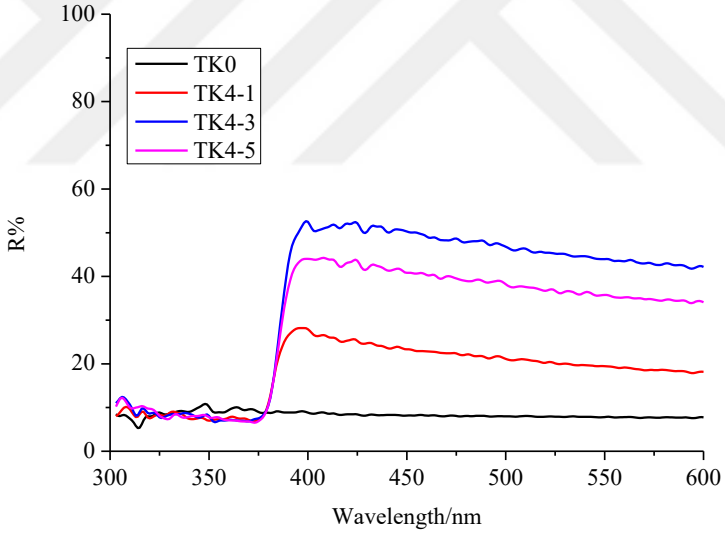


Figure 4.49 UV-Visible Reflectance Spectra of the TK0, TK4-1, TK4-3 and TK4-5

In Figure 4.49, SDS modified ZnO was added to acrylic resin as a amounts of 1, 3 and 5%. TK4-3 sample was very effective in these series. It absorbs in the UV region and reflects in visible region as 45%.

CHAPTER FIVE
CONCLUSIONS

ZnO samples synthesized by different methods, different zinc salts, precipitants and solvents. They are all in nanoscale. According to the synthesis methods and conditions, the surface morphologies are different as seen in the SEM images. Temperature, pH, solvent and effluent conditions were very effective. It was observed that influence of pH greatly effects on morphological properties. In our case, as the pH was increased, the particle sizes decreased. This may be due to the formation of the Zn(OH)x species in the solution. As pH increased, the broadening (FWHM) of the diffraction peaks increased and the intensities of diffraction line decreased. This affect the crystallite size which was calculated by using Debye Scherrer's formula. This argument was also supported (Singh, & Haque, 2016). On the other hand, it was also observed that crystal size increases with increase in pH value (Chithra, Sathya, & Pushpanathan, 2015; Verma, Bhatia, & Bedi, 2017). These workers gave 9 values as the most suitable pH value in ZnO synthesis. They said that the crystal size increases with pH. The calcination at 60°C was given better results than the calcination at 80°C. This may be due to the growth mechanism of the ZnO. In general, formation of crystals at lower temperatures affects the morphology of the ZnO particles. This means that the sizes and shapes of the particles would be changed depending upon the temperature. The yield of ZnO increased with the decreasing the concentration of Zn^{2+} in solution. As the number of carbon atom increased from C_1, C_2, C_3 and C_4 as solvents, the particles became more pronounced and the particle size became smaller. Usage of Butanol as solvent was found to be more effective on particle sizes.

The modified ZnO samples applied onto the glass were analyzed on a UV-VIS Spectrophotometer. The performance of the pure polymer between 300 and 400 nm was very low. The presence of ZnO ensures that the polymer absorbs light better. Modification of the surfaces of ZnO nanoparticles with the surfactants, SDS and CTAB were very effective than APTES. These results were closely related with the anionic, neutral, and cationic nature of the used capping agents such as SDS, CTAB

or APTES and their interaction with the surface of ZnO. Sodium dodecyl sulfate, SDS is an anionic surfactant used in many cleaning and hygiene products. CTAB is a cationic surfactant. On the other hand, (3-Aminopropyl) triethoxysilane (APTES) is an amino silane frequently used in the process of silanization, the functionalization of surfaces with alkoxysilane molecules. It can also be used for covalent attaching of organic films to metal oxides such as silica, titania and ZnO. Experimentally it was observed that Zinc oxide is positively charged in aqueous solution. The surface charge on zinc oxide in aqueous solution has been studied (Degen, & Kosec, 2000). Aqueous suspensions of zinc oxide could not be stabilized electrostatically because of the decreasing pH of suspensions in the region between 7 and 12 as a result the transformation of colloidal $Zn(OH)_{2(S)}$ particles to $Zn(OH)_{2(aq)}$ ions. When the zinc oxide is immersed in the water the surface of the oxide is hydrolyzed and a layer of hydroxide is built up. It is well established that zinc hydroxide is slightly soluble in water, becoming more soluble as the pH is either lowered or raised. Interaction of zinc hydroxide with $–NH_2$ functional groups of APTES is well-known.

As a result, ZnO specimens were found to be nano-sized, UV-filtered and semi-conducting. XRD patterns of the ZnO samples revealed good crystallinity and phase purity. The ZnO specimens prepared are suitable for use as fillers in the production of polymer composite materials. ZnO sample obtained from Molumer can be used safely as a source material in the preparation of polymer composites as UV absorber.

In the future studies, usage of the surfactants and the investigation of the effectiveness of the modification in the preparation of ZnO must be studied. Especially, usage of surfactants as capping agents in the synthesis of ZnO nanoparticles should be investigated in details.

REFERENCES

Allied Market Research titled, "Nano Zinc Oxide Market by Application - Global Opportunity Analysis and Industry Forecast, 2014 – 2022". Retrieved July 20, 2017, https://www.alliedmarketresearch.com/nano-zinc-oxide-market.

Atchudan, R., Edison, T. N. J. I., Perumal, S., Shanmugam, M., & Lee, Y. R. (2017). Direct solvothermal synthesis of zinc oxide nanoparticle decorated graphene oxide nanocomposite for efficient photodegradation of azo-dyes. *Journal of Photochemistry and Photobiology A: Chemistry*, *337*, 100-111.

Bacaksiz, E., Parlak, M., Tomakin, M., Özçelik, A., Karakız, M., & Altunbaş, M. (2008). The effects of zinc nitrate, zinc acetate and zinc chloride precursors on investigation of structural and optical properties of ZnO thin films. *Journal of Alloys and Compounds*, *466*(1), 447-450.

Barhoum, A., Melcher, J., Van Assche, G., Rahier, H., Bechelany, M., Fleisch, M., & Bahnemann, D. (2017). Synthesis, growth mechanism, and photocatalytic activity of Zinc oxide nanostructures: porous microparticles versus nonporous nanoparticles. *Journal of Materials Science*, *52*(5), 2746-2762.

Bharti, D. B., & Bharati, A. V. (2017). Synthesis of ZnO nanoparticles using a hydrothermal method and a study its optical activity. *Luminescence*, *32*(3), 317-320.

Bhattacharyya, S., & Gedanken, A. (2008). A template-free, sonochemical route to porous ZnO nano-disks. *Microporous and Mesoporous Materials*, *110*(2), 553-559.

Bel Hadj Tahar, N., Bel Hadj Tahar, R., Ben Salah, A., & Savall, A. (2008). Effects of Individual Layer Thickness on the Microstructure and Optoelectronic Properties of Sol–Gel-Derived Zinc Oxide Thin Films. *Journal of the American Ceramic Society*, *91*(3), 846-851.

Cao, M., Wang, F., Zhu, J., Zhang, X., Qin, Y., & Wang, L. (2017). Shape-controlled synthesis of flower-like ZnO microstructures and their enhanced photocatalytic properties. *Materials Letters*, *192*, 1-4.

Chaari, M., & Matoussi, A. (2012). Electrical conduction and dielectric studies of ZnO pellets. *Physica B: Condensed Matter*, *407*(17), 3441-3447.

Chen, D., Jiao, X., & Cheng, G. (1999). Hydrothermal synthesis of zinc oxide powders with different morphologies. *Solid State Communications*, *113*(6), 363-366.

Chiang, C. H., Ishida, H., & Koenig, J. L. (1980). The structure of γ-aminopropyltriethoxysilane on glass surfaces. *Journal of Colloid and Interface Science*, *74*(2), 396-404.

Chithra, M. J., Sathya, M., & Pushpanathan, K. (2015). Effect of pH on crystal size and photoluminescence property of ZnO nanoparticles prepared by chemical precipitation method. *Acta Metallurgica Sinica (English Letters)*, *28*(3), 394-404.

Choi, D. S., Hansen, M., Van Keuren, E., & Hahm, J. I. (2017). Highly photoresponsive, ZnO nanorod-based photodetector for operation in the visible spectral range *Nanotechnology*, *28*(14), 145203.

Culler, S. R., Ishida, H., & Koenig, J. L. (1985). Structure of silane coupling agents adsorbed on silicon powder. *Journal of Colloid and Interface Science*, *106*(2), 334-346.

Dem'Yanets, L.N., Li, L.E., Uvarova, T.G. (2006). Zinc oxide: Hydrothermal growth of nano- and bulk crystals and their luminescent properties. *Journal of Materials Science, 41,* 1439–1444.

Degen, A., & Kosec, M. (2000). Effect of pH and impurities on the surface charge of zinc oxide in aqueous solution. *Journal of the European Ceramic Society*, *20*(6), 667-673.

Dharma, J., Pisal, A., & Shelton, C. T. (2009). Simple method of measuring the band gap energy value of TiO_2 in the powder form using a UV/Vis/NIR spectrometer. *Application Note Shelton, CT: PerkinElmer*.

Dong, B., Yu, X., Dong, Z., Yang, X., & Wu, Y. (2017). Facile synthesis of ZnO nanoparticles for the photocatalytic degradation of methylene blue. *Journal of Sol-Gel Science and Technology*, *82*(1), 167-176.

Dolgonos, A., Mason, T. O., & Poeppelmeier, K. R. (2016). Direct optical band gap measurement in polycrystalline semiconductors: A critical look at the Tauc method. *Journal of Solid State Chemistry*, *240*, 43-48.

Ghasaban, S., Atai, M., & Imani, M. (2017). Simple mass production of zinc oxide nanostructures via low-temperature hydrothermal synthesis. *Materials Research Express*, *4*(3), 035010.

Grasset, F., Saito, N., Li, D., Park, D., Sakaguchi, I., Ohashi, N., Haneda, H., Roisnel, T., Mornet, S., & Duguet, E. (2003). Surface modification of zinc oxide nanoparticles by aminopropyltriethoxysilane. *Journal of Alloys and Compounds*, *360*(1), 298-311.

Gu, H., Yu, L., Wang, J., Yao, J., & Chen, F. (2017). A sol-gel preparation of ZnO/graphene composite with enhanced electronic properties. *Materials Letters*, *196*, 168-171.

Guzmán-Carrillo, H. R., Rivera-Muñoz, E. M., Cayetano-Castro, N., Herrera-Basurto, R., Barquera-Bibiano, Z., Mercader-Trejo, F., & Manzano-Ramírez, A. (2017). Facile control of ZnO nanostructures by varying molar concentration of zinc acetate. *Materials Research Bulletin*, *90*, 138-144.

Hjiri, M., Zahmouli, N., Dhahri, R., Leonardi, S. G., El Mir, L., & Neri, G. (2017). Doped-ZnO nanoparticles for selective gas sensors. *Journal of Materials Science: Materials in Electronics*, *28*(13), 9667-9674.

Hong, R., Pan, T. & Qian, J., &Li, H. (2006).Synthesis and surface modification of ZnO nanoparticles.*Chem. Eng. J.*, *119*, 71–81.

Ismail, A.A., El-Midany, A., Abdel-Aal, E.A., & El-Shall, H. (2005). Application of statistical design to optimize the preparation of ZnO nanoparticles via hydro thermal technique. *Materials Letters*, *59*, 1924–1928.

Janíková, B., Tokarský, J., Kutláková, K. M., Kormunda, M., & Neuwirthová, L. (2017). Photoactive and non-hazardous kaolin/ZnO composites prepared by calcination of sodium zinc carbonate. *Applied Clay Science, 143,* 345-353.

Kakhki, R. M., Tayebee, R., & Ahsani, F. (2017). New and highly efficient Ag doped ZnO visible nano photocatalyst for removing of methylene blue. *Journal of Materials Science: Materials in Electronics*, *28*(8), 5941-5952.

Kim, K. B., Kim, Y. W., Lim, S. K., Roh, T. H., Bang, D. Y., Choi, S. M., ... & Seo, H. S. (2017). Risk assessment of zinc oxide, a cosmetic ingredient used as a UV filter of sunscreens. *Journal of Toxicology and Environmental Health, Part B*, *20*(3), 155-182.

Kumar, R., Umar, A., Kumar, G., & Nalwa, H. S. (2017). Antimicrobial Properties of ZnO Nanomaterials: A Review. *Ceramics International 43*, 3940-3961.

Lachom, V., Poolcharuansin, P., & Laokul, P. (2017). Preparation, characterizations and photocatalytic activity of a ZnO/TiO_2 nanocomposite. *Materials Research Express*, *4*(3), 035006.

Li, H. (2004). *IR Studies of the Interaction of Surfactants and Polyelectrolytes Adsorbed on TiO_2 Particles*. The Graduate School The University of Maine, PhD Thesis.

Li, P., Wei, Y., Liu, H., Wang, X.K. (2005). Growth of well-defined ZnO microparticles with additives from aqueous solution. *J. Solid State Chem., 178,* 855–860.

Li, X., Sun, P., Yang, T., Zhao, J., Wang, Z., Wang, W., ... & Du, Y. (2013). Template-free microwave-assisted synthesis of ZnO hollow microspheres and their application in gas sensing. *CrystEngComm*, *15*(15), 2949-2955.

Lou, X., Shen, H. S., & Shen, Y. S. (1991). Development of ZnO series ceramic semiconductor gas sensors. *J. Sens. Trans. Technol*, *3*(1), 1-5.

Ludi, B., & Niederberger, M. (2013). Zinc oxide nanoparticles: chemical mechanisms and classical and non-classical crystallization. *Dalton Transactions*, *42*(35), 12554-12568.

Ma, C. L., & Sun, X. D. (2002). Preparation of nanocrystalline metal oxide powders with the surfactant-mediated method. *Inorganic Chemistry Communications*, *5*(10), 751-755.

Madhu, C., Kaur, I., & Kaur, N. (2017). Synthesis and investigation of photonic properties of surface modified ZnO nanoparticles with imine linked receptor as coupling agent-for application in LEDs. *Journal of Materials Science: Materials in Electronics*, *28*(9), 6388-6398.

Mahmud, S., Johar Abdullah, M., Putrus, G. A., Chong, J., & Karim Mohamad, A. (2006). Nanostructure of ZnO fabricated via French process and its correlation to electrical properties of semiconducting varistors. *Synthesis and Reactivity in Inorganic and Metal-Organic and Nano-Metal Chemistry*, *36*(2), 155-159.

Majoul, N., Aouida, S., & Bessaïs, B. (2015). Progress of porous silicon APTES-functionalization by FTIR investigations. *Applied Surface Science*, *331*, 388-391.

McDevitt, N. T., & Baun, W. L. (1964). Infrared absorption study of metal oxides in the low frequency region (700-240 cm− 1). *Spectrochimica Acta*, *20*(5), 799-808.

Multian, V. V., Uklein, A. V., Zaderko, A. N., Kozhanov, V. O., Boldyrieva, O. Y., Linnik, R. P., ... & Gayvoronsky, V. Y. (2017). Synthesis, Characterization, Luminescent and Nonlinear Optical Responses of Nanosized ZnO. *Nanoscale Research Letters*, *12*(1), 164.

Musić, S., Dragčević, Đ., Popović, S., & Ivanda, M. (2005). Precipitation of ZnO particles and their properties. *Materials Letters, 59*(19), 2388-2393.

Noshirvani, N., Ghanbarzadeh, B., Mokarram, R. R., Hashemi, M., & Coma, V. (2017). Preparation and characterization of active emulsified films based on chitosan-carboxymethyl cellulose containing zinc oxide nano particles. *International Journal of Biological Macromolecules, 99*, 530-538.

Onodera, A., & Takesada, M. (2012). Electronic Ferroelectricity in II-VI Semiconductor ZnO. In *Advances in Ferroelectrics*. InTech.

Özgür, Ü., Alivov, Y. I., Liu, C., Teke, A., Reshchikov, M., Doğan, S., Avrutin, V., Cho, S.J., & Morkoc, H. (2005). A comprehensive review of ZnO materials and devices. *Journal of Applied Physics*, *98*(4), 11. 041301.

Pandey, M., & Tripathi, B. D. (2017). Synthesis, characterization and application of zinc oxide nano particles for removal of hexavalent chromium. *Research on Chemical Intermediates, 43*(1), 121-140.

Pena-Alonso, R., Rubio, F., Rubio, J., & Oteo, J. L. (2007). Study of the hydrolysis and condensation of γ-Aminopropyltriethoxysilane by FT-IR spectroscopy. *Journal of Materials Science, 42*(2), 595-603.

Pysklo, L., Pawlowski, P., Parasiewicz, W., & Slusarski, L. (2007). Study on reduction of zinc oxide level in rubber compounds. Part I Influence of zinc oxide specific surface area and the interphase transfer catalyst 18-crown-6. *KGK. Kautschuk, Gummi, Kunststoffe, 60*(10), 548-553.

Quy, C. T., Hung, C. M., Van Duy, N., Hoa, N. D., Jiao, M., & Nguyen, H. (2017). Ethanol-Sensing Characteristics of Nanostructured ZnO: Nanorods, Nanowires, and Porous Nanoparticles. *Journal of Electronic Materials*, *46*(6), 3406-3411.

Radzimska, A.-K. & Jesionowski, T. (2014). Zinc Oxide-From Synthesis to Application: A Review. *Materials 7,* 2833-2881.

Ramelan, A. H., Wahyuningsih, S., Munawaroh, H., & Narayan, R. (2017, February). ZnO wide bandgap semiconductors preparation for optoelectronic devices. In *IOP Conference Series: Materials Science and Engineering* (176, 1, p. 012008). IOP Publishing.

Reichardt, C., & Welton, T. (2011). *Solvents and solvent effects in organic chemistry*. John Wiley & Sons.

Rilda, Y., Kurniawan, S., & Arif, S. (2015). Synthesis and Modification of the Morphology Of Zinc Oxide (ZnO) Nanoparticles With Induced Biopolymer Chitosan. *Journal of Pharmaceutical, Biological and Chemical Sciences*, *6*, 1511-1518.

Ristić, M., Musić, S., Ivanda, M., & Popović, S. (2005). Sol–gel synthesis and characterization of nanocrystalline ZnO powders. *Journal of Alloys and Compounds*, *397*(1), L1-L4.

Segets, D., Gradl, J., Taylor, R. K., Vassilev, V., & Peukert, W. (2009). Analysis of optical absorbance spectra for the determination of ZnO nanoparticle size distribution, solubility, and surface energy. *ACS Nano*, *3*(7), 1703-1710.

Singh, M. K., Agarwal, A., Gopal, R., Swarnkar, R. K., & Kotnala, R. K. (2011). Dumbbell shaped nickel nanocrystals synthesized by a laser induced fragmentation method. *Journal of Materials Chemistry*, *21*(30), 11074-11079.

Singh, N., & Haque, F. Z. (2016). Synthesis of zinc oxide nanoparticles with different pH by aqueous solution growth technique. *Optik-International Journal for Light and Electron Optics*, *127*(1), 174-177.

Shingange, K., Tshabalala, Z. P., Dhonge, B. P., Ntwaeaborwa, O. M., Motaung, D. E., & Mhlongo, G. H. (2017). 0D to 3D ZnO nanostructures and their luminescence, magnetic and sensing properties: Influence of pH and annealing. *Materials Research Bulletin*, *85*, 52-63.

Socrates, G. (2001). *Infrared and Raman Characteristic Group Frequencies: Tables and Charts*. John Wiley & Sons.

Srivastava, O. K., & Secco, E. A. (1967). Studies on metal hydroxy compounds. II. Infrared spectra of zinc derivatives ε-$Zn(OH)_2$, β-ZnOHCl, ZnOHF, $Zn_5(OH)_8Cl_2$, and $Zn_5(OH)_8Cl_2$ H_2O. *Canadian Journal of Chemistry*, *45*(6), 585-588.

Suyambulingam, G. R. T., Jeyasubramanian, K., Mariappan, V. K., Veluswamy, P., Ikeda, H., & Krishnamoorthy, K. (2017). Excellent floating and load bearing properties of superhydrophobic ZnO/copper stearate nanocoating. *Chemical Engineering Journal*, *320*, 468-477.

Tauc, J., Grigorovici, R., & Vancu, A. (1966). Optical properties and electronic structure of amorphous germanium. *Physica Status Solidi (b)*, *15*(2), 627-637.

Tauc, J. (1968). Optical properties and electronic structure of amorphous Ge and Si. *Materials Research Bulletin*, *3*(1), 37-46.

Thankachan, R. M., Joy, N., Abraham, J., Kalarikkal, N., Thomas, S., & Oluwafemi, O. S. (2017). Enhanced photocatalytic performance of ZnO nanostructures produced via a quick microwave assisted route for the degradation of rhodamine in aqueous solution. *Materials Research Bulletin*, *85*, 131-139.

Tian, B., Liu, S., Zhang, Y., Li, C., & Wang, Z. (2017). Hydrophilic, mesoporous structural ZnO nanospheres for pH-triggered release of drug. *Materials Letters*, *188*, 165-168.

Verma, N., Bhatia, S., & Bedi, R. K. (2017). Role of pH on electrical, optical and photocatalytic properties of ZnO based nanoparticles. *Journal of Materials Science: Materials in Electronics*, *28*(13), 9788-9797.

Widiyastuti W., Machmudah S., Nurtono T., Winardi S., Balgis R., Ogi T., & Okuyama K., (2017). Morphology and optical properties of zinc oxide nanoparticles synthesized by solvothermal method. *Chemical Engineering Transactions, 56*, 955-960.

Wolski, L., Whitten, J. E., Sobczak, I., & Ziolek, M. (2017). The effect of the preparation procedure on the morphology, texture and photocatalytic properties of ZnO. *Materials Research Bulletin, 85*, 35-46.

Wang, J., Cao, J., Fang, B., Lu, P., Deng, S., & Wang, H. (2005). Synthesis and characterization of multipod, flower-like, and shuttle-like ZnO frameworks in ionic liquids. *Materials Letters, 59*(11), 1405-1408.

Wang, Z.L. (2008). Splendid one-dimensional nanostructures of zinc oxide: A new nanomaterial family for nanotechnology. *ACS Nano, 2*, 1987–1992.

Wang, Y., Zhang, C., Bi, S. & Luo, G. (2010). Preparation of ZnO nanoparticles using the direct precipitation method in a membrane dispersion micro-structured reactor. *Powder Technology, 202,* 130-136.

Zhou, Y., Xu, L., Wu, Z., Li, P., & He, J. (2017). Optical and photocatalytic properties of nanocrystalline ZnO powders synthesized by a low-temperature hydrothermal method. *Optik-International Journal for Light and Electron Optics, 130*, 673-680.

Znaidi, L. (2010). Sol–gel-deposited ZnO thin films: A review. *Materials Science and Engineering: B, 174*(1), 18-30.